EPSRC Centre for Doctoral Training in

Future Power Networks and Smart Grids

Characteristics of Partial Discharge Under High Voltage AC & DC Conditions

A thesis presented in fulfilment of the
University of Strathclyde requirements for the degree of
Doctor of Philosophy

Euan Andrew Morris MEng

2020

Department of Electronic & Electrical Engineering

University of Strathclyde

Glasgow, UK

University of Strathclyde Glasgow

EPSRC Engineering and Physical Sciences Research Council

HVT RESEARCH GROUP

Authors Declaration

This thesis is the result of the author's original research. It has been composed by the author and has not been previously submitted for examination which has led to the award of a degree. The copyright of this thesis belongs to the author under the terms of the United Kingdom Copyright Acts as qualified by University of Strathclyde Regulation 3.50. Due acknowledgement must always be made of the use of any material contained in, or derived from, this thesis.

Signed: Euan Andrew Morris

Date: 14/07/2020

Abstract

High voltage AC has been the technology of choice for electricity transmission since the creation of electric grids throughout the world. However due to a wide range of factors, including the availability of new AC-DC and DC-AC converter designs, an increasing requirement for subsea interconnections for off-shore wind and continental super-grids, a greater emphasis on efficient operation for cost and environmental reasons, and a desire for ever-increasing transmission distances, high voltage DC is increasingly seen as an attractive and viable choice.

While HVDC technologies have existed for as long as HVAC, their lack of significant use until recently mean that several gaps in knowledge exist, including in the area of condition monitoring of assets. One such condition monitoring technology is partial discharge monitoring, which, while it is a mature technology that is frequently used in AC systems, it has had limited deployment under DC conditions. As such it still lacks the field experience, well-developed standards, technical expertise, and overall knowledge base for DC that exists for AC.

This thesis presents research into the characteristics of partial discharge under both AC and DC conditions. A review of relevant literature is presented, followed by the research methodology, including the use of thin film polymer samples, and a 'coring' method for introducing an artificial void into a cable sample. Data and analysis are then presented which compare the presentation of PD in different materials, the impact of multiple void configurations on PD, and statistical analysis of the PD pulses themselves.

These analyses demonstrate clear differences between the behaviour of PD, and the characteristics of the PD pulses themselves, under the different voltage types, void configurations, and materials investigated, with potential reasons for these differences discussed, and suggestions made for how knowledge of these differences should affect the detection of PD, and, therefore improve condition monitoring of both AC and DC equipment.

Table of Contents

List of Figures

List of Tables

List of Abbreviations

ABS	Acrylonitrile butadiene styrene
AC	Alternating current
ASCII	American Standard Code for Information Interchange
CSC	Current source converter
CSV	Comma-separated values
DC	Direct current
DOI	Digital object identifier
EBA	Ethylene butyl acrylate
EVA	Ethylene-vinyl acetate
FEA	Finite element analysis
GF	Gas-filled
HFCT	High frequency current transformer
HPOF	High-pressure oil-filled
HVAC	High voltage alternating current
HVDC	High voltage direct current
IEC	International Electrotechnical Commission
IGBT	Insulated-gate bipolar transistor
IGCT	Integrated gate-commutated thyristor
ISO	International Organization for Standardization
LCC	Line-commutated converter
LDPE	Low-density polyethylene
MIND	Mass impregnated non-draining
MMC	Modular multi-level converter
PD	Partial discharge
PDIV	Partial discharge inception voltage
PE	Polyethylene
PET	Polyethylene terephthalate
PP	Polypropylene
PPLP	Polypropylene laminated paper
PRPD	Phase-resolved partial discharge

PSA Pulse sequence analysis

PVC Polyvinyl chloride

SCOF Self-contained oil-filled

TDR Time-domain reflectometry

TXT Text file

UHF Ultra high frequency

VSC Voltage source converter

XLPE Cross-linked polyethylene

Acknowledgement

The work presented in this thesis was made possible because of the help and support of many people to whom I'd like to give my thanks.

Firstly, thanks must go to my supervisor Professor WH Siew, who has given continuous support and advice throughout every stage of the PhD process. Technical support was also provided by the project industrial partner SSEN, and in particular Dr Gerry Cleary, to whom I am grateful, with additional support from David Stroud and Tawanda Chitifa.

Significant support, particularly in the early stages of this project was provided by my colleagues at the HVT research group, so my thanks go to, Dr Eddie Corr, Dr Rong Tang, Professor Brian Stewart, and my second supervisor, Dr Martin Given.

My thanks, must also go to students and staff at the Future Power Networks and Smart Grids CDT. Specifically, the CDT's director Professor Stephen McArthur, co-director Professor Tim Green, and administrator, Ms Shirley Kirk, as well as all the members of my CDT cohort (2014) and the 2015 cohort, and in particular the members of the Professional Engineer Development Society committee for the years I was Chair.

Additionally, I am extremely grateful to Mr Francis Cox, and all the technicians in the HVT and EEE workshops, whose technical support was vital throughout the project.

Lastly, I am extremely grateful for the critical emotional support that was provided by all my friends and family, in particular, my parents, my brother, and, of course, my spouse, Alyx.

1. Introduction

This chapter presents the background, motivation and objectives for the research conducted, as well as an outline of the thesis describing subsequent chapters, and the published contribution from this research.

1.1. Background

1.1.1. High Voltage Direct Current Transmission

Since the early conception of the electric generator, the benefits of mass-supply of electrical energy have been clear. The first power stations utilising generators produced low voltage direct current (DC), and were only capable of suppling very local loads, usually electric lighting. However, the development of alternating current (AC) generators and transformers allowed for the generation and supply of high voltage electricity over long distances, leading to the birth of the transmission network. From these early days of electricity supply, until recently, the vast majority of transmission was achieved through AC, with a large number of condition monitoring methods, standards and equipment being developed over the decades to ensure reliable and efficient operation.

As a result of a wide range of factors, including new AC-DC and DC-AC converter designs, an increased requirement for subsea transmission, environmental and efficiency concerns, and the desire for increased transmission distances, transmission lines carrying high voltage direct current (HVDC) are increasingly a more attractive choice. However, the same field experience, international standards, technical expertise, and general knowledge base that exist for AC transmission systems do not yet exist for DC.

One area in which the gap between knowledge of AC systems and DC systems is particularly apparent is the field of partial discharge (PD) measurement. PD monitoring is an important tool in the condition-based maintenance of AC circuits, but further research is required for a similar level of knowledge of the correlation of PD signals and equipment condition to give improved reliability for DC circuits.

1.1.2. Partial Discharge Monitoring

PD monitoring is of pre-eminent importance among methods of monitoring the health of high voltage AC assets, and has been a subject of study since the early twentieth century [1]. Over the decades research has been undertaken covering the mechanisms and forms of PD[2], the effects of PD on cable health[3], the characteristics of PD pulses[4], the separation of PD from noise[5], as well as the differences in PD behaviour in different equipment[6] for example power cables, transformers, motors and generators. Additionally methods of PD detection have also developed significantly, from the earliest PD detection performed with analogue devices[1], through to the use of crystal controller pulse counters to detect pulse density and height[7], onto the advent of analogue to digital converters allowing for pulse distribution analysis, and finally with the rise of personal computers allowing for smarter PD analysis through the use of software techniques[8], [9] including neutral networks[10]. Due to these developments partial discharge monitoring is a well-accepted indicator of the condition of insulation, and is commonly used industrially to prevent unplanned outages [11].

1.2. Motivation

Given the correct conditions, HVDC systems can be the only economic choice for the bulk transmission of electricity[12]. In some cases, this is due to existing AC transmission networks being congested, or when the connection of two or more asynchronous AC networks is required, but the most common reason is when connection is required over longer distances. Typically, the idea of the 'break-even distance', is considered the criterion for when a DC system might be selected over an AC system, i.e. when the savings from DC transmission lines balance with the additional costs of the converter stations that DC systems require. The value of break-even distance has changed as the cost of converter stations has decreased, from a typical value around a decade ago of 800-1000 km[13] to around 500 km more recently[12]. The break-even distance can be even lower in circumstances when an AC line would require significant reactive power compensation (due to cables having a capacitance which increases with length and which decreases the cable current carrying capacity), or if additional AC

circuits would be required for stability purposes (as the maximum power transfer for a circuit is inversely proportional to the reactance of the cable, and this reactance increases with cable length) . Additionally, in cases when subsea cables are desirable (such as the connection of off-shore wind generation), HVDC can become economical at distances as short as 40-50 km[12], [14] due to the significant capacitance of AC submarine cables. Given the rapid growth, and planned further expansion, of offshore wind, particularly in the waters around the UK, the number of HVDC lines installed is also set to significantly increase. However, as discussed above, the HVDC systems do not have the wealth of research and field experience that HVAC systems enjoy. There is therefore a clear and strong motivation for significant research into condition monitoring of HVDC systems using PD, and indeed as discussed below, this field has seen significant focus in recent years.

Topics explored of particular relevance to HVDC have included: PD with high frequency characteristics[15] as harmonics are commonly generated by converter stations, the impact of void size on PD development under DC conditions[16], PD patterns during accelerated aging under DC conditions[17], modelling of space charge and its impact on PD[18] as space charge can accumulate in DC cables, due to the lack of the constant polarity reversal found under AC conditions, the impact of electric field distribution[19] as this is more consistent under DC conditions, and the use of neural networks and other machine learning techniques to diagnose and categorise partial discharges[20] based on the limited knowledge of PD under DC conditions.

However, despite this, there remains a significant knowledge gap in relation to condition monitoring of HVDC assets including converter stations and harmonic filters, with cable monitoring in particular being of importance, due to the inaccessibility of these assets making routine (i.e. time-based) maintenance expensive at best, and entirely impractical at worst[21].

Repairing or replacing assets upon failure (i.e. break-down maintenance) is also not a practical solution, as there is a significant loss of income when assets fail.

Therefore, the only desirable maintenance strategy is that of condition-based maintenance, which, for AC cables, involves significant use of PD monitoring. However, for PD monitoring to be practical for DC cables, given the different behaviour of PD under DC conditions, the patterns and characteristics of DC PD, and the relation to AC PD under similar conditions must be better understood.

In particular, the effect that the insulation type (impacted by the type of HVDC used- discussed in Chapter 2) has on PD patterns and PD pulses themselves must be explored, as well as the impact of voltage polarity. Consideration of pulse shape and their relationship to various parameters is also of key interest for denoising of PD data[22].

1.3. Research Aim & Objectives

1.3.1. Research Aim

- The aim of this project was to allow for the better detection of partial discharges in power cables situated in electrically noisy environments, or in cases, such as longer cables, when PD signal strength is likely to be small due to a long distance between the PD source and detector, by collecting PD pulses generated under different conditions, performing analysis to determine how these conditions impacted the characteristics of the PD, and to produce a database of the captured pulses to allow this analysis to aid in further research in this field.

1.3.2. Research Objectives

To achieve this aim, the objectives of the research presented by this thesis were:

- To determine the impact of material type on the characteristics of PD
- To further investigate the impact of multiple voids, and their configuration, on partial discharge characteristics under AC and DC conditions
- To find the impact of voltage polarity on partial discharge characteristics under DC conditions.
- To discover the impact of material type, void configuration and voltage type on the size and shape of PD pulses.

- To determine if the impact of the conditions under which the PD originates has a significant enough impact that it should be considered when PD detection is undertaken, particularly when this detection would otherwise be difficult due to low signal strength and/or high background noise.
- To explore novel methods of artificial void creation in cable samples, and to compare cable results to insulation sample results to ensure the practical applicability of the latter.
- To create a database of PD results to allow this analysis to aid in the development of PD detection and monitoring applications, for example, in the creation of algorithms to distinguish PD signals from background electrical noise.

1.4. Thesis Outline

Following this chapter, Chapter 2 presents a review of the literature considered as foundational for the research which was carried out. This includes background information on the development of power cable insulation, various partial discharge detection techniques (with an emphasis on detection in cables) and their use and history, the mechanisms of PDs in voids under both AC and DC conditions, as well as definitions for common terms used in partial discharge research, including in this work, and recommended methods for representing PD data.

Chapter 3 concerns the methodology used for this research, and details information about the laboratory in which the experimental results were obtained, the equipment which was used to carry out the experiments, and the design of the experimental methods themselves, including the creation of the test rigs and samples for testing.

Chapter 4 begins the original contribution and presents results and analysis from the testing of single void thin film samples of polyethylene and polypropylene under both AC and DC conditions. These results are used to validate the test sample creation method, the design of the test rig, and the suitability of the test

circuit and equipment. In addition, investigation into the effect of the material type, as well as voltage type, on the presentation of PD is discussed.

Chapter 5 provides data and analysis for testing of both single void and multiple void thin film samples (of different configurations) of polyethylene and polypropylene under AC conditions. These results are used to investigate the impact of void configuration and material type on the inception and development of PD.

Chapter 6 presents analysis of data captured under DC conditions during testing of thin film polyethylene samples containing both single and multiple voids. This analysis investigates the impact of different void configurations on the presentation of PD under DC conditions. Additionally, this analysis is compared with analysis from Chapter 5 concerning AC analysis under the same conditions, to determine the impact of voltage type.

Chapter 7 is concerned with the analysis of data captured from testing under both AC and DC conditions on a test sample, containing a single void, created from a section of cross-linked polyethylene cable. These results are used to validate the coring method used to create the defect in a cable sample, as well as to allow comparative analysis of data collected from a sample of real cable with data from the artificial voids.

Chapter 8 presents statistical analysis of the individual PD pulses captured in each of the material types, for the different void configurations and under the different voltage types. This data allows for investigation of the difference in various PD pulse metrics based on the conditions under which the pulse originates.

Chapter 9 presents the overall conclusions of the work, based on the analysis in the preceding chapters, and makes recommendations for further work to extend this analysis.

1.5. Contribution

1.5.1. Research Contribution

The contributions from this thesis are summarised as follows:

- The behaviour of PD in samples created from thin films of polyethylene and polypropylene containing a single void under AC conditions was explored.
  - This was used to confirm that the PD behaviour in the samples was as expected, using the AC test method and sample creation method.
  - In addition, differences between PD behaviour in each material were investigated, determining which analysis methods found these behavioural differences, and which did not.
- Investigation of PD in polyethylene samples containing a single void was also undertaken under DC conditions
  - The DC test method was presented, and applied to confirm that PD can be successfully detected under these conditions.
- Samples containing different void configurations were tested under both AC and DC conditions, to determine the impact of voltage type and void configuration.
  - It was found that, under both AC and DC conditions, the partial discharge inception voltage (PDIV) was affected by the different void configurations, with a clear reduction when parallel voids were present, and limited effect when serial voids were. PDIV were significantly higher under DC compared to AC conditions
  - A measurable impact of different void configuration was found on the characteristics of PD, including the patterns on standard PD plots (discussed below), and the pulse sequence analysis (PSA) comparing the PD pulses to those which occurred before them. These differences were greater under DC conditions than under AC, with greater ranges of measured characteristics found when multiple voids were present.

- AC testing of samples with different void configurations also compared the impact of material type (between polypropylene and polyethylene) on PD behaviour.
    - The material type was found to have a noticeable impact on the PD behaviour, with differences in the spread of both pulse size, and pulse phase location for each material. Suggesting that material type should be considered when PD detection methods are being developed
- DC testing on the samples with different void configurations was also used to find the impact of voltage polarity on PD behaviour.
    - The voltage polarity was found to a have a measurable impact on PD behaviour, with positive polarity stress tending to lead to shorter recurrence times for PD compared to negative polarity stress. Suggesting that voltage polarity should be considered when PD detection methods are being developed for use under DC conditions.
- PD pulses themselves were statistically analysed to determine the impact of material type, void configuration and voltage type on the size and shape of the pulses.
    - Clear differences were found in PD pulses occurring under the different conditions, with noticeable impacts on pulse height, pulse width, rise time, and fall time evident.
    - From this, a suggestion is made for the material, and voltage type and polarity to be considered when designing denoising algorithms for PD detection under those conditions.
- A 'coring' method was used to create a void type defect in a sample of cable.
    - This method successfully introduced a void, in which PD was detected under AC, and positive and negative DC, conditions.
    - From this it was found that the behaviour in the single void in an XLPE cable was similar to that in the single-void thin-film low-

density polyethylene samples. Confirming that the results from thin film samples were of practical relevance.

- An open access database (assessable through the University of Strathclyde's PURE data repository) of all the collected data was created[23].
  - This contains the PD pulses captured at two scales, the scale of individual PD pulse capturing information about the PD pulse itself, and the scale of a 50 Hz waveform to capture the PD apparent charge and phase.
  - Data captured for this database were used in the design of a wavelet algorithm for denoising of PD data[24].

1.5.2. Journal Contributions

1. **E.A. Morris**, W.H. Siew, M.J. Given, and G.P. Cleary, *"Influence of DC voltage polarity on partial discharge characteristics of void defects"* IET High Voltage (in progress).
2. **E.A. Morris**, W.H. Siew, M.J. Given, and G.P. Cleary, *"Influence of material type and void configuration on PD under AC and DC conditions."*, CIGRE Science and Engineering (in progress).
3. **E.A. Morris**, W.H. Siew, M.J. Given, and G.P. Cleary, *"Partial Discharge Measurements of Voids in Layered Polymers and Cable Sample."*, Elsevier Data in Brief (in progress).

1.5.3. Conference Contributions

1. **E. A. Morris**, W. H. Siew, and M. J. Given, *"DC Partial Discharge in Polymeric Cable Insulation."*, Conference on Electrical Insulation and Dielectric Phenomena, 2018, pp. 494–497[25].
2. **E. A. Morris** and W. H. Siew, *"Partial Discharge Activity in Polymeric Cable Insulation under High Voltage AC and DC."*, International Universities Power Engineering Conference (UPEC), 2017, pp. 1–4 [26].
3. **E. A. Morris** and W. H. Siew*, "A Comparison of AC And DC Partial Discharge Activity in Polymeric Cable Insulation."*, 21st IEEE International Pulsed Power Conference, 2017, pp. 1–4 [27].

1.5.4. Colloquia Contributions

1. **E. A. Morris**, W. H. Siew, and M. J. Given, "*Partial Discharge Detection and Location for HVDC Cables."*, Universities High Voltage Network (UHVNet), 2016.
2. **E. A. Morris**, W. H. Siew, and M. J. Given, *"Partial Discharge Detection for Polymeric HVDC Cables."*, Universities High Voltage Network (UHVNet), 2017.
3. **E. A. Morris,** G. P. Cleary, and W. H. Siew, *"Characterisation of Partial Discharge in HVDC Cables."*, Smart Future Energy Systems (SmartFuturES) Colloquium, 2018.

2. Partial Discharge Mechanisms and Measurement

This chapter presents an overview of the literature pertinent to this research and includes definitions for common terms used in partial discharge research, including in this work.

2.1. HVDC Transmission

2.1.1. Early History

The origins of HVDC transmission, as with the birth of electric transmission and distribution as a whole, are in the last years of the 19th century. In 1882 the Pearl Street power station began supplying electricity at DC voltages to the financial district in New York City [28], and, in the same year, in Germany a 50 km transmission line was constructed between Miesbach and Munich, operating at 2 kV [29] DC. However, technological limitations meant that there were significant drawbacks to transmitting electricity using DC voltages rather that at AC. Most significant amongst these was the cost of converting between voltages that are economical for transmission, and those which are safe and practical for use by consumers [29]. Therefore for the bulk of electricity distribution and transmission from the early 20th century onwards AC voltages were used [30].

2.1.2. Further Research & Advantages of HVDC

This difficultly (and cost) of converting between different voltages, remained the major barrier to HVDC transmission however, as transmission technologies, HVDC systems have several advantages, and HVAC several disadvantages, significantly:

- HVDC transmission cables suffer from fewer loss mechanisms than HVAC transmission as shown in Table 1.
- Transmission capacity and distance limited by inductive and capacitive elements of AC cables[30].
- Higher cable utilisation under DC voltages due to lack of ‘skin-effect’[31], the tendency of AC current density to be largest nearest the surface of the conductor due to the magnetic field created by the alternating electric field inherent to AC, reducing the effective area of the cable.

- A reduction of number of lines required for the same power transfer[31].
- HVDC transmission systems have no need for the reactive compensation required by HVAC systems[30].

Table 1 – AC and DC cable loss mechanism comparison (from [32]*).*

AC Cables	DC Cables
• Ohmic losses in conductor • Induced losses in conductor • Induced losses in sheath • Induced losses in armouring • Induced losses from adjacent cables • Cable current due to length	• Ohmic losses in conductor

Due to the disadvantages with AC systems, research continued into HVDC transmission. The first obstacle to be overcome was the need for a rectifier (a device which converts AC to DC) capable of operating at high voltages. The first device capable of this was the high voltage mercury valve arc valve developed by Uno Lamm and his team[28] in 1929. This, along with research into converter topologies, DC insulators, and other foundational topics in the 1930s, laid the groundwork on which modern HVDC transmission is built[28].

2.1.3. Economic Viability & Break-Even Distance

The 1930s also saw research into the economics of HVDC transmission as compared to HVAC, which saw the emergence of what is now known as the 'break-even distance'. This is the distance at which the cost of DC terminals, DC cables, and DC losses, outweigh the costs of AC terminals, cables, and losses. This point occurs due to the fact that the costs which are higher for DC (namely the station terminals) are fixed regardless of line length, whereas the costs which are higher for AC (cable costs and losses) increase on a per-kilometre basis (this is illustrated diagrammatically in Figure 1).

These developments were built on throughout the mid-to-late 1940s, and 1950s, when the commercial viability of HVDC seemed certain[28]. In particular, the use of HVDC links for undersea connections, was estimated to be the most attractive

commercially, due to the high cost of reactive compensation required for HVAC subsea connections[30]. The first commercial HVDC link was constructed in 1950 between the Swedish mainland and the island of Gotland[28], operating at 100 kV with a capacity of 20 MW. This stimulated a range of feasibility studies into HVDC links across Europe and North America, of which the first to be commissioned was the 'Cross Channel' link between the south of England and the north of France in 1961.

The next major development in HVDC technology came with the invention of the thyristor (a solid-state switching device which allowed for the creation of more efficient converters), in the late 1970s, with improvements in thyristor, converter, and control design continuing through the 1980s and 1990s allowing for increasing voltage levels and capacities.

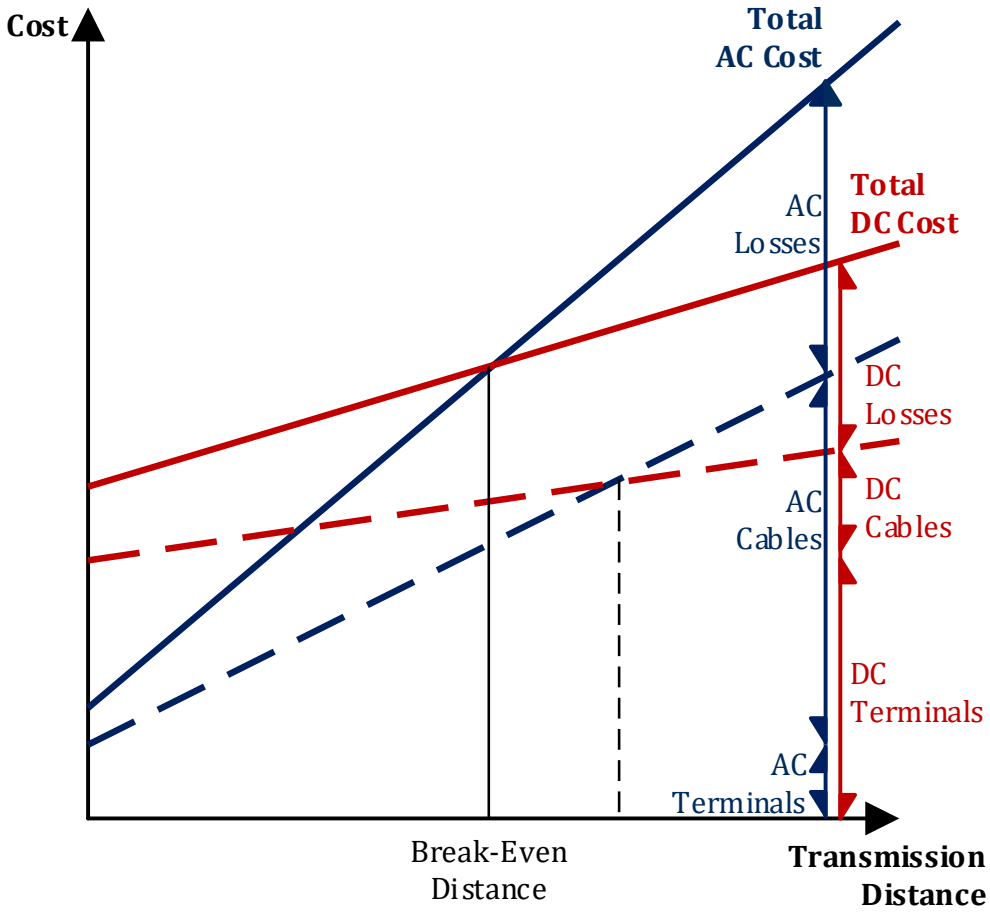

Figure 1 – Illustration of the costs versus distance of AC (blue) and DC (red) transmission lines with losses included (solid line) and excluded (dotted line) based on [29].

2.1.4. Further Developments & Converter Topologies

Thyristor (and mercury valve) based HV AC to DC and DC to AC converters are current source converters (CSC) (shown in Figure 2) also known as line-commutated converters (LCC), but the development of insulated gate bipolar transistors (IGBTs) capable of operating at high voltages, allowed for the use of voltage source converters (VSC) (shown in Figure 3) or self-commutated converters[33].

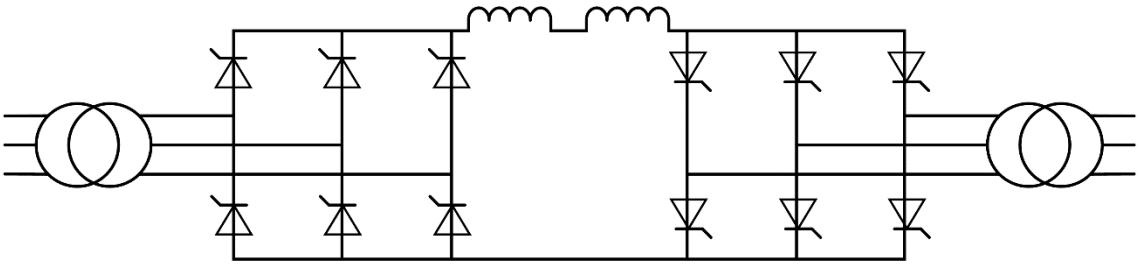

Figure 2 – Circuit diagram illustrating the LCC converter, showing the thyristors and smoothing reactors.

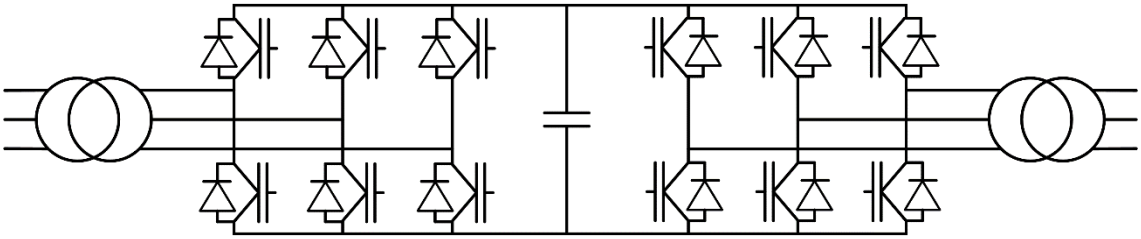

Figure 3 – Circuit diagram illustrating the VSC converter, showing the IGBTs and DC capacitor.

Each technology operates differently and has positive attributes and drawbacks as summarised in Table 2.

Table 2 – Summary and advantages/disadvantages of LCC and VSC converter topologies from[33].

LCC	VSC
• Use thyristors which can withstand voltage in either polarity • Output voltage can be either polarity to charge power flow direction • Current direction does not change	• Use IGBTs which can pass current in either direction • Output voltage polarity does not change • Current direction changes to charge power flow direction

• Thyristors can turn on by control action • Turn-off (or 'commutation') rely on external circuit • Requires use of mass-impregnated cables (or PPLP)	• IGBTS can turn on or off by control action • Turn-off is independent of external circuit (hence 'self-commutation') • Requires use of XLPE cables
Advantages	
• Available at high power level • High reliability • Low power loss from converters • Good overload capacity • Lower cost	• Self-commutating • Finer Reactive power control • Better suited for multi-terminal applications • Compact site area (50-60% of similar LCC)
Disadvantages	
• Generates harmonic distortion physically large AC & DC harmonic filters required • Requires AC voltage for commutation • Requires stronger AC system	• Lower power capacity due to IGBT current capacity • Higher converter losses • Less mature technology • Higher cost (10-15%)

As can be seen from Table 2, the technology chosen for the HVDC converts affects the choice of cable insulation[34], this is further discussed below.

2.1.5. State-of-the-art Research & Future Topics

Much of HVDC research in the early 21st century focused on designs for multi-level VSC converters, with the aim of reducing power losses and increasing the operating power level to that of LCC converters and beyond. The first commercial multi-level converter was installed in 2010 and used the modular multi-level converter (MMC) topology[35]. Compared to conventional VSC converters MMC converters have the advantage of being[33]:

- Modular and scalable
- Highly efficient

- Capable of producing lower harmonics (unwanted higher frequency components which affect the quality of the DC output).

Much of the on-going research in the HVDC field is in improving MMC converters, including; improving reliability[36], improving MMC efficiency[37], the use of MMCs in multi-terminal applications, and the use of integrated gate-commutated thyristors (IGCT) in place of IGBTs[38].

Other topics of research include hybrid LCC-VSC HVDC[39], control of HVDC systems including with regards to providing grid support in the form of system inertia (which slows the impact of changes in system frequency, ensuring the system is more stable)[40], protection of HVDC systems[41], and, most pertinent to this project, condition monitoring of HVDC assets[42].

2.2. Power Cable Insulation

Power cables are a fundamental part of any transmission system, and whether designed to carry AC or DC, will typically have the same configuration, shown in Figure 4[43].

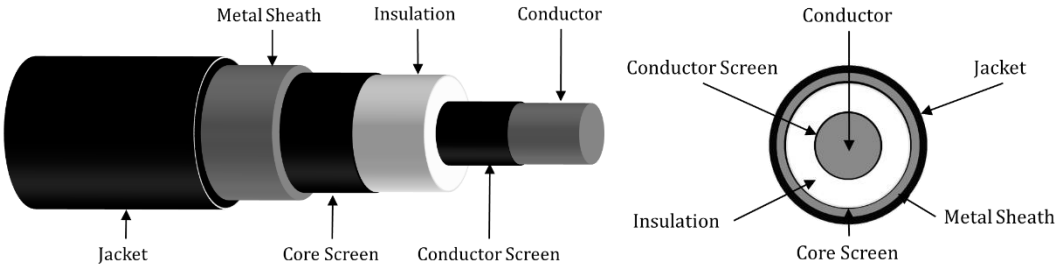

Figure 4 – Diagram showing standard components of power cables, in isometric view (left) and face-on view (right) based on [43].

The jacket, or oversheath, is the external cable covering, it provides mechanical strength and prevents damage from moisture or other contaminates, a thermoplastic is typically used to make the jacket. Other cable armouring may be used on top of the jacket, particularly in the case of submarine cables.

The metal sheath, or outer conductor, acts as the earthing for the cable and conducts leakage and fault currents if required, as well as acting as an electromagnetic shield. The metal sheath is typically made from lead, copper, or aluminium.

The core screen, or outer semicon, is bonded to the insulation to prevent air gaps, and to provide a better electric field distribution (preventing areas of high local field strength which can lead to breakdown). The core screen is made from a polymer, such as XLPE, EVA (ethylene-vinyl acetate) or EBA (ethylene butyl acrylate), which contains conducive materials, such as carbon black or graphite.

The insulation isolates the conductor from ground (and other objects that may come in contact with the cable). The insulator must be capable of withstanding the rated voltage of the cable, as well as the temperature the conductor reaches at the rated current of the cable. Many materials can be used for cable insulation, as discussed in the next section.

The conductor screen, or inner semicon, provides the same function as the core screen, and is made of the same material.

The conductor is the current-carrying part of the cable and, as such, is made from a material with high electrical conductivity, typically either copper or aluminium.

2.2.1. Historic

When the first HVDC links were being installed from the 1950s-70s there were four cable insulation types available[44]:

- Mass impregnated non-draining (MIND)
- Self-contained oil filled (SCOF)
- High-pressure oil filled (HPOF)
- Gas-filled (GF)

All of which use oil-paper insulation. Technological limitations of maintaining oil and gas pressure in longer distance cables, as well as manufacturing and even environmental concerns, meant that MIND insulation, where the paper insulation is saturated with a non-draining resin compound, was the most popular option. However, MIND insulation has several disadvantages, in particular the maximum conductor temperature is relatively low (around 55°C) limiting the current rating of the cable[44], encouraging research into alternatives.

2.2.2. Polymeric

2.2.2.1. Extruded Insulation

Research into the potential use of polymers as insulating materials, specifically extruded insulation, began in the 1970s with designs based on standard polyethylene (PE) and cross-linked polyethene (XLPE). However, these designs were found to fail under test due to the build-up of space charge (electrons on the surface of the insulation), particularly under DC polarity reversal [44], which occurs when power flow is reversed in an LCC system. It wasn't until the creation of the first VSC HVDC link (to Gotland in 1999) that a practical extruded insulation cable (using XLPE) could be used, due to the lack of voltage polarity reversal in VSC operation. Since then a great number of XLPE insulated cables are used in HVDC applications, all of which connect VSC stations.

2.2.2.2. Paper Laminate

Clearly, there is also a requirement for an alternative to MIND cables that are suitable for use with LCC, when that configuration is desirable. The solution is the use of polypropylene (PP) in the form of polypropylene laminated paper (PPLP). PPLP was originally developed as a replacement for HVAC MIND cables, in the 1970s, however recently it has been used for HVDC applications[45].

Whichever insulating material is chosen, it is desirable to assess the health of condition of the insulation while the cable is in service. Partial discharge measurement is an important method of accomplishing this, and, as such, has been a subject of intense study from the beginnings of large-scale electricity transmission.

2.3. Partial Discharge Mechanisms

Partial discharge (PD) is a type of electrical discharge that occurs in a localised area of insulation that itself is between two conductors, but that does not completely connect the conductors[46]. PD occurs due to imperfections or defects within insulation, for example voids or cavities. Discharges can, over time, damage insulation until there is a complete path between conductors and the equipment containing the insulation fails[1].

The first recorded discovery of what is now known to be partial discharge, made long before the development of electricity transmission and distribution, was by physicist Georg Chrsitoph Lichtenberg in 1777[47]. The phenomenon Lichtenberg discovered was that radial or tree-like patterns were formed on an insulating surface when a sharp pointed electrode at a high voltage was discharged onto that surface. At the time it was thought these patterns (which were named Lichtenberg figures) were related to positive and negative 'fluids', but around one hundred years after their discovery it was found that the true cause was small electrical discharges that propagated along the surface[48].

From an electrical engineering standpoint, the research into partial discharge began in 1936, when the first measurement of PD within a defected insulating material was reported. Although the term 'partial discharge' was not applied, with the phenomenon described as "breakdown due to a slowly progressive treeing and coring [sic] in the dielectric caused by ionisation by collision[49]".

Research continued in the late 1940s, which saw development both in the understanding of the physics behind the mechanisms of PD and methods for their detection[48], with commercial PD detectors becoming available in the late 1950s.

Early research focused on the correlation between PD patterns when plotted with respect to phase angle and pulse magnitude (known as phase resolved partial discharge or PRPD plots, discussed below) and type of defect, with the first digital recording of PD occurring in the late 1976.

The thesis is focused on void-type PD, or PD occurring within cavities in solid insulation. Void-type partial discharge is the most significant when discussing the impact, and monitoring, of PD in power cables, and, as such, there has been significant research focused in this area since the advent of computerised detection in the late 1980s [50], [51], [60], [61], [52]–[59].

2.3.1. Void Type Mechanisms

Within solid insulation, internal discharges can occur in defects within that insulation. These defects can occur in the form of gas-filled cavities that develop

during the extrusion of polymers, or the casting of resins, including in resin-impregnated paper[1]. Additionally, cavities can be formed due to contaminants within insulation, which can create a local electric field sufficient for a dielectric breakdown, creating a cavity. Oil-filled cavities can also develop in a similar manner in oil filled cables, or those insulated with oil-impregnated paper. These cavities can be considered to behave in a similar manner to gas-filled cavities [62].

In whichever manner they form, it has been found that these cavities will have a breakdown field strength given by Paschen's Law[63] (which was formulated to determine the breakdown field strength of a gap between metal electrodes) . This holds that the potential at which breakdown occurs is a non-linear function of the product of the cavity dimensions and the pressure of the gas in the cavity[64]. When plotted this non-linear function is known as a Paschen Curve.

$$V_{BD} = \frac{B \times p \times d}{ln(A \times p \times d) - ln\left[\ln\left(1 + \frac{1}{\gamma}\right)\right]} \qquad (2.1)$$

Where V_{BD} is the breakdown voltage (in volts), γ is the secondary ionisation co-efficient (the number of electrons emitted from the cathode per incident positive ion, dependent on the cathode material), A and B are constants reflecting the saturation ionisation (in per metre-pascal), and minimum energy required for ionisation within a given gas (in volts per metre-pascal), respectively, p is the pressure (in pascals) and d is the cavity gap distance (in metres)[65].

The values for A and B cannot currently be mathematically derived for a given gas and must be determined experimentally. For air, A is 11 $m^{-1}{\cdot}Pa^{-1}$, and B is 277 $V{\cdot}m^{-1}{\cdot}Pa^{-1}$. Examples of Paschen Curves for common gases are shown in Figure 5.

Paschen's Law is derived from the observation that the breakdown voltage of a gas is dependent on the electron mean free path (the average distance an electron travels before hitting an atom) which is related to pressure (i.e. the number of atoms in a given volume of a gas), and on the distance between the electrodes[65] (or in the case of a discharge within a cavity, the length of the cavity

perpendicular to the electrodes). At higher pressures there is a short mean free path, meaning that electrons are likely to collide with atoms before they have sufficient energy for ionisation, whereas at low pressures electrodes may gain ionisation energy but not hit an atom before reaching the anode (or in the case of a cavity discharge, the surface of the cavity).

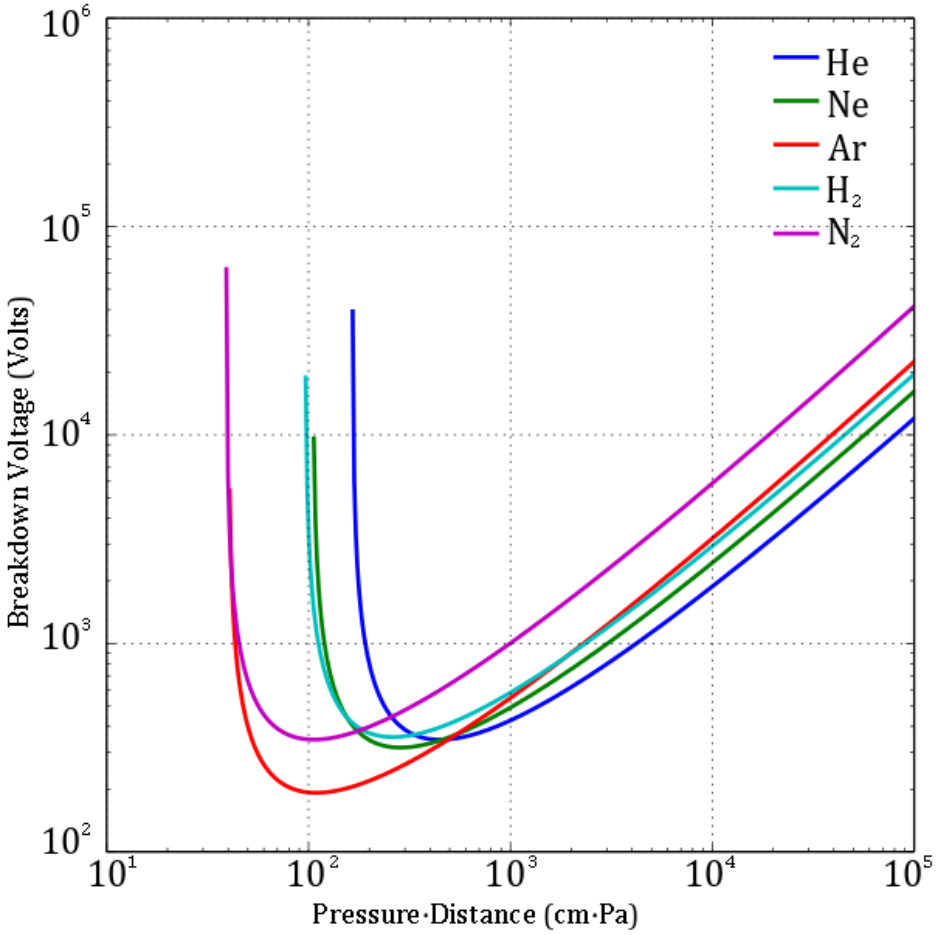

Figure 5 – Paschen's curves for common gases (based on [66]*).*

The partial discharge inception voltage (PDIV) therefore, is the minimum steady state voltage applied to an object at which the breakdown voltage (V_{min}) is reached within a cavity or defect within that object (as discussed below for practical purposes this value may be different depending on if an AC or DC voltage is applied). Once this point is reached, a discharge will occur provided a free electron is present within the cavity to begin ionisation. There is a time lag (t_L) associated with both the appearance of this electron (known as the statistical time) and with the time taken for the ionisation process to begin (known as the

formative time), with the time lag being the sum of these times. Over this time lag, the voltage in the cavity will increase past the breakdown voltage by an amount (ΔV) with the PD occurring at a voltage greater than the minimum ($V_i = V_{min} + \Delta V$). After ignition, the discharge will extinguish due to change build-up on the void surface and the voltage in the cavity will fall to a residual voltage (V_R), with PD reoccurrence being possible once the cavity voltage exceeds the breakdown voltage again, with the time this takes being termed the recovery time (t_R). Figure 6 shows this process schematically (where V_{max} is the voltage that would exist across the cavity if no discharge were ever to occur).

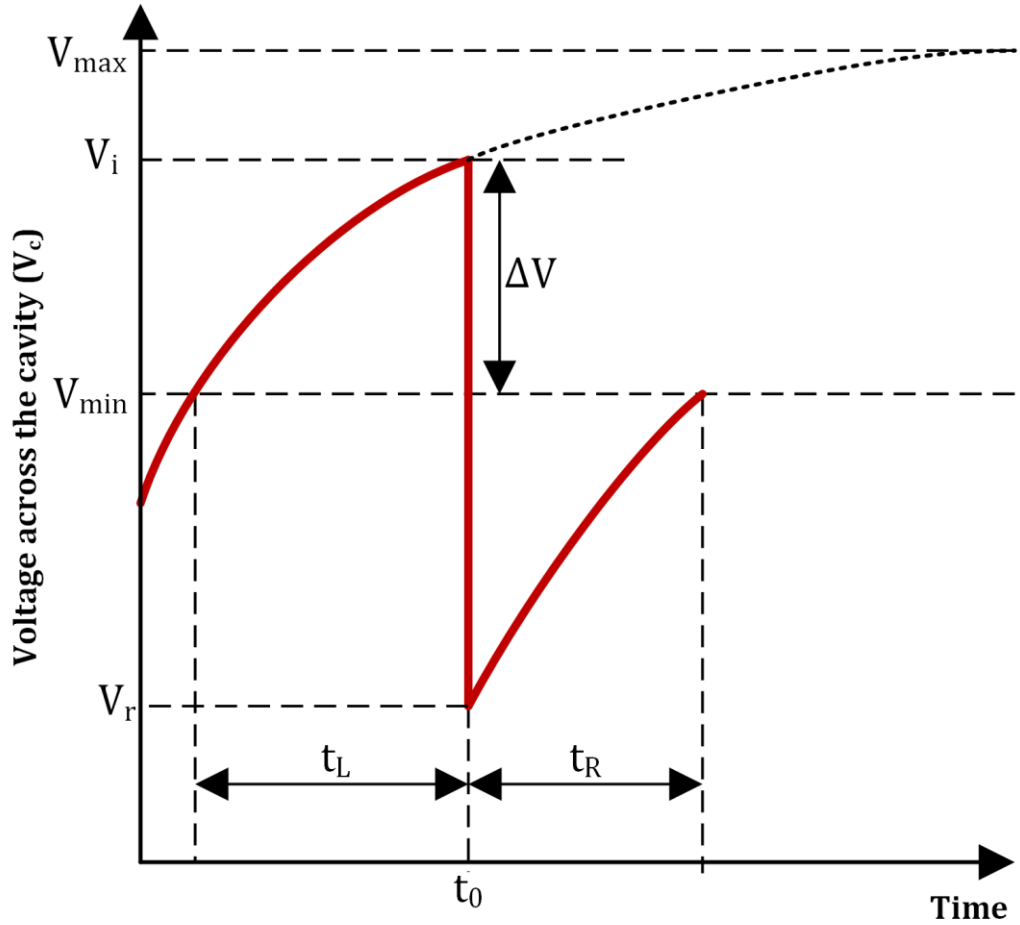

Figure 6 – Development of voltage across a cavity during PD events (based on [67]*).*

2.1.1.1. *Townsend and Streamer Discharge*

The degree to which the voltage in the cavity exceeds the breakdown voltage (ΔV) before the free electron initiates the breakdown (after time t_L) has an impact on the nature of the breakdown itself. If t_L is short, and thus V_i is close to V_{min} then

the breakdown will be 'Townsend-like'. For longer values of t_L and thus higher values of ΔV, the probability that the discharge will be 'streamer-like' increases[68].

In a Townsend discharge (illustrated in Figure 7), the ionisation process involves the free electrons being accelerated by the electric field, colliding with gas molecules, which creates further electrons, which collide with further gas molecules, and so on, creating an avalanche through which electrical conduction is possible[69].

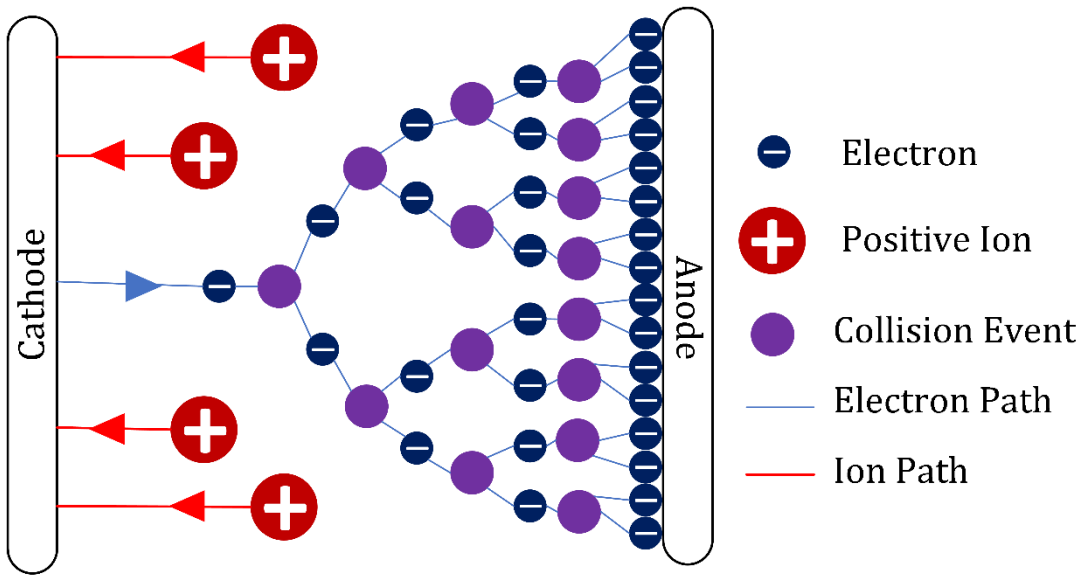

Figure 7 – Illustration of Townsend avalanche (based on [69]*).*

For steamer discharge (illustrated in Figure 8), the avalanche creates positive space charge, as the accelerated electrons resultant from the ionisation leave behind slower moving positive ions. This forms a space charge first near the anode, and then rapidly across the gap (as the avalanche travels towards the anode), which, upon reaching the anode forms a conducting channel[68].

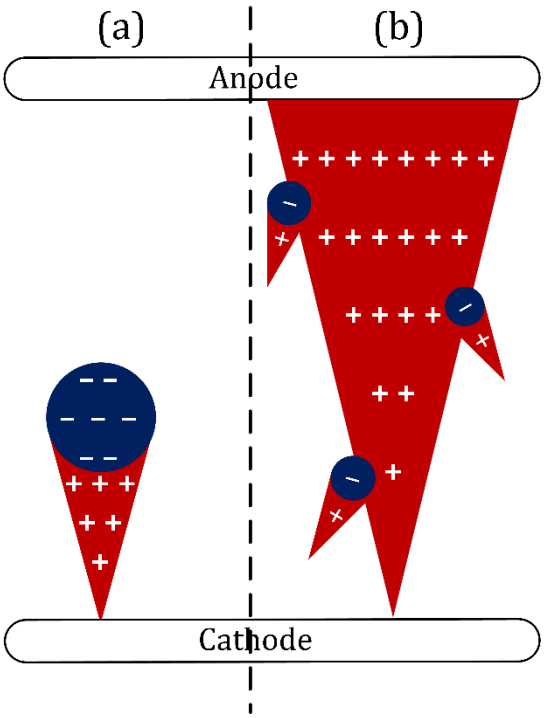

Figure 8 – Illustration of the development of streamer discharge (based on [70]*).*
Showing (a) the development of the initial avalanche and the resultant positive space charge(b) the creation of the positive space charge channel (streamer)and development of secondary avalanches.

The mechanisms for PD in a void-type defect is the same under both AC and DC stresses, although values for ΔV (and thus overall pulse magnitude) in DC tend to be smaller. Another significant variation, however, is the mechanism by which PD pulses recur, as explained below.

2.3.1.1. Recurrence of PD Under AC Conditions

The cavities or voids in which partial discharges occur can be modelling using the three-capacitance or 'abc' model, where the void, the insulating material in series with the void, and the rest of the insulating material are represented by capacitances c, b, and a, respectively. A representation of a void type defect is shown in Figure 9 with the equivalent circuit of this schematic shown in Figure 10.

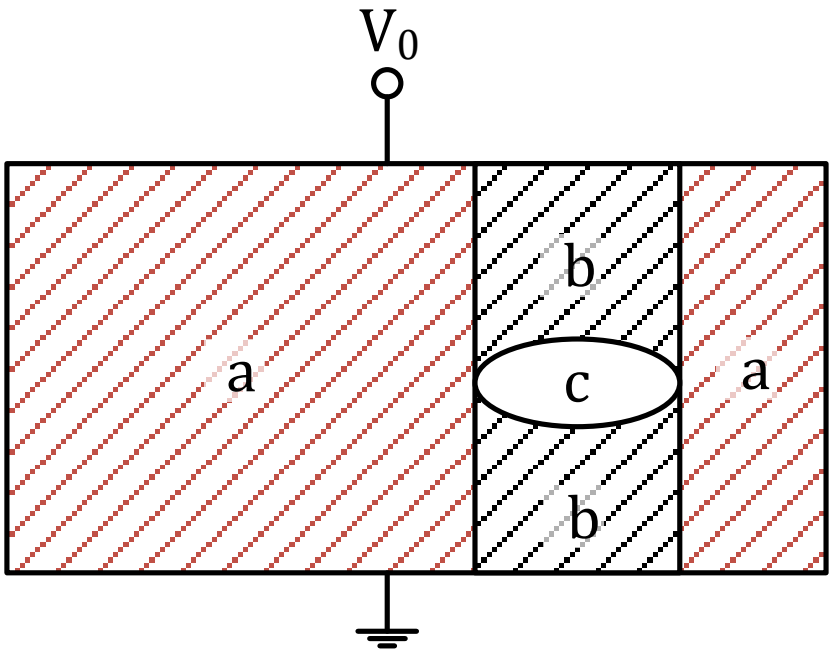

Figure 9 – Schematic of void type defect showing: (c) the gas- or oil-filled cavity, (b) the insulating material in series with the void, and (a) the rest of the insulating material based on [71].

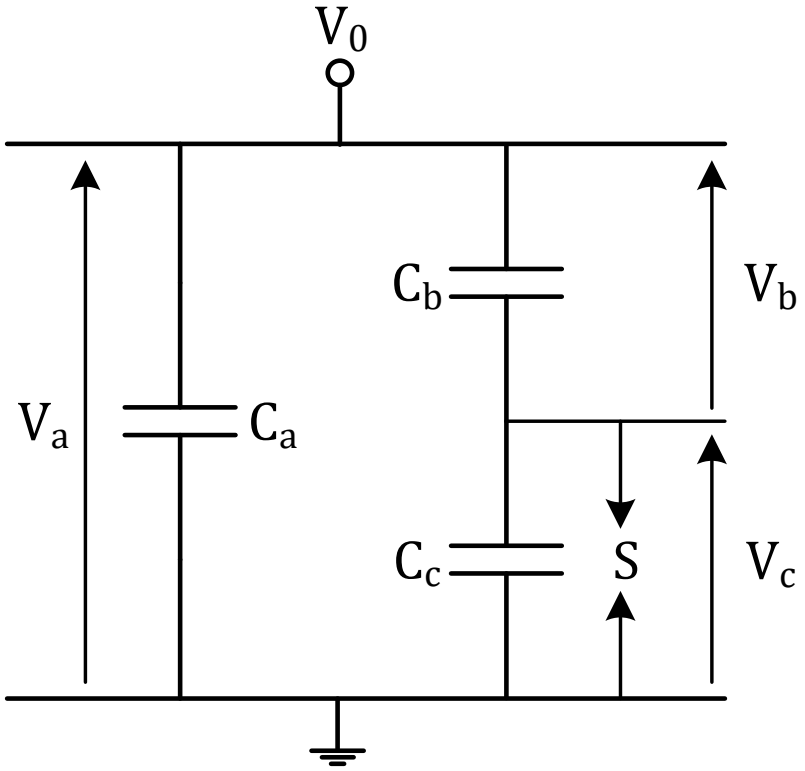

Figure 10 – Equivalent circuit of the three-capacitance model showing: (C_c) the equivalent capacitance of the cavity, (C_b) the equivalent capacitance of the insulating material in series with the void, and (C_a) the equivalent capacitance the rest of the insulating material, based on [1].

When the applied voltage (V_0) leads to a voltage across the void (V_c) of greater than the breakdown voltage, then partial discharge can occur (i.e. V_0 is equal to or greater than the PDIV), at which point the field in the void falls to its residual value, before beginning to rise again (as shown in Figure 6). From this it follows that under an AC voltage, the PD can reoccur in each AC cycle around both the positive and negative peak (giving an average recurrence of once every 10 ms under 50 Hz AC). This recurrence is not generally exactly at these peaks, for several reason, first the time taken to reach the breakdown strength within the void is often lower than that generated by the maximum peak, second the residual value of the field within the void can vary. In practice this means that, in void type defects, PD pulses will tend to occur in the first and third quadrants of the AC waveform, that is, leading the positive and negative peaks[1].

2.3.1.2. Recurrence of PD Under DC Conditions

Under DC conditions the equivalent circuit for three-capacitance model must be extended to be of use. As the voltage applied is constant, the model would reach a steady-state upon which activity would cease. However, in reality there is dissipation of the built-up charge into the dielectric (which has finite resistivity), which can be modelled using resistors giving the circuit as shown in Figure 11.

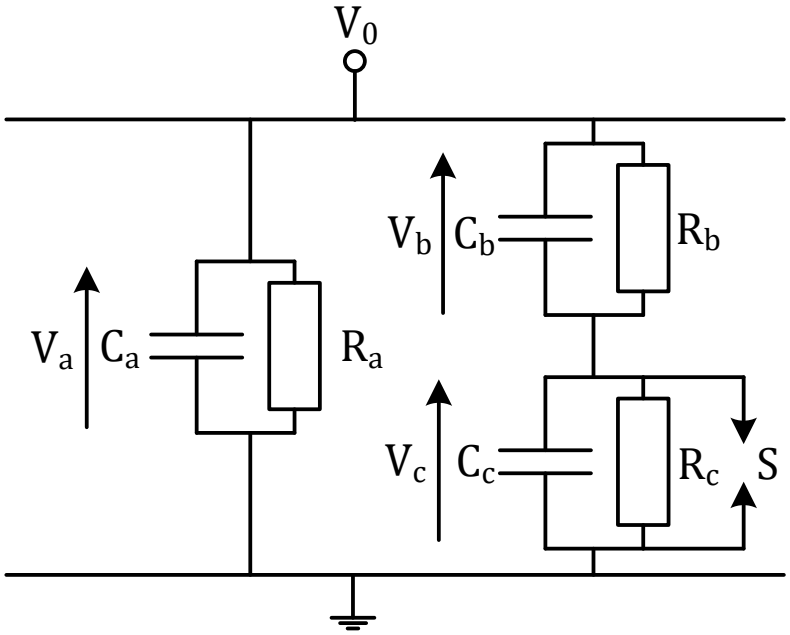

Figure 11 – Equivalent circuit of the three-capacitance model modified for DC conditions based on [67].

This charge dissipation is what allows for PD recurrence under DC conditions. If the PD processes are considered as represented by a spark gap (S in Figure 11), the time constant for charging the void can be given by:

$$\tau = \left(\frac{R_b R_c (C_b + C_c)}{R_b + R_c}\right) \tag{1.1}$$

To determine the frequency of recurrence of PD, n, consider the following:

$$n = \frac{1}{\Delta t} = \frac{1}{t_R + t_L} \tag{1.2}$$

Where n is the PD repetition rate, and Δt is the time interval given by the sum of the recovery time (t_R), which is the time taken for the field in the void to reach breakdown strength, and the time lag (t_L), which is the time taken for the appearance of the free electron.

The maximum rate of repetition therefore occurs when the time lag is close to zero, giving:

$$\Delta t = t_R = -\tau \times ln\left(\frac{V_{max} - V_{min}}{V_{max} - V_r}\right) \tag{1.3}$$

Where V_{max} is the maximum voltage that would exist across the void if a discharge were never to occur, V_{min} is the breakdown voltage, and V_r is the residual voltage across the void after a discharge). Assuming that V_{max} is significantly greater than V_r gives us the approximation:

$$\Delta t \approx \tau \times \left(\frac{V_{min} - V_r}{V_{max}}\right) \tag{1.4}$$

Giving a final approximation for the repetition rate as:

$$n \approx \frac{1}{\tau} \times \left(\frac{V_{max}}{V_{min} - V_r}\right) \tag{1.5}$$

Meaning that the repetition rate increases proportionally to the maximum potential across the void, which is proportional itself to the applied voltage, while

being inversely proportional to the minimum voltage for PD to occur, and the residual voltage after PD[72].

In practice, this means that determination of the PDIV for DC is more complicated than that for AC, as the repetition rate at V_{min} is nearly zero for DC[73], while it has an average value of once every 10 ms for AC. For this reason, the PDIV at DC is defined as the applied voltage at which one PD event occurs per minute[46]. This means charge dynamics under AC and DC are different, resulting in that PDIVs under DC are higher, while repetition rates, and peak pulse amplitudes are much lower[74]. PDIV is influenced by void size and shape[51], and the gas composition and pressure[75], amongst other factors.

2.3.1.3. Influence of Multiple Voids

Several studies have been performed to determine the influence of multiple voids on PD under AC conditions. Characteristics investigated have included: electric fields within voids[76], PD inception voltages[59], [77], pulse shapes[78], degradation of insulation [79]. Studies have achieved this through practical investigation as well as modelling [10], [80].

Key findings from the research so far consider that, under AC conditions, a serial arrangement of voids , i.e. one above the other in relation to the electrodes, tends to reduce the electric field strength in the voids[78], [81], while parallel voids, i.e. side-by-side in relation to the electrodes, tend to either have similar or greater field strengths to single voids. This means that parallel voids would be expected to have a lower PDIV (since the field strength in the parallel voids are higher for the same applied external voltage compared to a single void), while serial voids would be expected to have a higher PDIV when compared to single voids (since the field strength in the serial voids are lower for the same applied external voltage compared to a single void) . Other findings show that void separation is important, with void PD activity becoming more independent the greater the distance between the voids[82].

The impact of insulation material on the characteristics of PD under AC conditions when multiple voids are present has not been closely examined.

Different studies have been performed on polyethylene terephthalate (PET)[83], epoxy resin[84], and LDPE[59], [85], but no studies to date comparing different materials with multiple voids.

Additionally, the influence of multiple voids on DC partial discharge activity is also not so well explored, with one study using acrylonitrile butadiene styrene (ABS) samples containing a range of void configurations constructed using 3D printing[85]. No studies to date consider multiple voids in LDPE or polypropylene under DC conditions. These gaps in knowledge provide some of the motivation for the work in this thesis, since, as discussed above, the most common materials for HV cable insulation are polyethylene (in the form of XLPE) and polypropylene (in the form of PPLP), so PD activity in these materials is of particular industrial relevance.

2.3.2. Other Categories

Other categories of PD exist, apart from void type.

The previously mentioned Lichtenberg figures are an example of surface discharge, where a high electric field is applied parallel to an insulating surface. These types of discharges are common at the ends of cables where there are areas of high field strength.

Corona discharges occur within a localised region near a sharp or point on an electrode where a region of high electric stress can occur, which leads to the breakdown of surrounding gas. This type of discharge is a common problem in transmission lines[7], [72], [86], [87].

This thesis is focused on internal discharges in cables, so analyses of other categories of discharge are not included.

2.4. Measurement of Partial Discharge in Cables

There are many features of partial discharge phenomena that are can be used in their detection. PD pulses produce, to varying degrees: sound; light, current and voltage pulses; chemical by-products; and degradation of insulation[1], [48], [65], [88].

For the scope of this thesis, only electrical detection will be considered in detail, with other methods being summarised briefly.

2.4.1. Measurement Methods

2.4.1.1. *Electrical Detection*

Electrical detection of PD functions by measuring the current or voltage pulse resultant from a PD event. The exact properties of this signal are not fully understood, particularly at DC voltages. However, electrical detection of PD is governed by a set of standards, IEC 60270 'High-voltage test techniques – Partial discharge measurements'[46], the most recent version of which is (IEC 60270:2000/AMD1:2015). This standard applies to measurements of PD in electrical plant under AC (up to 400 Hz) or DC, and defines: common terms, quantities to be measured, measurement circuit specifications, recommended test procedures and measurement methods and advice on background electrical noise reduction.

From IEC 60270 the following definitions are of particular relevance:

Partial Discharge – '[a] localised electrical discharge that only partially bridges the insulation between conductors'

PD pulse – '[the] current or voltage pulse that results from a PD occurring within the object under test'

The 'object under test' can be simple, such as a sample of dielectric material, or complex, such as a piece of large HV plant.

Apparent charge (q) – 'that charge which, if injected within a very short time between the terminals of the test object in a specified test circuit, would give the same reading on the measuring instrument as the PD current pulse itself.' q is expressed in picocoulombs.

Apparent charge, therefore, is distinct from the charge of the pulse itself, which cannot be practically measured. The apparent charge of a pulse is also termed the pulse magnitude.

Pulse Repetition Rate (n) – '[the] ratio between the total number of PD pulses recorded in a selected time interval and the duration of this time interval'

Phase Angle (ϕ) and time of occurrence (t) – From:

$$\Phi_i = 360 \times \left(\frac{t_i}{T}\right) \tag{1.6}$$

'where t_i is the time measured between the preceding positive-going transition of the test voltage through zero, and the PD pulse, and T is the period of the test voltage.'

Φ is expressed in degrees, and is only applicable to measurements under AC.

PD pulse count (m) – '[the] total number of PD pulses which exceed a specified threshold level within a specified time interval Δt'

PD pattern – '[a] display of the apparent charge q versus the phase angle Φ of the PD pulses recorded during a specified time interval Δt'

For AC PD pulses can be displayed on a phase resolved-partial discharge (PRPD) plot which plots the number of PD pulses of a defined charge range against phase angle range.

The test circuit specifications and test procedure recommendations from IEC 60270, and how these inform the methodology of this thesis, are discussed in more detail in Chapter 3.

2.4.1.2. *Measurement under DC conditions*

IEC 60270 also provides specific recommendations for the evaluation of PD test results under DC conditions, with the recommendation that the apparent charge and the time of occurrence of the pulse (i.e. the time the object under test has been held at a constant DC voltage when the PD pulse occurs) be recorded. The recommendation is also made to ensure the time between successive pulses is easily determined.

2.4.1.3. *Measurement of Individual Pulse Characteristics*

As well as the above metrics, the characteristics of individual PD pulses can be recorded and subjected to analysis, an example of these characteristics is shown in Figure 12.

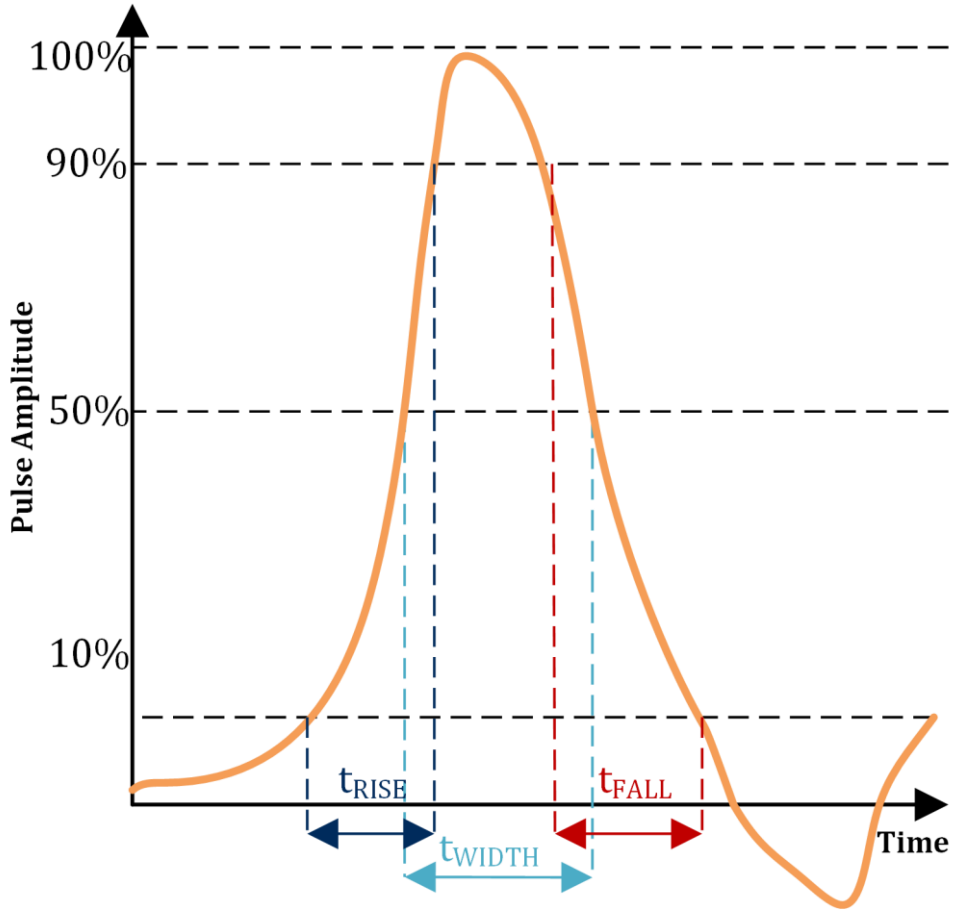

Figure 12 – Schematic of pulse indicating definitions of rise-time, pulse width, and, fall-time based on [89].

Rise-time – (t_{RISE}), the time taken for the PD pulse to reach 90% of peak value from 10%.

Pulse width – (t_{WIDTH}) the time between the pulse reaching 50% of the peak value on the rising edge to 50% on the falling edge.

Fall time – (t_{FALL}) the time taken for the pulse to fall from 90% of the peak value down to 10%.

Amplitude –the highest value reached by the pulse.

Individual characteristics can be analysed by examination of the standard deviation, skewness and kurtosis of the collected data sets of a number of PD pulses for each attribute, which can help express the probability of PD pulses having given characteristics under certain conditions.

Standard deviation is an expression of the amount by which members of a set differ from the mean value of that set. Standard deviation is calculated from:

$$\sigma = \sqrt[2]{\frac{1}{N}\sum_{i=1}^{N}(x_i - \mu)^2} \tag{1.7}$$

Skewness is a measure of the symmetry of the statistical distribution of the members of a data set around the mean of the set. A purely symmetrical data set (such as a normal distribution) has a skewness value of 0. A data set which is asymmetric with a bias above the mean (or to the right diagrammatically) has a positive skew value, while one with an asymmetrically bias below the mean (to the left) has a negative skew. Skewness is calculated from:

$$Skew = \frac{\frac{1}{N}\sum_{i=1}^{N}(x_i - \bar{x})^3}{\left(\sqrt[2]{\frac{1}{N}\sum_{i=1}^{n}(x_i - \bar{x})^2}\right)^3} \tag{1.8}$$

Kurtosis is a measure of the prominence of the outliers (or 'tails) of a data set, compared to the 'body' of the distribution. A normal distribution has a kurtosis value of 3. A set with a value less than 3 is termed 'platykurtic', suggesting a less pronounced peak, while a set with a value greater than 3 is 'leptokurtic' suggesting a sharper peak. Kurtosis is defined as:

$$Kurt = \frac{\frac{1}{N}\sum_{i=1}^{N}(x_i - \bar{x})^4}{\left(\frac{1}{N}\sum_{i=1}^{n}(x_i - \bar{x})^2\right)^2} \tag{1.9}$$

Normalised kurtosis is found by subtracting 3 from the calculated kurtosis values. This gives normal distributions a normalised kurtosis value of 0, platykurtic distributions a negative normalised kurtosis value, and leptokurtic distributions

a positive normalised kurtosis value. Where a kurtosis value is given in this thesis it is a normalised value.

2.4.1.4. *Other Methods*

Other methods of PD detection can include acoustic detection, visual/optical detection, chemical detection, and radio frequency (RF) detection (including at ultra-high frequencies (UHF)).

The earliest forms of PD monitoring were acoustic and radio frequency. Early acoustic detection was undertaken manually, with operators using a stethoscope-like tool to find the location of PD[28]. Modern acoustic detection is performed with microphones, with some success in detection of parameters such as apparent charge, repetition rate, and pulse pattern[90]. Early radio frequency detection involved portable radios, with more advanced antenna detection following, and UHF techniques representing the state of the art of this technique[91], [92].

Under certain circumstances, PD can be visible either to the naked eye, or to cameras (including ultra-violet cameras). Generally, these are PD of the corona type, as void-type discharges are contained within solid insulation[7], [93].

Finally, the chemical by-products of the PD breakdown can also be monitored. In oil-filled transformers, this would take the form of dissolved gas analysis, with similar methods possible in gas-insulated substations. Chemical analysis of defective solid insulation can also provide information about the nature of the defect and level of degradation[57], [81].

These methods are not considered for this thesis, as they have limited applicability to in-service cable monitoring.

2.4.1.5. *State of the art*

Significant research effort has been deployed in investigating PD phenomenon characteristics. The effect of transient voltages under AC conditions[94], [95], as well as AC ripple[83], [87], [96] on DC voltages has been explored. The impact of space charge (particularly under DC conditions)[97]–[103] and external

magnetic fields[104] have been investigated. Another area of research has aimed at determining how defects in insultation develop over time[61], [105], and the subsequent changes to PD patterns, e.g. the impact of the increasing void size[106], [107].

2.4.2. Representing and Analysing PD Data

2.4.2.1. *AC Data*

As discussed above, the IEC 60270 standard suggests that AC data be presented in the form of a PRPD plot[87], [93], [108], [109]. For these to be generated, the apparent charge of the PD current pulse, and the phase reference of the input AC waveform must be captured. These can then be plotted, with the resultant pattern suitable for analysis, as different defect types produce different PRPD patterns[110]–[113].

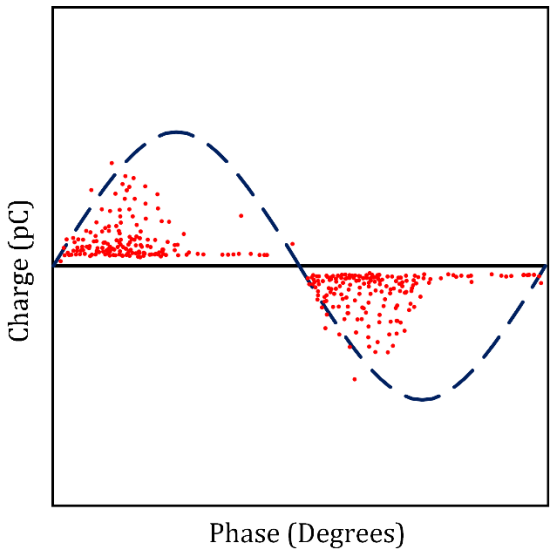

Figure 13 – Example of a typical PRPD plot showing PD in a void defect (based on [27]*)*

Another method of analysing AC PD data, also as recommended by IEC 60270, is the use of pulse sequence analysis (PSA)[46], [99], [114]. PSA considers various metrics relating to the relationship between a series of PD pulses, for example the time between PD pulses occurring, or the magnitude of the apparent charge of a PD pulse compared to its successor or predecessor[114], [115]. This data can be represented in many ways, including histograms of the measured parameters

discussed above, or scatter plots comparing multiple parameters[99], [108], [116].

Both PRPD plots and PSA are considered in this thesis for the collected data.

2.4.2.2. *DC Data*

IEC 60270 also makes suggestions for the collecting and representing of PD data under DC conditions. It recommends that measurements should be focused on recording: the apparent charge of each individual PD pulse, the cumulative charge over the test period, the number of pulses collected over the test period, and the pulse count falling into specified ranges of apparent charge[46].

Recommendations are also made for representing this data, as shown in Figure 14. These include plots of: (top left) the apparent charge of individual pulses against the measuring time, (top right) the cumulative charge from the individual pulses over the measuring time, (bottom left) histograms showing the number of PD pulse apparent charge magnitudes that exceed a specified threshold, and (bottom right) the number of pulses with apparent charge magnitudes that fall within a specified range.

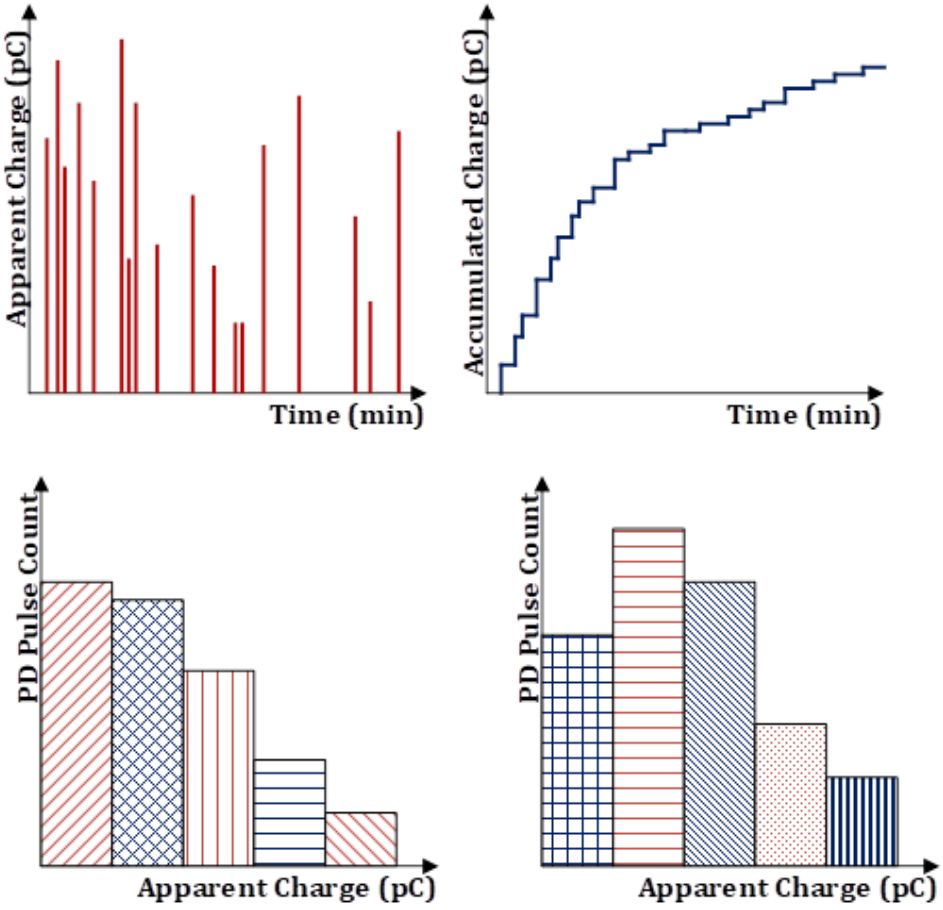

Figure 14 – IEC 60270 recommendations for displaying DC PD data (from [46]*).*

These recommended methods of displaying PD data captured under DC conditions are, amongst others, used in this thesis.

2.4.3. Denoising

As PD detection often occurs in the field, or in environments where significant electrical background noise is present, it is often necessary to extract PD signals from noisy signals by the use of denoising techniques[98], [117]–[119]. The most common of these are adaptive filter and wavelet-based techniques[24]. For adaptive filter techniques knowledge of the frequency spectrum of the PD signal and of the noise is used to design filters to reduce the strength of the noise signal while leaving the PD signal strength largely the same[120].

Wavelet-based techniques use a wavelet transform, a signal processing technique that maps a signal in the time-frequency domain. Wavelet transforms involve multiple stages of convolving signals with high- and low-pass filters, the results

of which are then used for the next stage of the transform. This iterative process continues until a set scale is reached. Wavelet denoising functions on the basis that signals tend to be concentrated while noise tends to be spread across a frequency spectrum, this allows for the application of correlation-based wavelet selection, or energy-based wavelet selection.

2.4.3.1. *State of the art*

In recent years, alternative wavelet selection techniques have been proposed, including entropy-based wavelet selection. This technique uses wavelet entropy to measure the randomness of wavelet coefficients (the lower the entropy the lower the randomness). As noise tends to be random, while signals are more consistent, this method can successfully remove noise from PD signals[24].

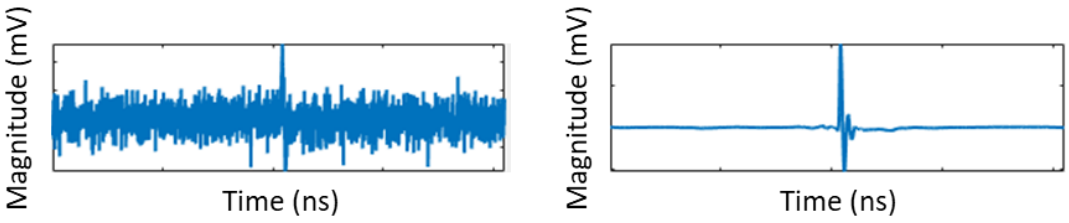

Figure 15 – Example of signal denoising showing: noisy signal (left) and denoised signal (right) (from [24]*).*

Although denoising itself is not considered in this thesis (as measurements were taken in a low-noise environment), the analysis and data collected is of use in the design of denoising algorithms[24].

2.4.4. Locating Defects

Defects in cables can be located either through off-line measurement (when the cable is de-energised from service)[121], or on-line measurement (when the PD is measured in a cable in operation)[91]. Techniques for measuring PD and defect location can vary depending on the operational status of the cable.

2.4.4.1. *Off-line Testing*

Off-line PD testing is performed on a cable that is de-energised and decoupled from the power grid. This can be done either in a laboratory or in the field. For off-line PD testing, a measurement circuit and an external power supply are required, the specifics of which can be variable.

Off-line measurements can be taken with either capacitive or inductive sensors. Capacitive sensors consist of a band-pass filter created in accordance with IEC 60270. This is done through the use of a coupling capacitor and a measuring impedance[122]–[124]. The Lemke Diagnostics LDS-6 used in the collection of data for this thesis is an example of a system which uses this detection method.

Inductive sensors are usually in the form of high frequency current transformers (HFCTs), which are placed around the cable earthing. This has the advantage of being galvanically isolated from the object under test (reducing, though not eliminating, the risk of damage to the measurement equipment during testing), but has the disadvantage of having lower sensitivity[125]–[128]. The LeCroy Waverunner 104Xi and HFCT set-up used in the collection of data for this thesis is an example of a system using this detection method.

Further description of the use and operation of these sensors is described in Chapter 3.

The main methods of determining the location of PD defects during off-line testing are time domain reflectometry (TDR) and double-sided measurements[129].

TDR involves connecting the measurement system to one end of the cable, and leaving the other end open[130]. This results in two signals being detected, the signal from the defect which travelled in the direction of the detector, and the reflected pulse resultant from the signal travelling towards the other end of the cable, reflected due to the other end being open. Using the difference in arrival times of the two signals, the location of the defect can be found[131]. Over longer distance cables, the attenuation (loss of signal strength due to the impedance of the cable) can be such that signals are hard to detect, requiring the use of more advanced denoising[132].

Double-sided measurements use a similar technique, only pulses are measured at both ends of the cable directly (not after reflection)[117], [129], [133]. The difference in arrival times is then used to estimate the location of the defect. This method has the disadvantage that the two measurement systems at each end of

the cable must be very well synchronised, as any difference in time base will result in an inaccurate estimation of fault location[122]. The advantage of double-sided measurements are the pulses have less distance to travel (as the second measurement is not of a pulse which has travelled the length of the cable before detection), so the attenuation of the signals is less.

TDR or double-sided measurements were not taken in the collection of data for this thesis, however the analysis presented may be of use for denoising the signals that could be detected by these methods.

2.4.4.2. *On-line Testing*

On-line testing is performed on cables that are in-service. Although measurements are done on active cables, in practice measurement systems are often installed while the cable is de-energised. However, the time required for installation is much shorter than for off-line testing, and equipment can be left in place to measure PD over long periods of time[123]. The fact that equipment can be left in place for long periods while the cable is in operation allows for continuous measurement of PD, as well as the identification of trends and degradation of cable integrity[134].

Measurement of PD during cable operation can also be done using either TDR or double-sided measurements, however the methods for doing so can be different when the cable is in service[130].

For on-line TDR, the same method for determining defect location is used, however a transponder is often placed at the other end of the cable from the measurement system. This transponder can inject a large pulse into the cable when the signal from the PD is detected, this is measured at the other end by the measurement system in place of the reflected pulse[135]. This is done as significantly more noise can be expected from an active cable or in an active substation than in a laboratory or de-energised substation[123].

This additional electrical noise also presents a problem for double-sided measurements. Therefore, post-processing is vital for on-line measurements of

PD using this method to distinguish PD pulse from background noise. Algorithms for achieving this are discussed above.

2.4.5. Impact on Cable Health

Partial discharges occurring in voids within cable insulation have been known to have a detrimental effect on cable health (beyond the presence of the void itself) since the 1960s[48]. This degradation of the insulation was found to be from two related properties, chemical degradation from the heat of the discharge, and further damage from the bombardment of particles generated by the discharge[63], [136]. This degradation leads to a roughened cavity surface, which enhances the field and localises the PDs. This eventually forms a path through the insulation from the conductor to earth causing the cable to fail.

2.5. Modelling of Partial Discharge

Partial discharge modelling can be used to: better inform understanding of PD behaviour under different conditions, understand the impact of different factors on the development of PD, and to inform insulation design.

For void-type defects, there are three models which are frequency used for these purposes – the three-capacitance model, the induced charge concept model, and finite element analysis (FEA) modelling[137].

While PD modelling was outside the scope of this thesis, as discussed above, insights into the behaviour of PD have come from these models.

2.5.1. Three-Capacitance Model

The three-capacitance model has been discussed above in section 2.3.1. This model was first proposed in 1951[138], and, as discussed, has been used to understand inception and recurrence of PD under both AC and DC conditions. The three-capacitance model cannot be used to model a single PD event however, as no consideration of charge accumulation is made using this technique[137].

2.5.2. Induced Charge Concept Model

Another analytical-based methodology, based on consideration of the charge distribution on the surface of the cavity, is the induced charge concept

model[139]–[141]. An electric dipole configuration (Figure 16) is formed from an estimation of the surface charges deposited on the void surface from the discharges, inducing charge on the electrode.

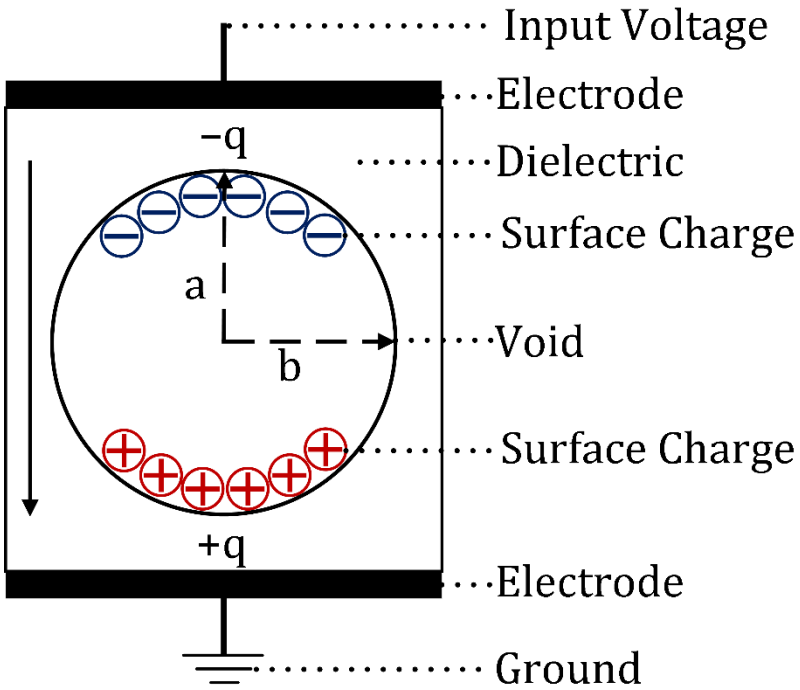

Figure 16 – Electric dipole configuration from induced charge concept model.

In Figure 16, a and b, are the dimensions of the void, parallel and perpendicular to the field lines, respectively. E_0 is the electric field strength, σ is the charge density on the cavity surface, and q is the induced or deposited charge from the partial discharges.

The overall polarity of the dipole (dipole moment, μ) can be calculated from:

$$\vec{\mu} = \int_S \vec{r}\sigma \, dS \tag{1.10}$$

Where r is the surface element (dS) radius vector.

While the induced charge, or the charge on the surface of the void, is calculated from:

$$q = -\vec{\mu} \cdot \vec{\nabla}\lambda \tag{1.11}$$

Where λ is a scalar function dependent on dS (a fuller definition of λ can be found in [141]).

With consideration of the applied voltage (V) and charge (Q) on the electrode, and that while the voltage drops by an amount (ΔV) after a PD, the charge on the electrode will increase from charge supplied by the external circuit (ΔQ) gives:

$$q \approx C\Delta V + \Delta Q \approx C\Delta V \tag{1.12}$$

Where C is the capacitance of the insulation, and ΔQ is negligible if the circuit impedance is large.

From this model, the electric field across the void can be calculated from:

$$E_{cav} = f_c E_0 + E_S \tag{1.13}$$

Where f_c is the field enhancement factor (from the void shape), and E_S is the field resultant from the partial discharge charges accumulating on the cavity surface. The field enhancement factor can be calculated from:

$$f_c = \frac{K\varepsilon_r}{1 + (K-1)\varepsilon_r} \tag{1.14}$$

Where K is a constant dependent on the ratio of *a* and *b.*

The induced charge concept model can be used to estimate the behaviour of PD in spherical, ellipsoidal and cylindrical voids, with a low simulation time. The assumption of a uniform electric field through the void, which is required for the model, may impact the model's accuracy, with this being more likely the larger the dimensions of the void[142].

2.5.3. Finite Element Analysis Model

Finite element analysis can also be used to model discharges in a cavity within a dielectric material. For FEA models, the electric field is determined numerically, which allows for non-uniform electric fields to be modelled, and the characteristics of the void pre-discharge can be defined. The simulation time for FEA modelling of PD can be very significant. PD events can be modelled using either an electric current FEA model[110], [143], [144], or an electrostatic FEA

model[145]. Electric current models can estimate the PD pulse current in real time, allowing for estimation of real and apparent charge, with an assumption that the PD affects the whole void evenly. An electrostatic model, in contrast, can model the distribution of charges on the cavity surface, although this does not estimate the real and apparent charge of the pulse, the charge magnitude can be calculated from the charge distribution[142].

3. Methodology

This chapter concerns the methodology for the creation of the test samples, and the test procedures themselves, including a description of the measurement equipment used, and its function.

3.1. Equipment

3.1.1. Laboratory

All measurements were taken in the David J Tedford High Voltage Technologies Laboratory, located at the University of Strathclyde. The laboratory is electrically shielded to form a Faraday cage, thus minimising the potential for external noise sources to interfere with data collection. The laboratory is also equipped with under-floor heating, which maintains the temperature in the lab within a consistent range, which was measured as between 20.4-21.6°C while the tests were performed.

3.1.2. Lemke Diagnostics LDS-6

Figure 17 – The Lemke Diagnostics LDS-6

The LDS-6 is a partial discharge measurement system designed by Lemke Diagnostics (now Doble Engineering Company). The LDS-6 has a measurement range of 1 pC to 100,000 pC, with the measurement range set during a calibration process. It consists of an adjustable wide band (100-500 kHz) preamplifier followed by an active integrator, which converts a voltage signal into an instantaneous sum of the pulse charge. This is captured, in real-time,

simultaneously with the input voltage (phase position) and event-time. The LDS-6 has a range of features allowing for the analysis of PD data, as well as diagnostic functions. Most significant of these is the ability to store phase-resolved PD data for external analysis at a phase resolution of 0.1°. These can be output as a TXT file (ASCII) which can be imported into MATLAB.

3.1.3. LDIC LDC-5 Calibrator

Figure 18 – The LDIC LDC-5 Calibrator

The LDC-5 generates pulses of set total charge, which can be used to calibrate the LDS-6, as well as other equipment. It can generate pulses of either 5 pC, 20 pC, 100 pC, or 500 pC.

3.1.4. LeCroy Waverunner 104Xi Oscilloscope

Figure 19 – The LeCroy Waverunner 104Xi Oscilloscope

The Waverunner 104Xi is a 4-channel oscilloscope with a maximum sample rate of 5 GS/s, and a bandwidth of 1 GHz. It has several modes of data acquisition, with the sequence method used here, this allowed for a set number of either PD pulses or AC cycles to be captured. Data can be output as separate CSV files for each monitoring channel, which can be used for external analysis. When compared to

the LDS-6, the 104Xi is less sensitive, but captures more information about each PD pulse.

3.1.5. AC Test Circuit

The AC test circuit, which is shown in Figure 20 is compliant with the IEC 60270 standard.

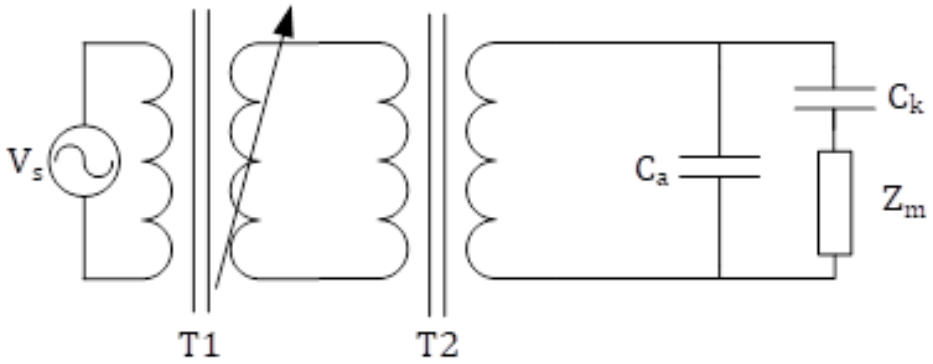

Figure 20 – Circuit for tests performed under AC stress, where: V_s is the voltage supply (230 V), T1 is the regulating transformer, T2 is the HV transformer, C_k is the coupling capacitor, C_a is the object under test, and Z_m is the measuring impedance.

3.1.5.1. *Regulating Transformer (Lemke)*

The first part of the AC test circuit, the regulating transformer (T1 in Figure 20 and Figure 21, which relates to the DC tests), provides a variable voltage input (0-380 V) to the HV transformer producing a voltage output of 0-10 kV. This voltage is varied by a three-phase motor, which controls the transformer tap position. This motor can be controlled by the LDS-6. The regulating transformer also provides a phase-reference for data acquisition performed through the LDS-6, with the phase shift established during the calibration process.

3.1.5.2. *Autotransformer (RS Components)*

If the regulating transformer is not in use, an autotransformer (also T1 in Figure 20 and Figure 21) is used to vary the voltage supplied to the HV transformer. While this has the disadvantage of lacking feedback to any control system, it does allow for more granular change than is possible with the regulating transformer. The autotransformer used allows for a variable output from 0-270V (giving a max output from the HV transformer of 71 kV, rather than 100 kV), and has a rating of 480 VA.

3.1.5.1. *HV Transformer (Lemke)*

The HV transformer (T2 in Figure 20 and Figure 21) is used to step the voltage up, with a ratio of 1:263, giving a maximum output of 100 kV with an input voltage of 380 V. The transformer has a continuous rating of 10 kVA, with a 10-hour rating of 20 kVA.

3.1.5.2. *Coupling Capacitor (Lemke)*

The HV transformer is connected to the object under test via a HV coupling capacitor (C_k in Figure 20 and Figure 21) with a capacitance of 1 nF (± 0.01 nF), rated at 100 kV AC.

3.1.5.3. *Measuring Impedance LDM 5/U (Lemke)*

The interface between the LDS-6 and the AC circuit is the LDM 5/U measuring impedance (Z_m in Figure 20 and Figure 21). The measuring impedance is connected in series with the coupling capacitor, and provides outputs to the LDS-6, or other measurement equipment, indicating the peak applied voltage, and peak apparent charge. The output channels are connected through coaxial output jacks, each with an output impedance of 1 kΩ.

3.1.5.4. *HVPD 100/50ALU HFCT*

An alternative to the LDM 5/U measuring impedance is the use of a high frequency current transformer (HFCT in Figure 21, the DC test circuit. In the AC circuit, Figure 20, this would take the place of Z_m) connected around the coupling of the test object to ground. The HFCT used from HVPD, had a transfer impedance of 4.3 mV/mA, a -3db frequency response of 100 Hz-25 MHz, suitable for PD measurement[146], and a rating of 350 A at 50 Hz.

3.1.6. DC Test Circuit

The DC test circuit (Figure 21) consisted of the AC test circuit components described above, as well as additional components to form a rectifier to produce a DC voltage.

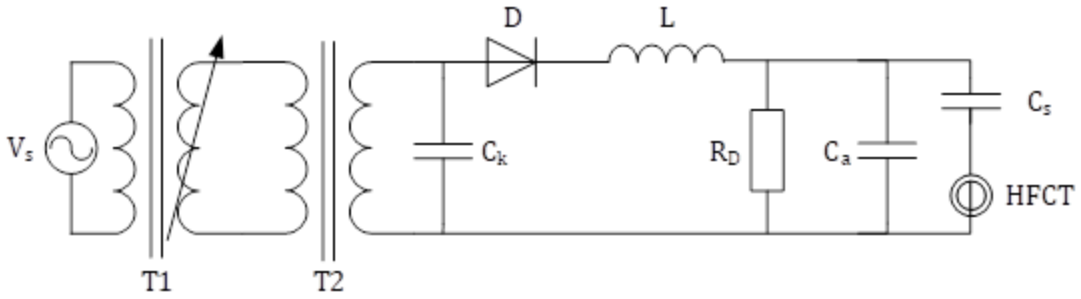

Figure 21 – Circuit for tests performed under DC stress, where: V_s is the voltage supply (230 V), T1 is the regulating transformer, T2 is the HV transformer, C_k is the coupling capacitor, D is the diode, L is the blocking impedance, R_D is the resistive divider, C_a is the object under test, C_S is the smoothing capacitor, and the HCFT is labelled as such.

3.1.6.1. *G 270 HV Rectifier (HighVolt)*

The diode rectifier (D in Figure 21) acts as a simple AC-DC converter (half-wave rectifier) and consists of a diode and a casing. The casing allows the diode to be turned around easily, allowing for voltage polarity reversal. The diode had a reverse voltage rating of 270 kV, and a current rating of 26 mA.

3.1.6.2. *C 10 HV Capacitor (HighVolt)*

The capacitor (C_k in Figure 21) smooths the waveform from the rectifier, and reduces the ripple current, producing a better DC output. In the DC circuit the capacitor had a capacitance of 10 nF, rated at 100 kV AC and 135 kV DC.

3.1.6.3. *LS 150-1/40 HV Blocking Impedance (HighVolt)*

The blocking impedance (L in Figure 21) acts as a high voltage filter, keeping interfering signals from the measurement equipment, and further smooths the output. The inductor was rated to 150 kV and 1 A, with a self-inductance of 40 mH.

3.1.6.4. *MRT 205-4 HV Resistive Divider (HighVolt)*

The resistive divider (R_D in Figure 21) is used to allow for the measurement from PD on test objects stressed by the DC circuit, without using the HFCT. The resistor had a resistance of 250 MΩ, with a ratio of 167.67. It was rated at 135 kV.

3.2. Creation of Test Objects

As discussed in Chapter 2, the behaviour of PD in void defects is investigated and discussed in this thesis. To create void defects, two methods were used. The first

was to create voids by layering thin-films of polymers, and the second was to introduce a void into the insulation layer of a sample of cable.

3.2.1. Thin-film Samples

3.2.1.1. *Materials*

The thin film samples were created from rolls of plastic film of either low-density polyethylene (LDPE) or polypropylene (PP), purchased from Goodfellow Cambridge LTD. In both cases the film was 0.05 mm thick. The LDPE roll was 300 mm in height and 10 m in length, while the PP roll was 600 mm in height and 5 m in length.

The properties of the LDPE, as provided by the manufacture, are shown in Table 3

Table 3 – Properties of low-density polyethylene[147].

Property	Value
Relative Permittivity	2.2-2.35
Dielectric Strength	27 MV/m
Surface Resistivity	10^{13} Ω/square

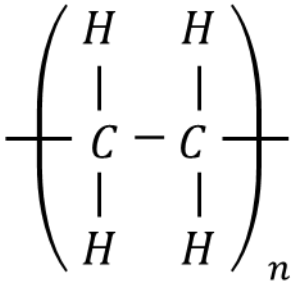

Figure 22 – Chemical formula for repeating unit of low-density polyethylene (based on [148]*).*

The properties of the PP, provided by the manufacturer, are shown in Table 4.

Table 4 – Properties of polypropylene[149].

Property	Value
Relative Permittivity	2.2-2.6
Dielectric Strength	30-40 MV/m
Surface Resistivity	10^{13} Ω/square

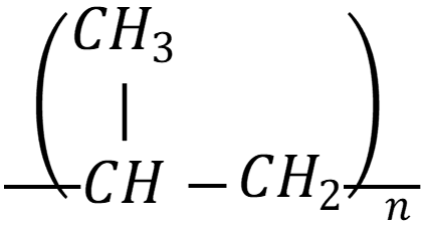

Figure 23 – Chemical formula for repeating unit of polypropylene (based on [150]*).*

3.2.1.2. *Creation*

The material on the rolls were cut, using a commercial guillotine trimmer, into squares of 150 mm in length These squares were layered to create the thin film samples, to create the void defects as seen in Figure 24, a commercial hole-punch was used, this cleanly removed a circular section from the films, of diameter 1 mm (the smallest section that could be practically removed). For each sample seven layers of thin film squares were used, giving an overall thickness of 0.35 mm. Three configurations of defected samples were created, along with a non-defected sample for each material which was stressed to ensure no discharges were detected for validation purposes, to ensure all PD detected was within the void. The three defected sample types were: single void configuration, two voids in parallel configuration, and two voids in serial configuration. These configurations were selected to investigate the impact of the orientation of the electric field on multiple voids in comparison to a single void. In both cases the separation between the voids was made as small as possible, to better represent multiple voids at the same site.

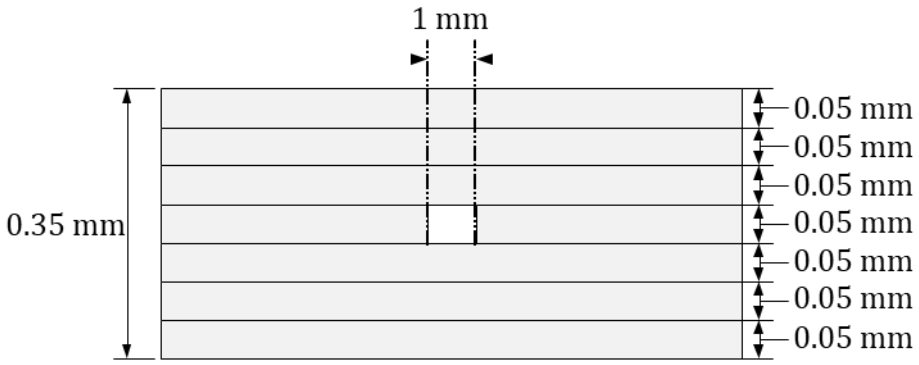

Figure 24 – Diagram illustrating single void thin film sample of either LDPE or PP.

The single void samples had the defect in the fourth (or middle) layer, giving 0.15 mm of intact material on either side of the void vertically, and 74.5 mm horizontally. This ensured that the single void would be in the same position within the applied electric field for each test.

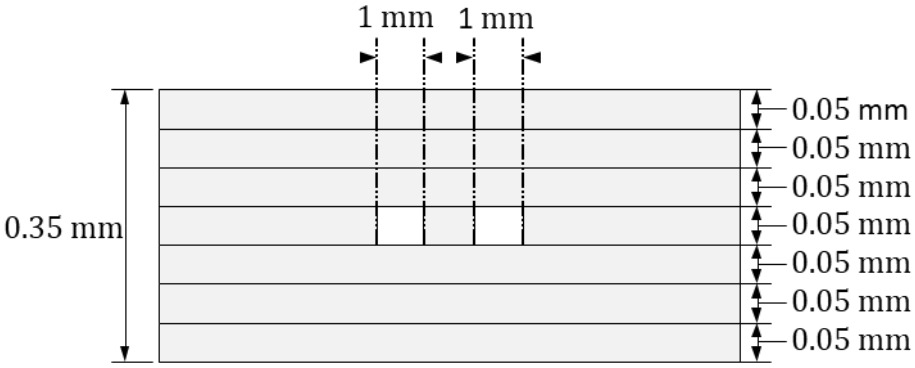

Figure 25 – Diagram illustrating parallel void thin film sample of either LDPE or PP.

For the two voids in parallel samples, the voids were also created in the fourth (middle) layer, with a separation of 1 mm (the smallest practical separation). This again gave 0.15mm of intact material on either side of the void vertically, with 73.5 mm of intact material horizontally in the plane of the voids, and 74.5 mm perpendicular to the plane of the voids.

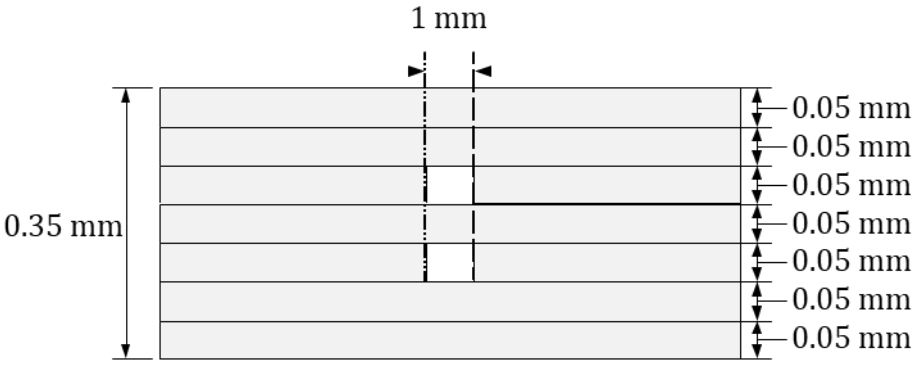

Figure 26 – Diagram illustrating serial void thin film sample of either LDPE or PP.

For the two voids in serial configuration, the sections were removed from the third and fifth layers, leaving one layer (0.05 mm) of fully intact material in between, and two layers (0.1 mm) on the other side of each defect. The voids were created in the middle of the layers, again leaving 74.5 mm of intact material horizontal to the void.

3.2.1.3. *Test Rig*

In order for voltages to be applied across the thin-film samples, and for partial discharges to be recorded, a test rig (Figure 27) was constructed. The rig consisted of two brass electrodes with diameters of 50 mm, one for connection to the coupling capacitor, and one for connection to earth. The electrodes had rounded edges to prevent corona discharge. The rest of the rig was comprised of cylinders constructed from the thermoplastic polymer acrylonitrile butadiene styrene (ABS), connected by screws and threads also made from ABS. Dimensions of the test rig are shown in Figure 28, Figure 29 and Figure 30.

The height of the top electrode could be varied by turning a handle at the top of the rig, which allowed for the distance between the electrodes to be varied. This make it possible for the space between the electrodes to be set to the height of the complete thin-film sample, ensuring no air gaps were present, and that no oil could enter the void or the sample layers. During testing the entire rig was placed in a tank filled with mineral oil, to ensure no air was present adjacent to the electrodes or thin film sample. Care was taken to ensure no air bubbles were present in the oil adjacent to either the electrodes or the sample, or between the layers of the sample.

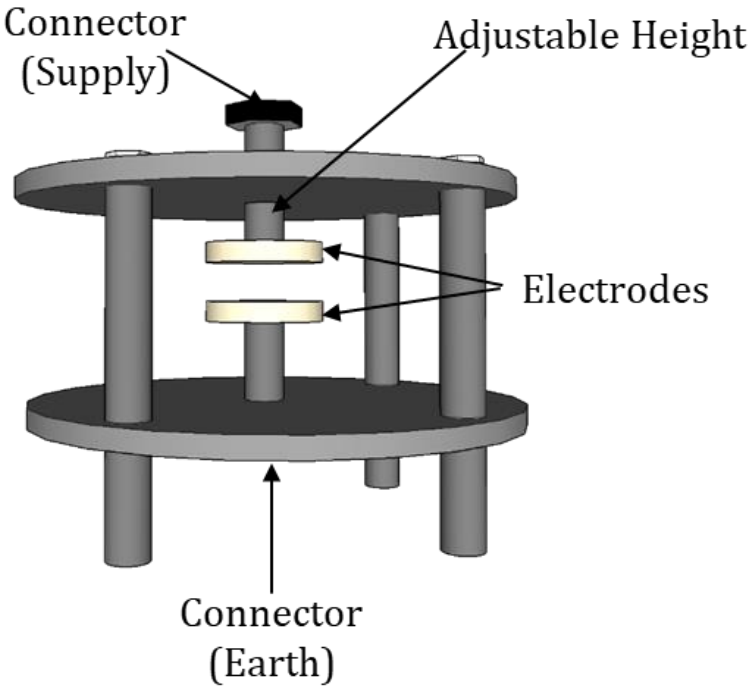

Figure 27 – Diagram illustrating test rig used for thin film samples.

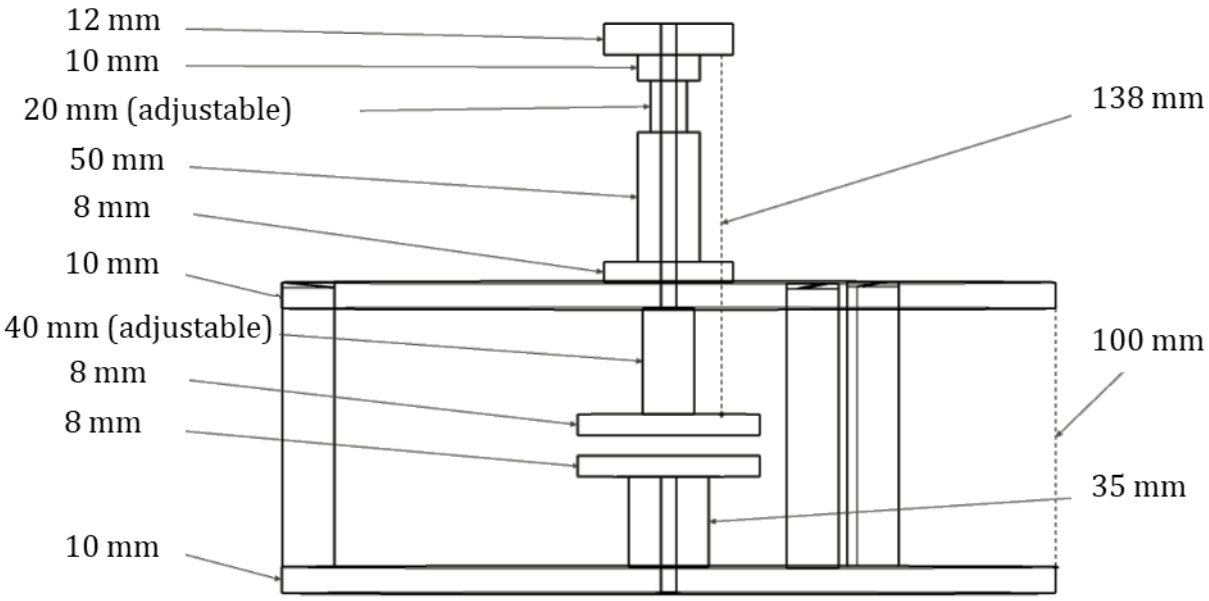

Figure 28 – Diagram of thin film test rig showing heights (side view).

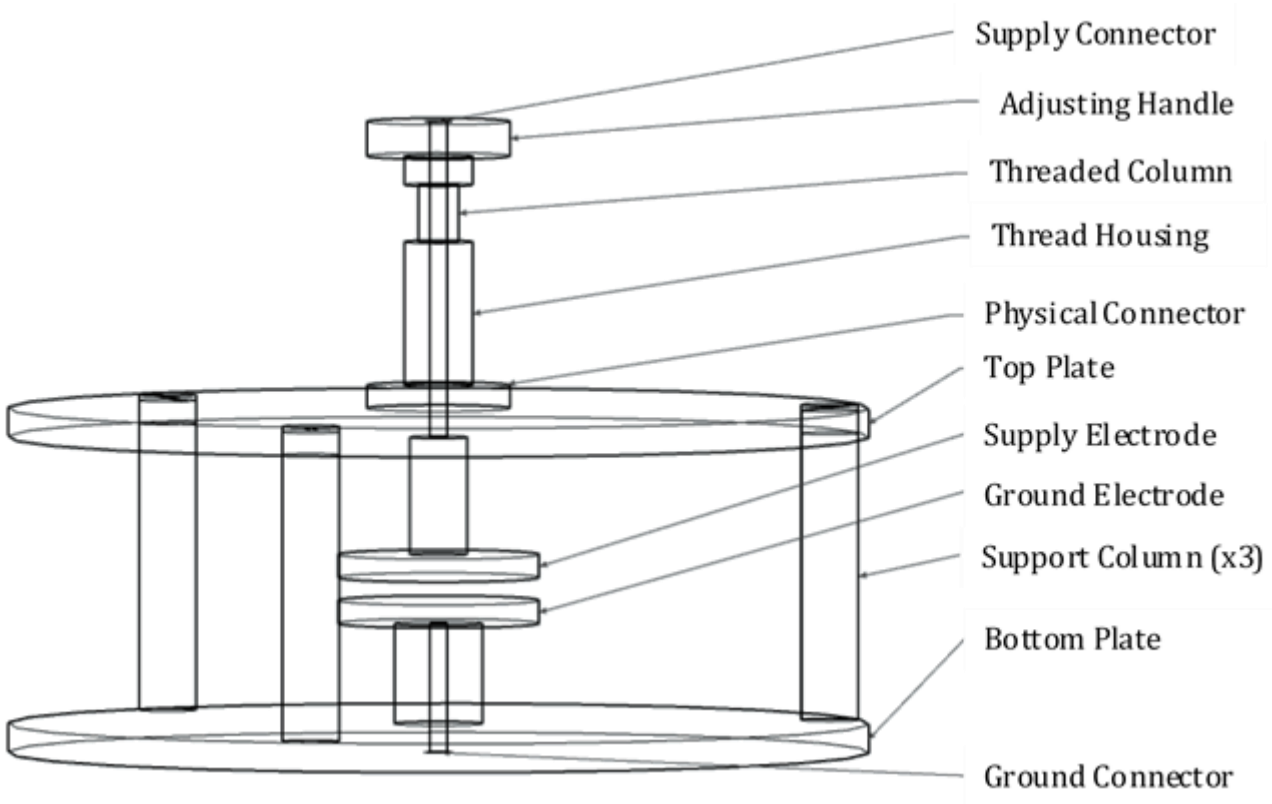

Figure 29 – Diagram of thin film test rig showing components (side view).

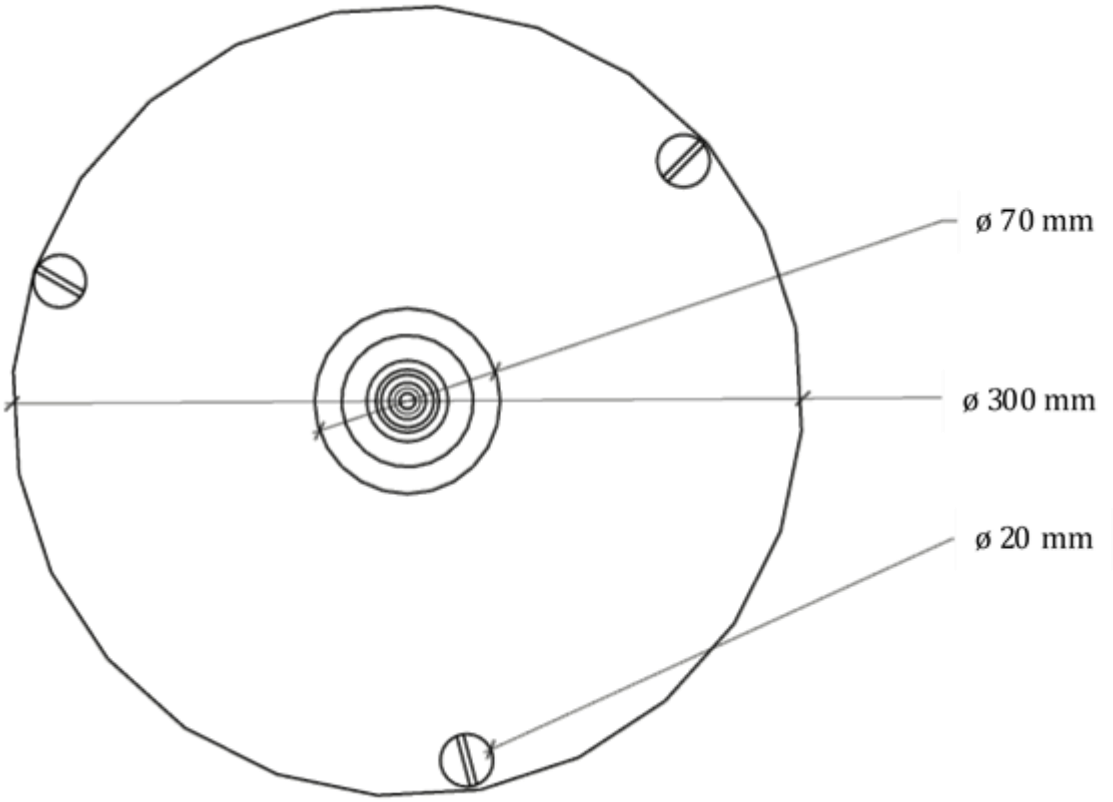

Figure 30 – Diagram of thin film test rig showing widths (top view).

3.2.2. Cable Sample

The cable sample was prepared from a section of cable insulated with cross-linked polyethylene (XLPE) that was designed for use under HVDC conditions. The exact specifications of the cable are withheld at the manufacturers' request, however generic details are shown in Table 5.

The cable sample was tested before the defect was introduced up to the maximum output of the test circuit under both AC and DC conditions to ensure that any discharges detected were due to the defect.

Table 5 – Properties of XLPE cable sample from manufacturer.

Property	**Value**
Conductor Material	Aluminium (Stranded)
Conductor Diameter	49.8 mm
Conductor Screen	XLPE (with conducting material)
Conductor Screen Thickness	1 mm
Insulation Material	XLPE
Insulation Thickness	24 mm
Insulation Relative Permittivity	2.5
Metallic Screen Material	Lead (Sheath)
Metallic Screen Thickness	4 mm
Outer Sheath Material	PVC
Outer Sheath Thickness	4 mm

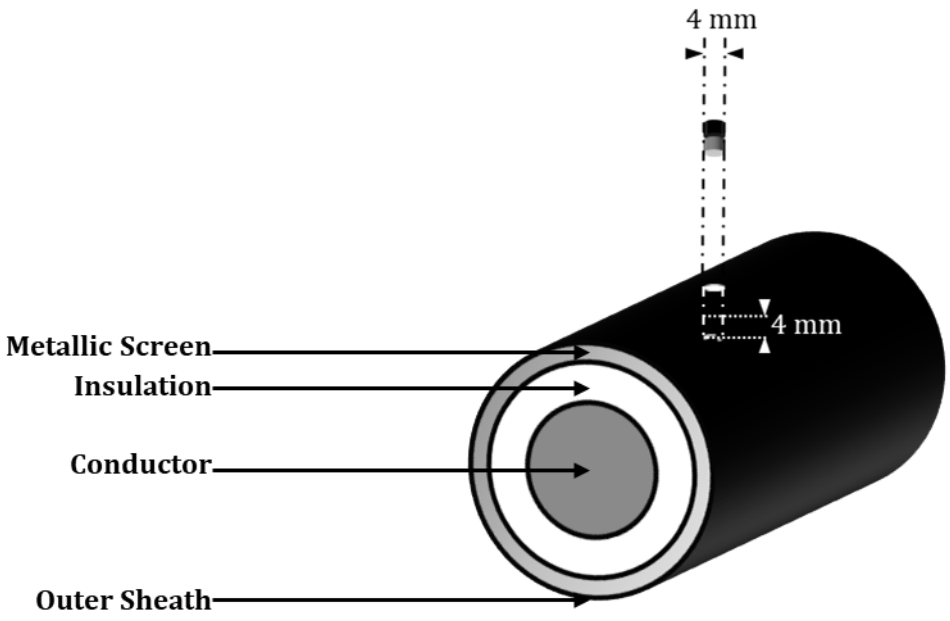

Figure 31 – Diagram illustrating artificial void in XLPE cable sample.

To create an artificial void in the cable sample a drill was used to create a cylindrical hole 4 mm in diameter to a depth of 13 mm (4 mm into the XLPE insulation layer). A core is then taken from a separate sample of the same cable of 4 mm in diameter and 9 mm in height (comprising the outer sheath and metallic screen). The core is the placed into the gap, so that the top of the core is flush with the outer sheath, ensuring the metallic screen is intact. This creates a cylindrical void of height 4 mm and diameter 4 mm, the smallest size which was practical.

The same void was used for each of the tests, with a 24-grounding period between tests.

3.3. Calibration

Before each test, the system was calibrated, according to the IEC 60270 standards, to ensure that the PD magnitude can be measured accurately. For measurements performed using the HFCT, the calibration determined the scale factor (k), the ratio between the measured voltage and the magnitude of a pulse. For measurements using the Lemke LDS-6 measurement system through the LDM 5/U measuring impedance, this scale factor is recorded by the device and applied to subsequent measurements automatically. For measurements through

the HFCT and the LeCroy Waverunner 104Xi oscilloscope the scale factor is noted and manually applied during analysis.

The calibration is performed using a Lemke Diagnostics LDC-5, which injects current pulses of known charge (5 pC, 20 pC, 100 pC, or 500 pC) into the system, with the charge selection made based on the expected range of magnitudes to be recorded. The output of the LDC-5 was validated by connecting directly to the 104Xi, a variation in magnitude of less than 10%, and a consistent rise time of less than 10 ns, comfortably within IEC 60270 requirements, was recorded over multiple tests.

3.4. Process

The test process was informed by IEC 60270 sections 8 (Tests, which covers testing under AC conditions), and 11 (Partial discharge measurements during tests with direct voltage).

1. Set-up – the test circuit is configured for the correct voltage type (AC or DC). When using the test rig the electrodes are cleaned and dried and the temperature of the mineral oil is checked. When using the cable sample, the ends of the cable are cleaned and dried, and a mouldable dielectric is applied (to prevent surface discharge).
2. Calibration – as described above, the system was calibrated and the scale factor, k, determined.
3. Final check – the circuit is visually inspected to ensure all connections are solid, and that the calibrator has been removed from the circuit (N.B. the test circuit is located in a test cage with an interlock system, preventing accidental energisation with anyone present within the cage).
4. Energisation – the circuit is energised, and voltage outputs are measured to ensure circuit is complete and no abnormal behaviour is observed.
5. Determination of PD inception voltage – the voltage is gradually increased at a rate of 100 V every 10 minutes until sustained discharge (at least 1 PD event detected per minute). This is the same for both AC and DC, although the number of PD events for AC was always much greater than 1 PD event

per minute (due to the mechanisms of PD recurrence discussed in Chapter 2)

6. PD measurement phase – the voltage is increased to 10% higher than the PDIV, and partial discharges are recorded. For the LDS-6, measurements are performed on each sample for two two-hour test periods, for the 104Xi 1000 pulses are recorded at the timescale of one AC waveform (20 ms), and 100 pulses are recorded at the timescale of one PD pulse (5 μs), after two hours of stressing, to allow for the activity of the sample to settle down (as discussed in Chapter 5).
7. De-energisation – the circuit is de-energised.
8. Earthing – the circuit is earthed to ensure that the capacitors and other components do not hold or develop significant charge. If the cable sample was used, this is also earthed.

3.5. Data Management

3.5.1. Data Collection

Data collected from the LDS-6 is in LXD format which can be read by the proprietary Lemke software. The same software can convert the data to ASCII as TXT files. Data from the 104Xi are in CSV format.

3.5.2. Documentation

Units and measurands are clearly labelled in files, with measurement parameters as defined in IEC 60270.

3.5.3. Storage and Back-up

Data are stored in the Sharefile cloud storage system for the University of Strathclyde 'Strathcloud' which provides multiple physical back-ups of the data.

3.5.4. Open Access

Data (TXT files for the LDS-6 data, and CSV files for the 104Xi data) from this thesis is located in the open-access database '*Partial Discharge Measurements of Voids in Layered Polymers and Cable Sample*' with the DOI 'https://doi.org/10.15129/156771c7-0566-43db-8d97-a11180e5d0d6' for use,

with attribution, by interested parties. This is facilitated by the University of Strathclyde's data repository 'Pure'.

3.6. Limitations

While the laboratory was shielded from external electrical noise, other equipment within the laboratory was capable of introducing noise into captured results. Care was therefore required when experiments were running that these did not conflict with experiments on other test rigs, or the use of other electrical appliances, such as those used for laboratory cleaning.

3.7. Conclusions

The aim of the chapter was to discuss the methodology followed for the capturing of the data that was used in future chapters. The equipment used, and the way this was connected and operated was described. In addition, the creation of test objects was detailed, including the novel 'coring' method for creating an artificial void in a sample of cable. Lastly, the collation of the collected data was discussed, and how this was done to allow for an open-access database of the PD pulses to be uploaded following completion of this project.

4. AC and DC Testing of Artificial Voids in Layered Polymers

This chapter presents the results of the initial AC and DC testing of the thin film samples with single void configurations. The methodology used for sample creation and testing is described in Chapter 3. The data captured in this section were recorded using the Lemke LDS-6. The aims of this chapter were to: first, ensure that the thin film sample creation method, and test cell, produced the expected results under AC conditions; secondly, to compare the results between the low-density polyethylene (LDPE) and polypropylene (PP) samples under AC conditions; and finally, to ensure that the methodology was valid for testing of LDPE under DC conditions.

4.1. PD Inception Voltages

The PD inception voltages for both AC stress and negative DC stress were determined by the process as detailed in Chapter 3. Table 6 shows the details of the PDIVs for the different sample configurations, including the mean measured input at the LV side of the transformer, the percentage range of these values, the calculated output at the HV side of the transformer (which corresponds to the PDIV itself), and the applied test voltage (an increase of 10% over the PDIV).

Table 6 - Partial discharge inception voltages for AC and DC tests on thin film samples using Lemke Diagnostics LDS-6.

Sample			PD Inception Voltage		Test (kV)
Voltage	**Material**	**Void Configuration**	**LV Input (V)**	**HV Output (kV)**	
AC	LDPE	Single	10.3	**3.5**	3.9
	PP	Single	10.2	**3.5**	3.9
−DC	LDPE	Single	24.0	**9.1**	10.0

Comparing the PDIVs (shown in Table 6) for the AC tests, it is found that the samples of the two materials behaved similarly. The PDIVs found were the same, within the same range for each, at a value of 3.5 kV. This suggests that for AC testing at least, the choice of material does not significantly impact the PDIV (this is explored further in Chapter 5). However, when considering the DC tests in comparison to the AC tests, the LDPE shows a different PDIV.

As shown above, the PDIV for the LDPE DC test was higher than that for the two AC samples. While the same definition of PDIV was used in each case (i.e. at least 1 PD event per minute), as discussed above, the recurrence rate of PD under DC conditions is considerably lower, so, as explained previously, while some early PD activity may have occurred at the same voltage as the AC PDIV, the repetition rate was not sufficient for this to be recorded as the PDIV.

From the analysis of the AC PDIVs therefore the conclusion can be drawn that the choice of dielectric does not seem to have a significant impact on the AC PDIVs for identical voids.

4.2. Test Results

The test results for this section are represented below, initially as standard PRPD plots and ϕ-q-n plots for the AC results, and as |Δq|-dt-n plots for the DC results. Subsequently phase distribution plots are also presented for the AC tests, while charge distribution plots are provided for the DC tests.

4.2.1. AC Test Results

AC tests were performed at a test voltage of 3.9 kV for both the LDPE and PP samples, with two samples of each tested for two contiguous two-hour test periods.

4.2.1.1. *PRPD*

Figure 32 shows the PRPD plots for the tests of the LDPE samples under AC stress. The patterns for each represent what would be considered typical of a void type defect under AC voltage, with the PD apparent charge leading the AC waveform, and the bulk of activity in the first and third quadrants. This is more evident in the second test period in sample 1, and less distinct between the test periods in sample 2.

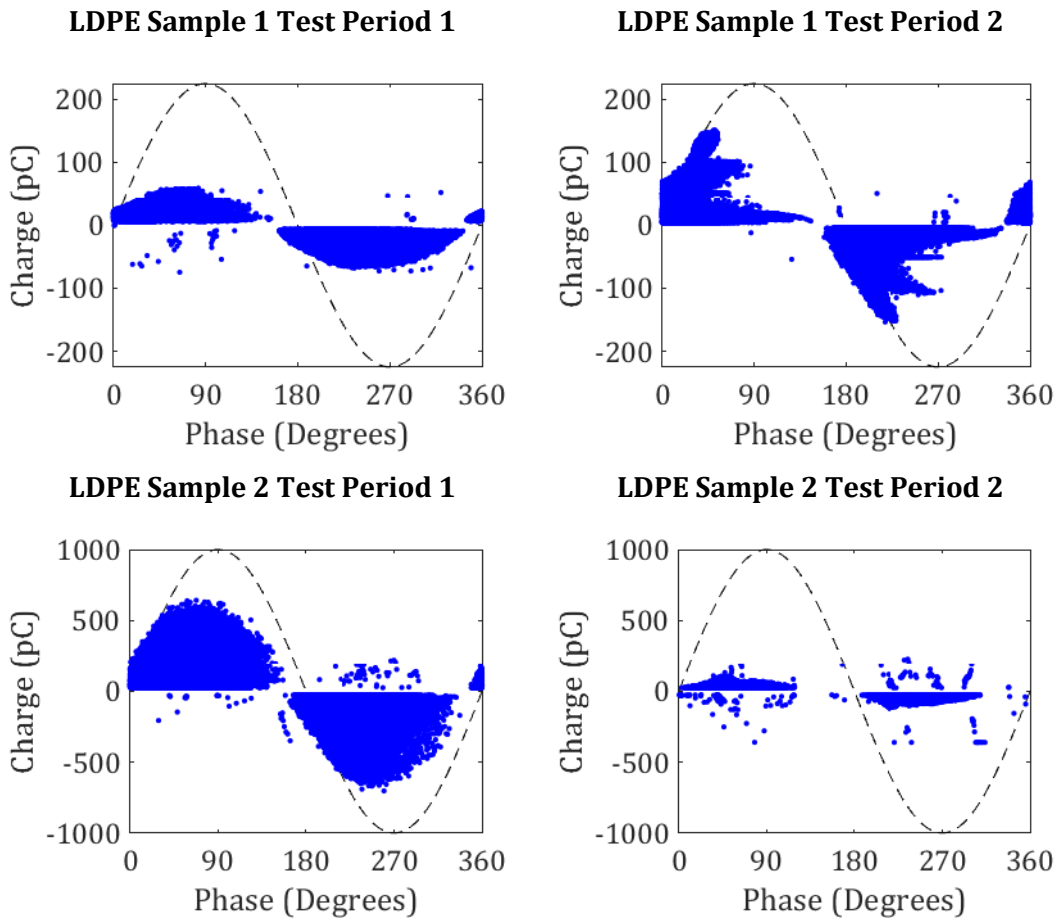

Figure 32 – PRPD plots for AC testing of single void LDPE samples, with sample 1 (top) and sample 2 (bottom).

The difference in these magnitudes may be related to the nature of the PD pulses that were generated, as streamer-like pulses are considered to have a higher apparent charge than Townsend-like pulses, with streamer-like discharges more common in void defects[1], [54], a difference in the proportion of streamer and Townsend-like pulses could therefore explain different behaviour between the samples. The equipment used in this section was not capable of recording individual pulses for this to be investigated, however this was possible in tests reported in subsequent chapters, where this question is explored further.

Figure 33 shows the PRPD plots for the AC testing of each of the PP samples. As with the LDPE samples, these PD patterns are indicative of a void-type defect under AC conditions (with peaks leading the AC waveform), and, also as with the LDPE, this is more evident in the second test period for each sample.

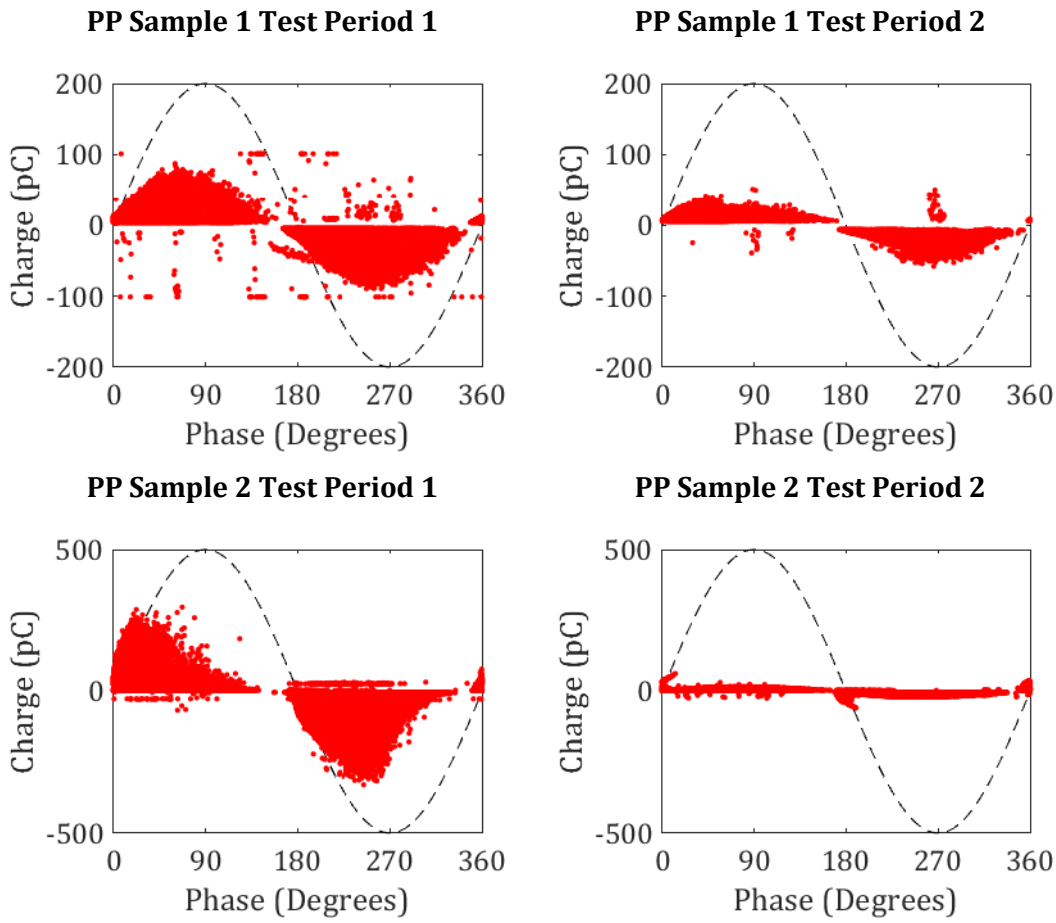

Figure 33 – PRPD plots for AC testing of single void PP samples, with sample 1 (top) and sample 2 (bottom).

The variation in different PD apparent charge values are in a similar range to those of the LDPE samples, possibly again due to different proportions of discharge types. As with the PDIV results, this suggests very little variation between the PD behaviour within the PP and LDPE.

4.2.1.2. *ϕ-q-n*

The PD behaviour is perhaps better represented on the ϕ-q-n plots, with Figure 34 showing these for the LDPE samples. From these it can be more clearly seen that the PD activity is concentrated in the first and third quadrant of the AC waveform. This activity distribution is also strongly correlated with void-type defects[151], [152].

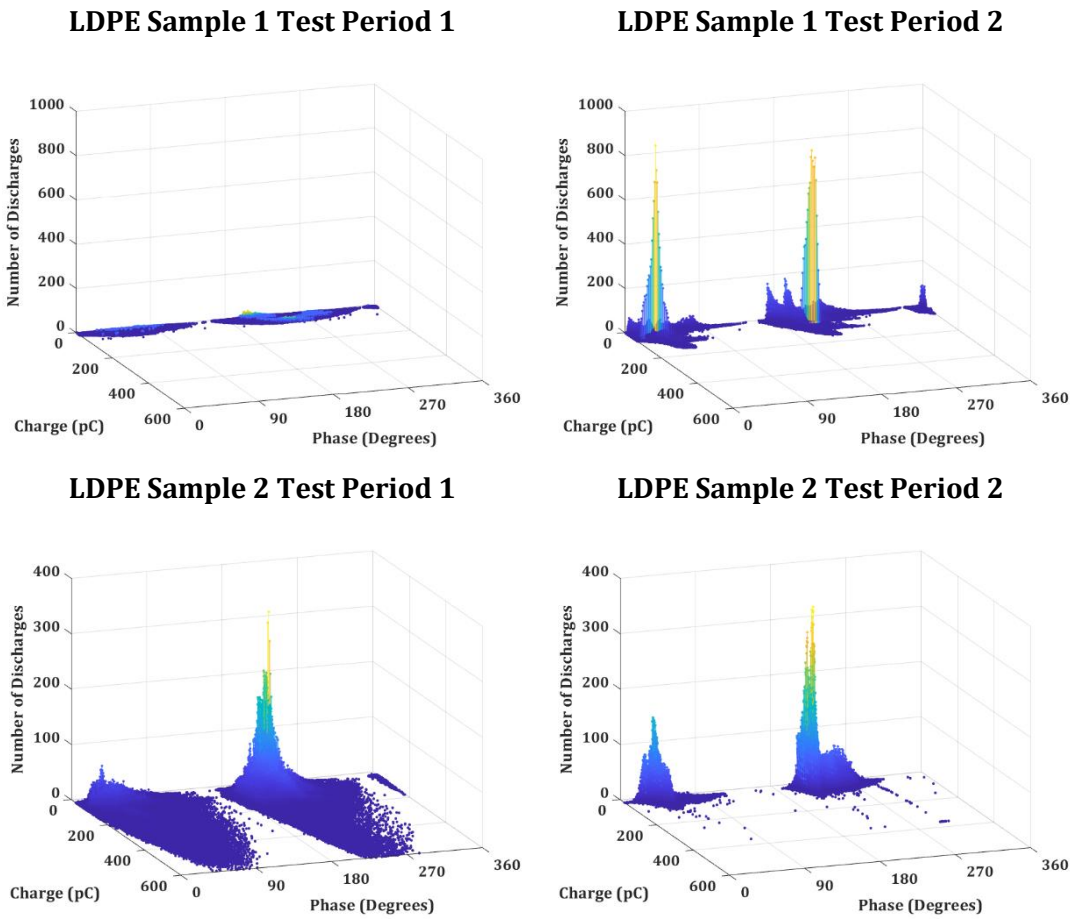

Figure 34 – ϕ-q-n plots for AC testing of single void LDPE samples, with sample 1 (top) and sample 2 (bottom).

Aspects of the behaviour of the samples in the two test periods were found to have similarities. In both cases the events became more concentrated around a smaller range of charge and phase values. Overall sample 2 was more consistently active than sample 1, with the first test period having a greater spread of pulses across the phase (samples 1 and 2) and peak apparent charge (sample 1 only). It has been suggested in previous research, in both epoxy resin samples[111] and LDPE samples[59] that these patterns have two components, the 'ear' which is formed from a large initial discharge in each half cycle, and a 'body' formed from the subsequent PDs. It has also been suggested[153] that is the due to the large 'ear' discharge increasing the availability of free electrons, which reduces the overvoltage for the remained 'body' discharges, as the time lag is reduced.

As can be seen in Figure 35 this rabbit like pattern is also found in the tests of the polypropylene samples.

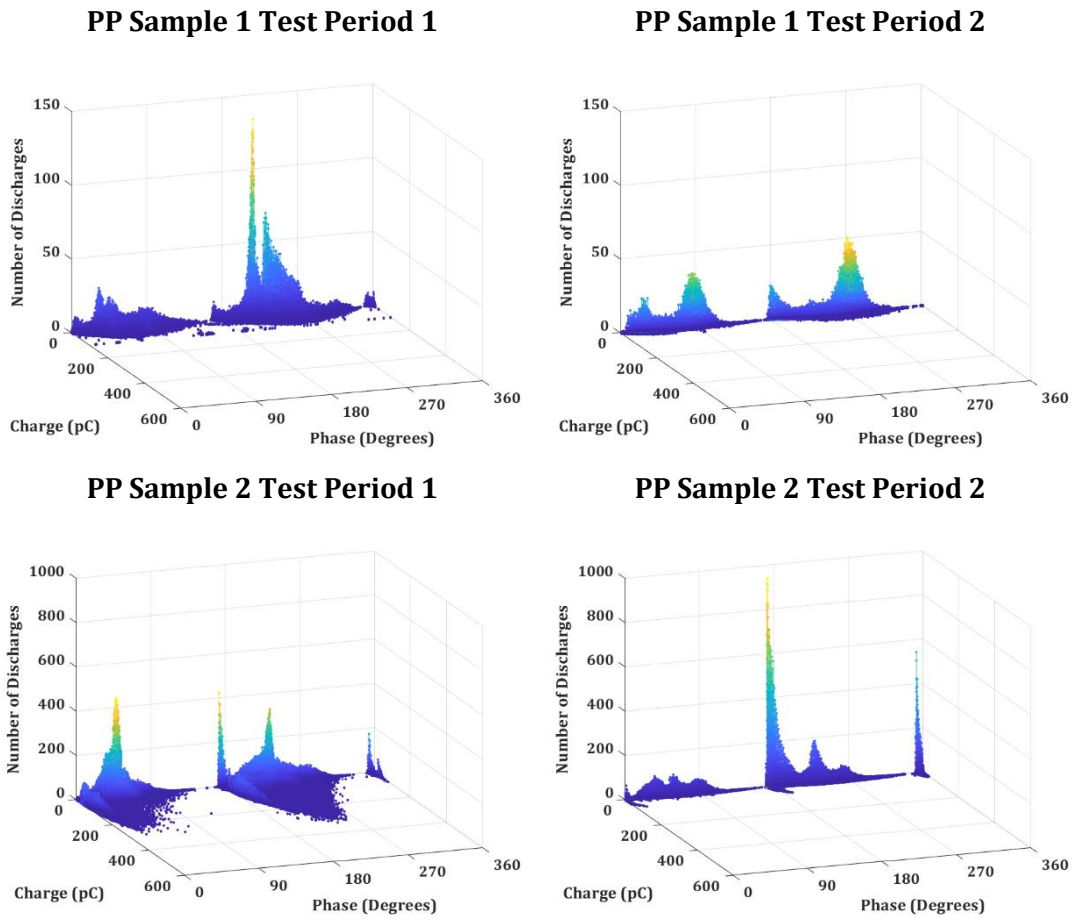

Figure 35 – ϕ-q-n plots for AC testing of single void PP samples with sample 1 (top) and sample 2 (bottom).

As discussed above, it is generally assumed that larger PD pulses (resultant from larger values of overvoltage or ΔV) represent steamer-like breakdown, while smaller PD pulse amplitudes are indicative of Townsend breakdown[7]. Therefore, it can be assumed that Townsend-like discharges have small peaks and long durations, and streamer-like discharges have tall peaks and short durations[52]. As previously indicated, individual pulses were not measured. However, for both the LDPE and polypropylene samples, it appears from visual inspection of the ϕ-q-n that the bulk of the discharges, which occur at lower apparent charges are of the steamer-like type, while a minority of pulses, occurring at higher amplitudes, are of the Townsend type. In both materials, the tendency appears to be that the amplitudes are lower for the second test period, suggesting this dominance of streamer-like pulses, increases over time.

As with the PRPD plots, the ϕ-q-n plots do not indicate significant differences between the PD activity in the polyethylene compared to the polypropylene, with similar variations between samples as well as between testing periods.

4.2.1.3. *Phase Distribution*

The distribution of PD pulse characteristics across the phase of the voltage can be plotted, specifically the peak absolute apparent charge, the mean absolute charge, the number of PD events per cycle, and the total absolute charge. The discharges for the first LDPE sample are shown in Figure 36, with the equivalent for the second LDPE sample shown in Figure 37.

In both samples, the distribution of the peak maximum charge more closely mirrors the phase of the input AC waveform during the first test period, with the PD more evenly distributed across the cycle in the second. In both samples for both test periods the PD pulse peaks slightly lead the peaks of the waveform, as might be expected from the PRPD and ϕ-q-n plots.

The number of PD events per cycle was also similar across both samples, with the peak in the first half of the waveform nearing 1 PD per cycle, and the peak in the second being 2 PDs per cycle for the first test period. These settled down in the second test period to 1 PD per cycle as the peak for both halves of the waveform. This similarity contrasts with the difference between the two samples in terms of the peak, mean, and total apparent charge. Specifically, values increase in the second test period for sample 1, and decreasing for sample 2. This suggests that, as indicated by the PRPD and ϕ-q-n plots, the activity 'settles down' in the second test period, however this can be accompanied by either an increase or decrease in the maximum and average sizes of the PD events, even as they occur at similar rates.

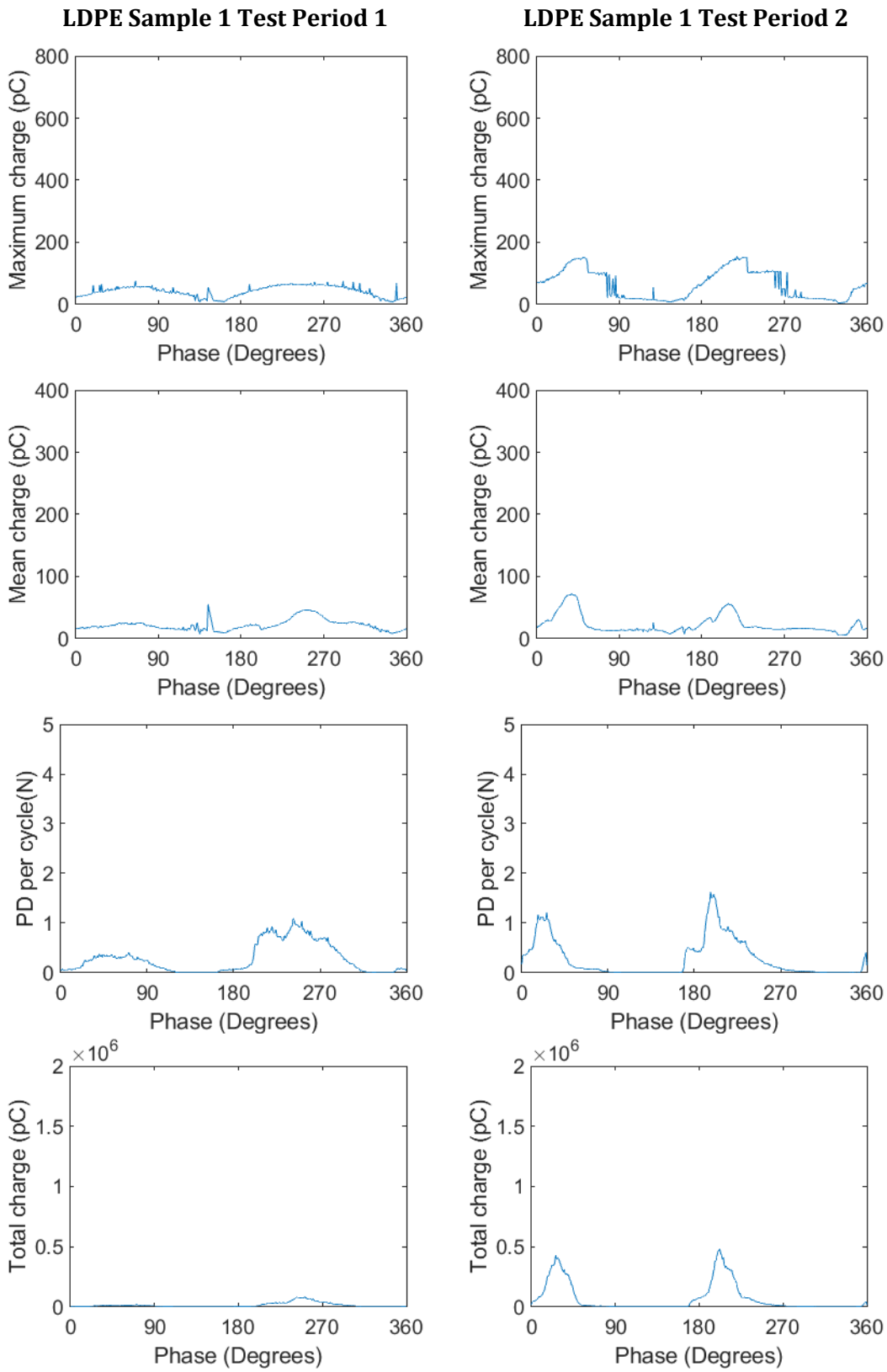

Figure 36 – Plots of phase distribution of: (top) maximum pulse amplitude, (top middle) mean pulse amplitude, (bottom middle) PDs per cycle, and, (bottom) total charge, in LDPE sample 1 for test period 1 (left) and test period 2 (right).

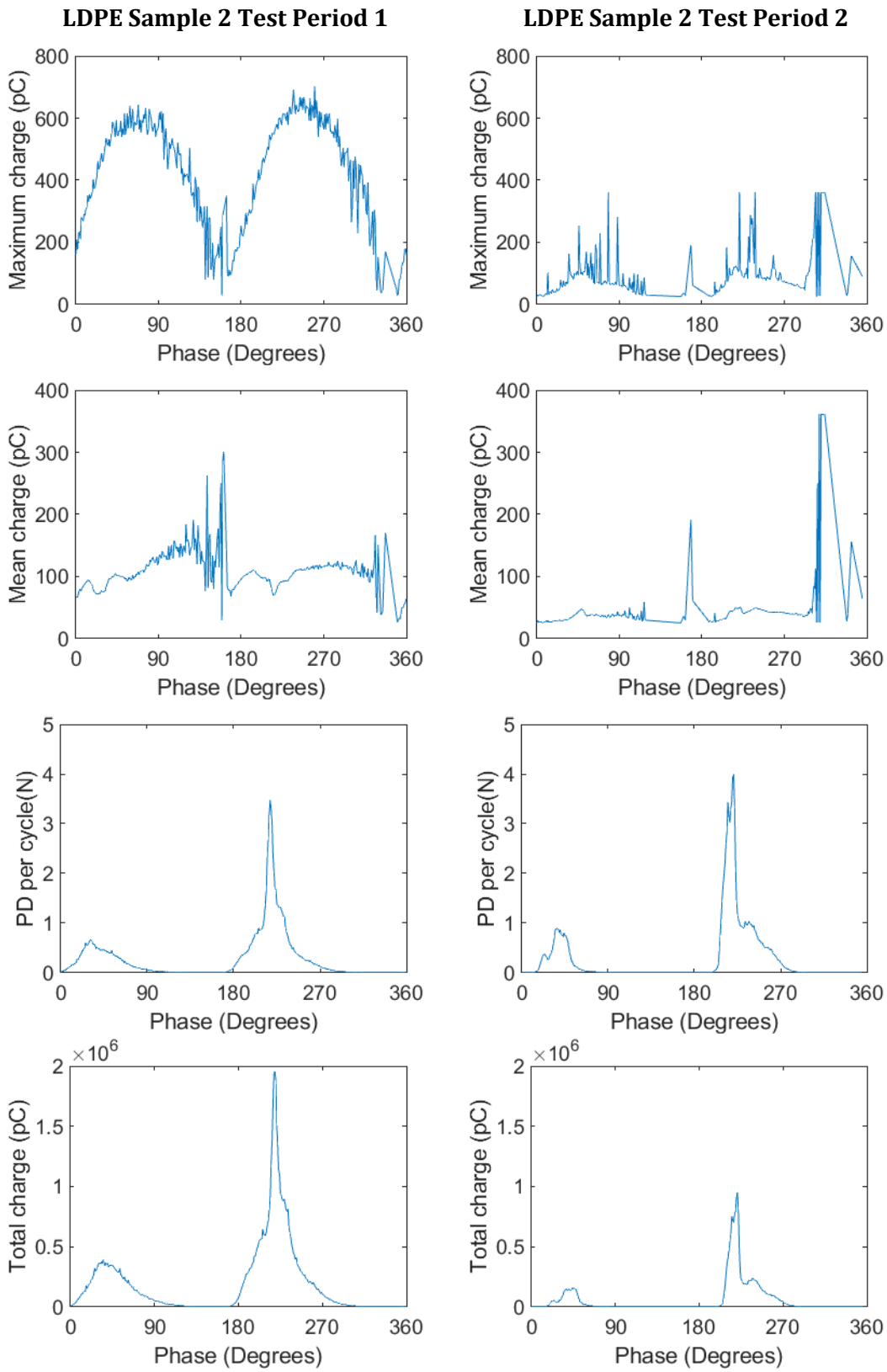

Figure 37 – Plots of phase distribution of: (top) maximum pulse amplitude, (top middle) mean pulse amplitude, (bottom middle) PDs per cycle, and, (bottom) total charge, in LDPE sample 2 for test period 1 (left) and test period 2 (right).

For the polypropylene the phase distributions for the first sample are shown in Figure 38, with those for the second sample shown in Figure 39.

The maximum apparent charge plots for the first test period for these samples, closely resemble the first test period for the LDPE samples, with the pattern closely following the AC waveform, however for the polypropylene samples, this pattern is also clear for the second test period as well.

Unlike with the LDPE samples, the mean apparent charge distribution is more even in the second test period for both polypropylene samples. The PD per cycle, for the first sample resembles the LDPE samples ('settling down' to a peak of 1 per cycle leading both the positive and negative peaks of the AC waveform in the second test period compared to the first). The second sample has a higher average PD per cycle (up to 4) leading the positive peak of the AC waveform.

It appears therefore, that while both the LDPE samples and polypropylene samples show a settling down in the second period, this behaviour is different for each material. In the LDPE samples, the distribution of the number of PD events becomes steadier, while the distribution of the size of these events increases. In contrast in the polypropylene samples, the number of PD events continues to be variable, while their apparent charge values appear to be more evenly distributed in the second test period.

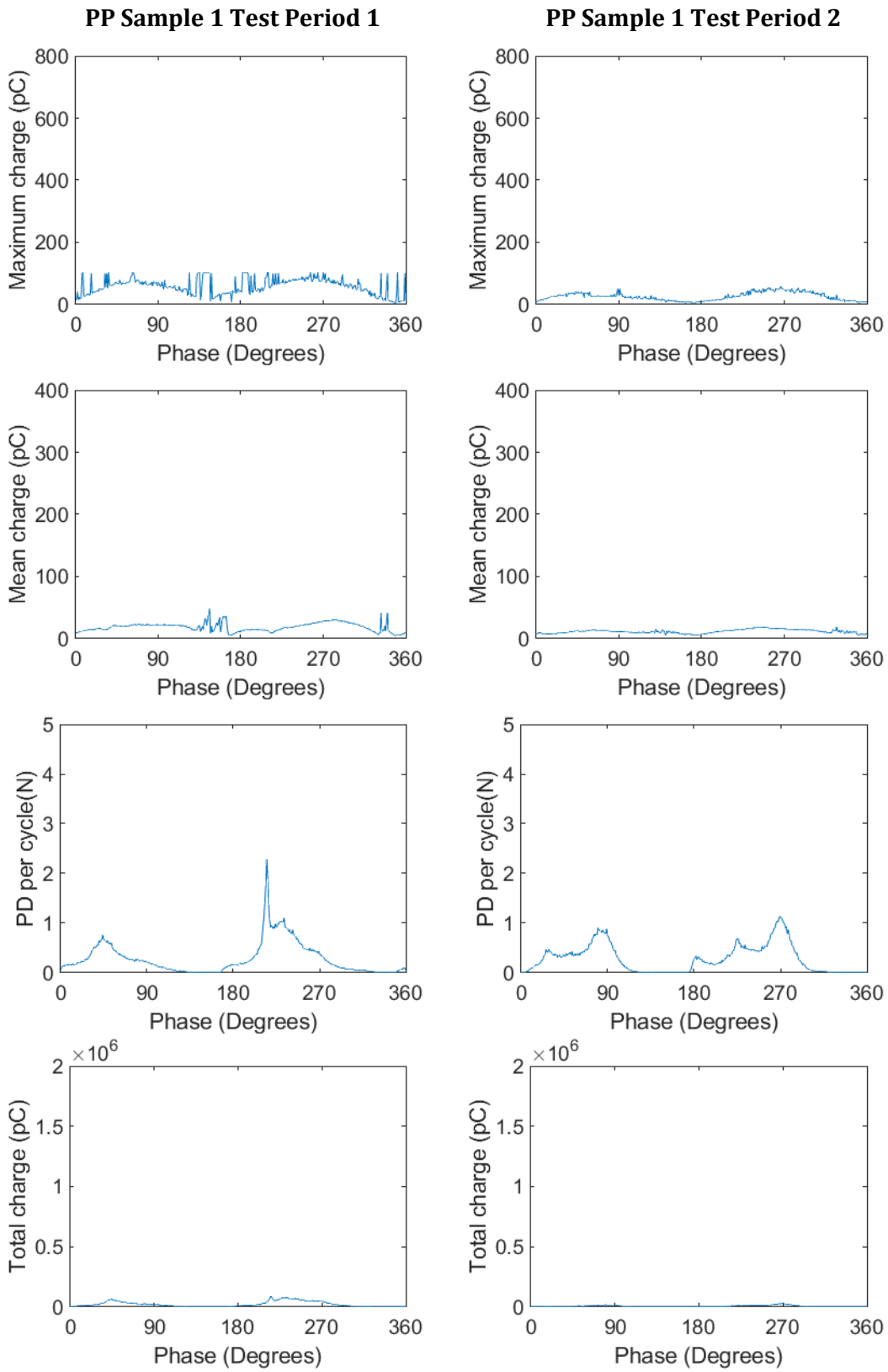

Figure 38 – Plots of phase distribution of: (top) maximum pulse amplitude, (top middle) mean pulse amplitude, (bottom middle) PDs per cycle, and, (bottom) total charge, in PP sample 1 for test period 1 (left) and test period 2 (right).

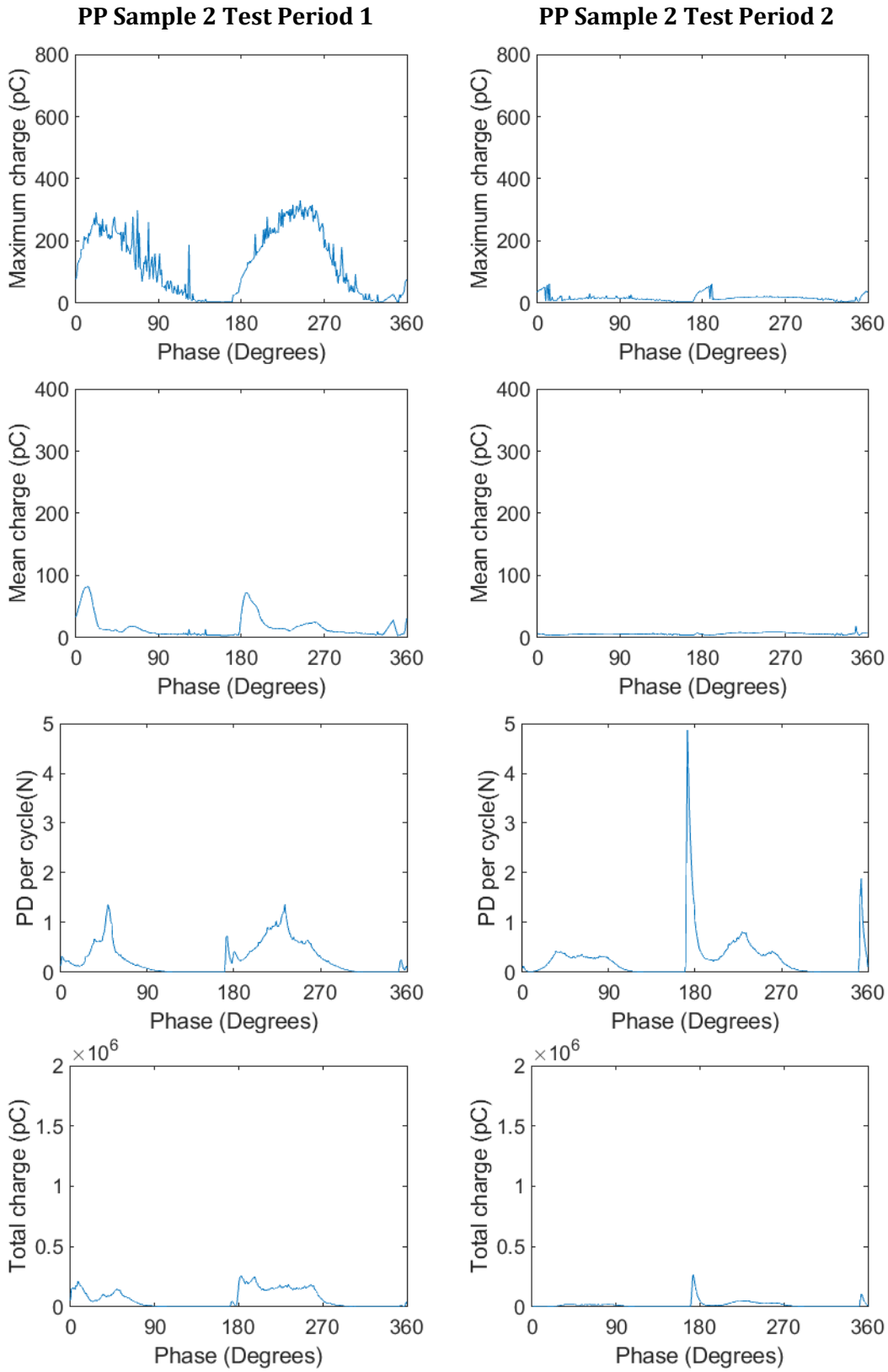

Figure 39 – Plots of phase distribution of: (top) maximum pulse amplitude, (top middle) mean pulse amplitude, (bottom middle) PDs per cycle, and, (bottom) total charge, in PP sample 2 for test period 1 (left) and test period 2 (right).

4.2.1.4. *Charge Distribution*

The distribution of the PD pulses across values of peak apparent charge for the two LDPE samples are displayed in Figure 40. In this regard, the two LDPE samples exhibit similar behaviour. In both samples, the spread of PD peak apparent charge magnitudes is higher in the first test period, which a noticeable reduction in the second test period. This matches the behaviour observed in the PDPR and ϕ-q-n plots, where the PD activity was noted to 'settle down' in the second test period compared to the first. There are differences between the two test samples also, with the second sample for both test periods, showing a more concentrated distribution, which again aligns with observations from the ϕ-q-n plots.

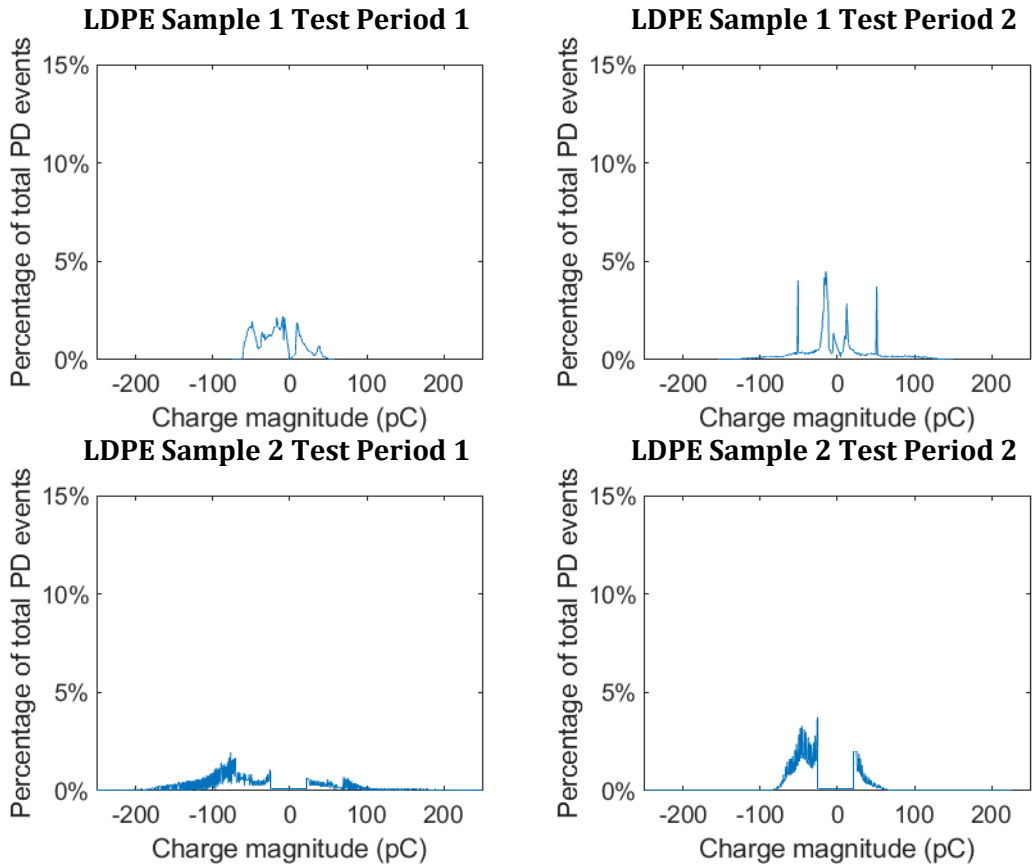

Figure 40 – Plots of PD per cycle of given peak charge magnitudes for single void LDPE sample 1 (top) and 2 (bottom).

The charge distributions of the polypropylene samples also display a similar 'settle-down' between the first and second test periods as the LDPE samples, as can be seen in Figure 41, with a greater percentage of PD events occurring at apparent charge magnitudes closer to zero. As before, the second test period shows a more concentrated distribution, however this difference is significantly less pronounced than in the LDPE samples, as the initial distribution is not as spread-out.

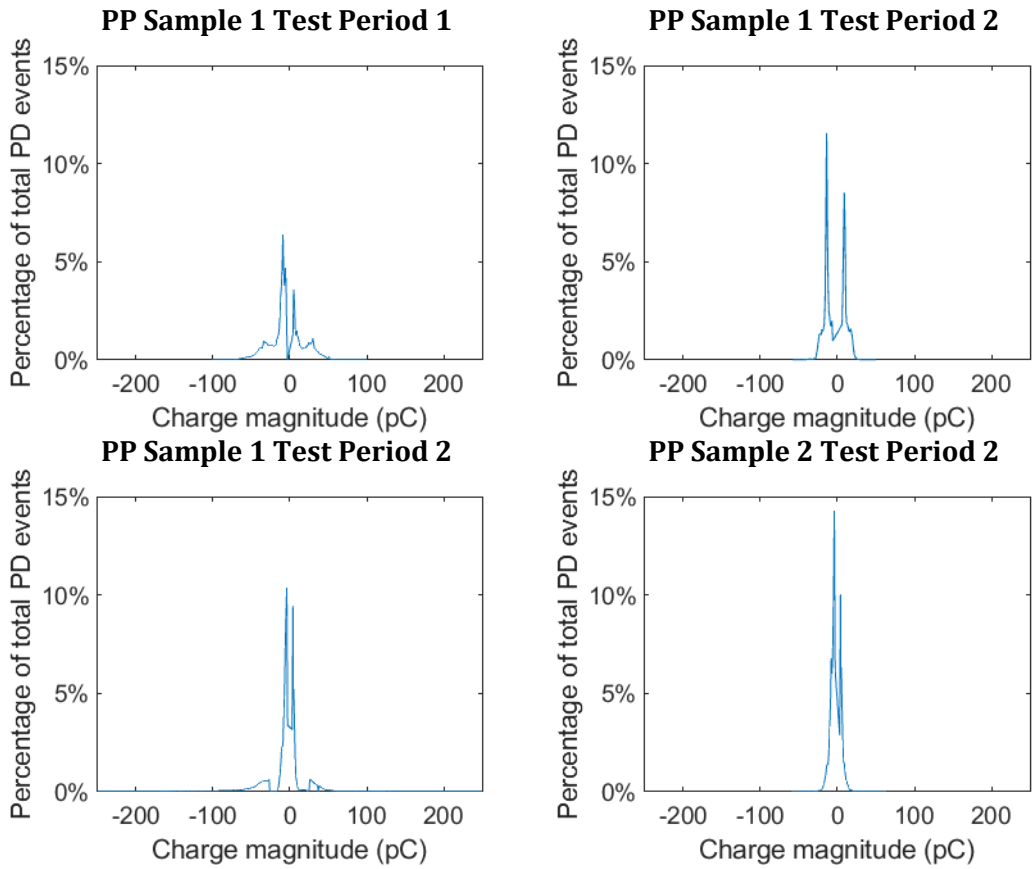

Figure 41 – Plots of PD per cycle of given peak charge magnitudes for single void PP sample 1 (top) and 2 (bottom).

Overall, the charge distribution shows that PD behaviour in both the LDPE and polypropylene samples are similar, with more pulses found in a lower range of charge magnitudes which are closer to zero, as the samples are tested for longer.

4.2.2. DC Test Results

The results of the DC testing of the LDPE are presented as: (I) plots of the number of PD events of a given charge, and time since previous discharge (|Δq|-dt-n plots); (II) plots of the frequency of peak pulse magnitude of the PD events compared to the previous PD;(III) frequency of the time between PD events; and; (IV) the cumulative charge over the test period.

4.2.2.1. *|Δq|-dt-n*

Figure 42 shows the |Δq|-dt-n plots for the DC testing of the LDPE sample in both test periods. For the first two-hour test period, the most common occurrence is an apparent charge pulse falling in the lowest bin ranges (0-25 s and 0-670 pC), occurring time after the previous discharge also in the lowest bin ranges (0-25 s and 0-670 pC). This is consistent with the process of PD reoccurrence under DC, with the value of apparent charge being closely related to the value of the overvoltage (which, as discussed in Chapter 2, is the amount by which the field strength across the void exceeds the minimum value for breakdown to occur), so a short recovery time, would give a small apparent charge. This suggests strongly that the thin film testing methodology as used here (and outlined in chapter 3), is suitable for testing under DC conditions[71].

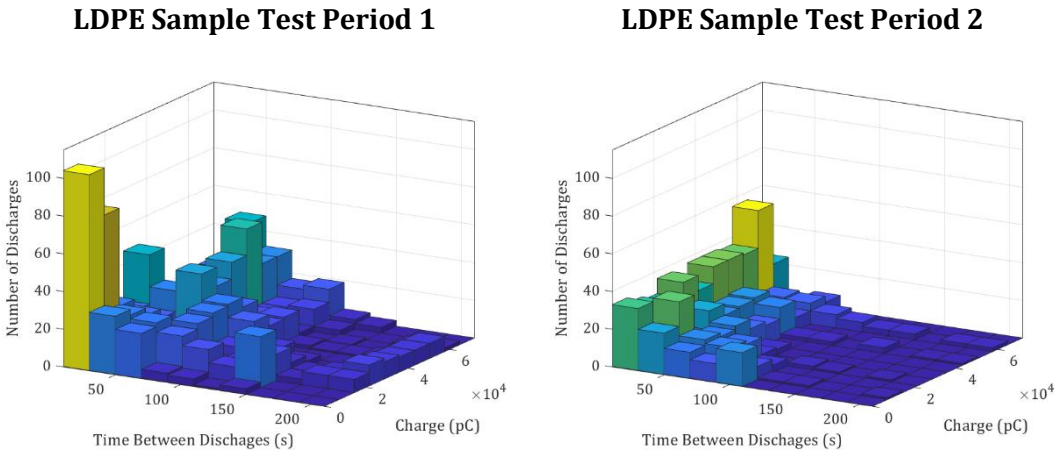

Figure 42 – |Δq|-dt-n plots for DC testing of single void LDPE sample.
Colours indicate the relative number of values falling in each bin from yellow (highest) to dark blue (lowest).

4.2.2.2. *Charge and Time Distribution*

In both test periods the difference in apparent charge magnitude from the preceding pulse was distributed geometrically (Figure 43), with the most likely values of difference being found in the lowest bin, and the probability of occurrence decreasing as the value of the difference in charge increases. As with the AC testing, the spread of detected values decreased in the second test period, suggesting a similar 'settling down' effect between the two test periods.

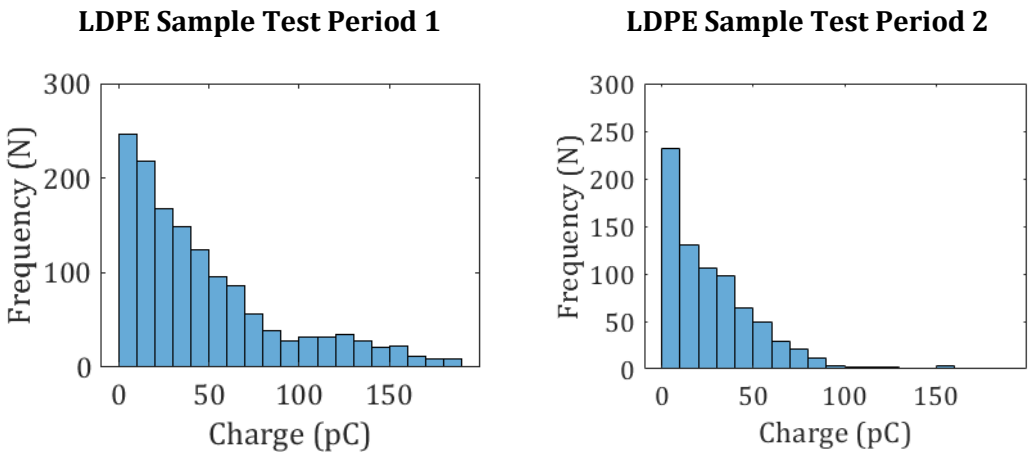

Figure 43 – Plots of frequency of difference from preceding pulse for DC testing of single void LDPE sample.

A similar pattern can be seen in Figure 44, which shows the distribution of the time between the PD pulses.

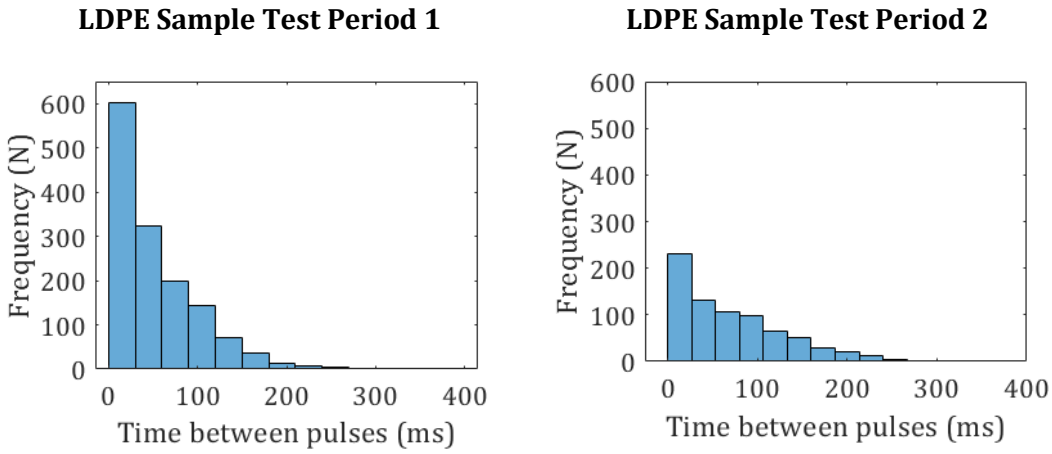

Figure 44 – Plots of frequency of time between pulses for DC testing of single void LDPE sample.

From this it can be seen that the most likely length of time between pulses is close to zero, with longer times becoming increasingly unlikely. In the second test

period the overall number of pulses is lower, and the likelihood of longer times between pulses becomes greater.

Figure 45 shows the cumulative charge plots for the two test periods. This shows that the total apparent charge recorded increases steadily over both test periods, with a sharper increase in the first test period, this matches with previous observations of the decreased number of PD pulses, and is comparable to previous work in this area[42].

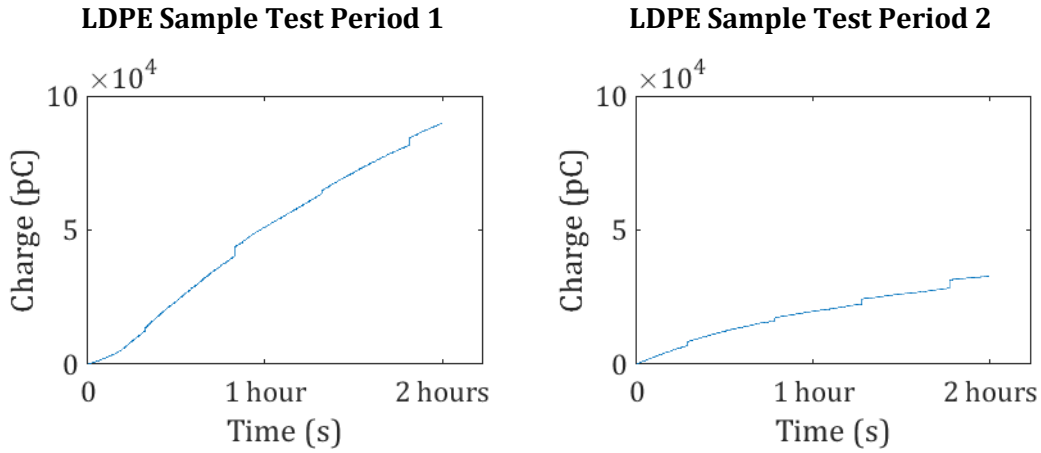

Figure 45 – Cumulative charge plots for DC testing of single void LDPE sample.

4.3. Conclusions

The first aim of this section was to ensure that the test equipment and methodology were suitable for the creation and detection of void-type defects which produce PD when subjected to sufficient electrical stress. The results of the AC testing, as displayed as PRPD and ϕ-q-n plots, were consistent with the results that would be expected from void-type defects, which confirms that the methodology and equipment are sufficient for this task.

Next, a comparison of the behaviour of PD in similar defects in two materials, low-density polyethylene and polypropylene, was made. Analysis of the PDIVs found that the material had no effect on the PD inception.

Analysis of the PRPD and ϕ-q-n plots for the AC testing of both materials also suggested similar PD activity regardless of the material, with greater differences between different samples of the same material, than between the two materials.

Differences between the materials were more apparent in comparisons of the distribution of the total recorded apparent charge of the PD events across the phase. With both the LDPE and polypropylene samples appearing to 'settle down' in the second test period as compared to the first, but in a different matter in each material. In LDPE, the distribution of the PD events became steadier, while the distribution of the size of these events increases. While in the polypropylene, the number of PD events continued to be variable, while the apparent charge values appear to be more evenly distributed in the second test period.

Other differences in PD behaviour between the materials was also apparent from the distribution of PD charge magnitudes as a percentage of the total PD events. With the LDPE showing a greater range of PD apparent charge magnitudes contributing to the total observed charge, and the polypropylene samples being more concentrated in values closer to zero.

Lastly LDPE samples were subject to DC stresses to confirm that the thin film methodology and measurement set-up were suitable for DC testing. This was confirmed by the results obtained, which were consistent with previous testing performed on void-type defects created by other methods, as well as the understood physical mechanisms of PD under DC conditions.

Due to the observation of the PD 'settling down' after the first two-hour test period, data recorded in subsequent chapters began after a two-hour period of test voltage application.

4.4. Evaluation

Overall, this section demonstrates that validity of the testing methodology applied, with void-type defects successfully created, and PD consistent with void-type defects measured under both AC and DC conditions. This allowed for a comparison of LDPE and polypropylene samples under AC conditions, and DC testing results for LDPE to be generated.

The equipment used for the PD measurement in this section was the Lemke Diagnostics LDS-6. This unit broke irreparably during the collection of data of this chapter, so the number of samples that could be tested, particularly under DC

conditions was reduced, which is a limitation of this section. Future chapters will present data collected via the LeCroy Waverunner 104Xi.

5. AC Analysis of Void Configurations in Layered Polymers

This section details the results from the AC testing of the thin film samples with different void configurations. Specifically, samples with a single void, with two voids in a parallel configuration and two voids in a serial configuration were tested (as detailed in Chapter 3). Five samples of each void configuration and polymer type were tested. The data presented in this chapter were captured using the LeCroy Waverunner 104Xi.

5.1. PD Inception Voltages

PD inception voltages were determined via the process described in Chapter 3. As such the mean measured voltage at the input side of the transformer, the percentage range of these values, and the inferred voltage at the output of the transformer (the PDIV) are presented. As before the test voltage was 10% higher than the PDIV.

Table 7 – Partial discharge inception voltages for AC tests of thin film samples using LeCroy Waverunner 104Xi.

			PD Inception Voltage			Test (kV)
Voltage	**Sample Material**	**Void Configuration**	**LV Input (V)**	**Range**	**HV Output (kV)**	
AC	LDPE	Single	15.6	±2%	**4.1**	4.5
		Parallel	13.2	±3%	**3.5**	3.9
		Serial	16.1	±3%	**4.2**	4.6
	PP	Single	14.7	±2%	**3.9**	4.3
		Parallel	12.7	±4%	**3.3**	3.6
		Serial	15.8	±3%	**4.1**	4.5

The LDPE samples consistently had a higher PDIV than the polypropylene samples, regardless of void configuration. When compared to the results for the PDIVs for the tests on the single void samples (Table 6) using the LDS-6, the PDIVs found with the LeCroy Waverunner 104Xi. This is likely due to the 104Xi being less sensitive than the LDS-6, meaning that the applied voltage at with PD was detected was higher. The differences between these measurement devices was further discussed in Chapter 3.

In both materials, the presence of parallel voids decreased the PDIV, with the presence of serial voids producing a (smaller) increase in the PDIV. This suggests that the orientation of defects relative to the electric field applied to the material has an impact on the formation of partial discharges. Serial voids decrease the amount of solid insulation material across the field lines when compared to the single voids, while parallel voids do not. This means that the electric field within the parallel voids and single void for a given voltage will be similar, while for the serial voids this field would be weaker. The observation of a reduced PDIV for parallel voids when compared to a single void implies that multiple voids under the same field conditions leads to a higher likelihood of detectable PD at a lower value of applied voltage. This effect applies to partial discharge inception in both materials.

5.2. Test Results

Once the PDIVs were determined, each of the five samples for both materials were tested by the procedure described in Chapter 3. These results are presented below as phase-resolved partial discharge plots (PRPD); plots of phase, charge, and number of discharges(ϕ-q-n); and plots of the frequency of occurrence of charge magnitudes.

5.2.1. PRPD

The initial function of the PRPD plots is to confirm that PD has been detected within the void(s) in each of the samples. This allows for a comparison of the PD behaviour for the different void configurations.

5.2.1.1. *Single Void*

An example of the PRPD plot for the five single void LDPE samples is shown in Figure 46. In these the peak apparent charge values occur leading the positive and negative peaks of the AC waveform, as is typical of void-type defects. Comparing these with the plot for the single void polypropylene samples (shown in Figure 47), shows a similar pattern, again indicative of a void-type defect. The LDPE samples show a more concentrated pattern, with generally lower peak apparent charge values spread out more evenly across the AC cycle, in contrast the polypropylene samples show higher apparent charge values more

concentrated in the first and third quadrants. This difference was not apparent in the PRPD plots presented in Chapter 4; however, the plots of phase and charge distribution did suggest behaviour similar to this in both the LDPE and polypropylene samples. One possible reason for this difference is that the test voltage applied for tests recorded using the LeCroy Waverunner 104Xi was higher than that for the tests recorded using the Lemke Diagnostics LDS-6, as the former set-up is less sensitive to PD (not detecting values of pulse amplitude equivalent to an apparent charge of 100 pC or less, while the LDS-6 detected many pulses in this range), necessitating a higher voltage before PD inception is detected. For this reason, as well as simply being unable to record PD events of insufficient apparent charge magnitudes, the apparent charge values detected in this chapter are generally higher than in the previous chapter.

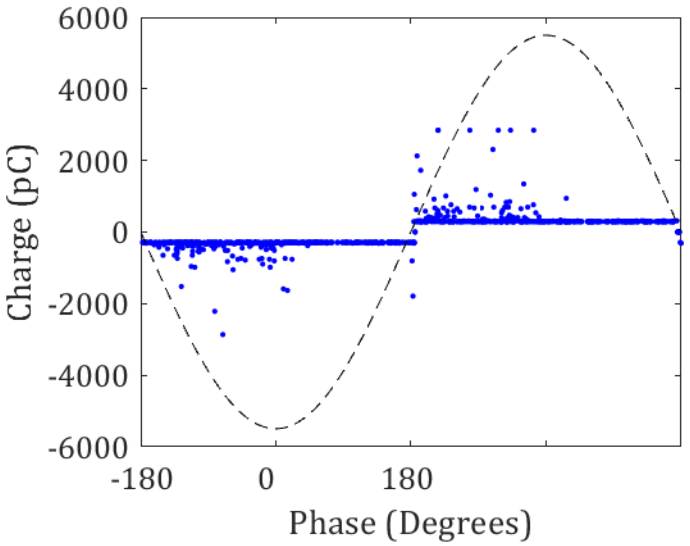

Figure 46 – PRPD plot for AC testing of single void LDPE samples.

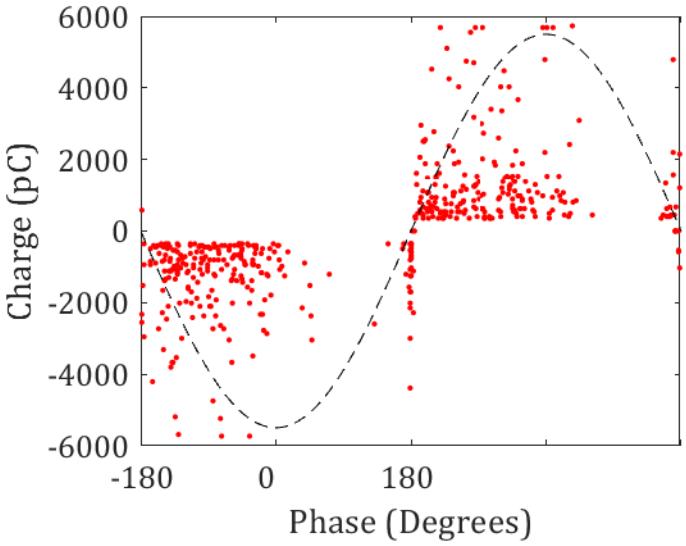

Figure 47 – PRPD plot for AC testing of single void PP samples.

5.2.1.2. *Parallel Voids*

The PRPD plots for the samples of LDPE with voids in a parallel configuration are shown in Figure 48, with PD patterns again indicative of void type defects. When compared with the single void patterns the distribution of the PD events across the phase is greater, while a greater number of PD events have an apparent charge closer to the detection threshold.

Considering the PRPD plot for the polypropylene samples with parallel voids, shown in Figure 49, differences can be seen with the parallel void LDPE patterns, with pulses significantly less distributed across the AC cycle. Comparing Figure 46 and Figure 48 (the patterns for the LDPE samples), with Figure 47 and Figure 49 (the patterns for the polypropylene samples), it can be seen there are more similarities among the PRPD patterns for the samples of the same material type, than for the same void configuration. This suggests that while the void configuration has an impact on the PD generation (by impacting the PDIV) the material type still has a noticeable effect on the PD presentation and development. It has been suggested the different molecular structure of materials, including differences in how easily electrons can be extracted from the void surface could have an impact on PD development[59], this would be a potential explanation for the differences in PD presentation between the materials..

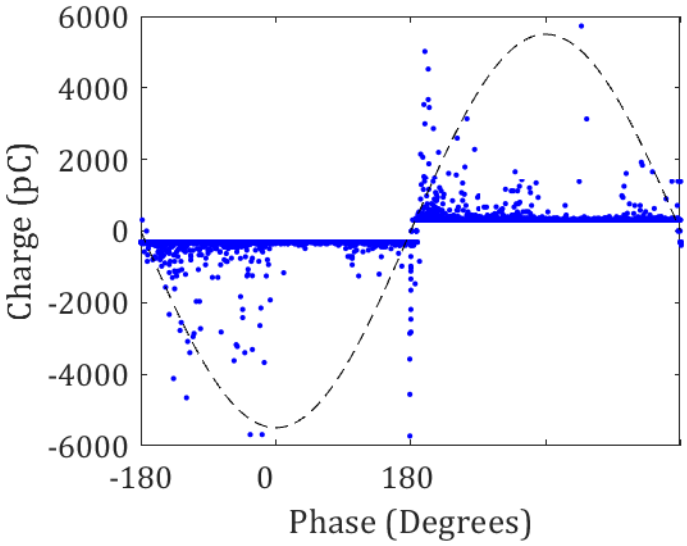

Figure 48 – PRPD plot for AC testing of parallel void LDPE samples.

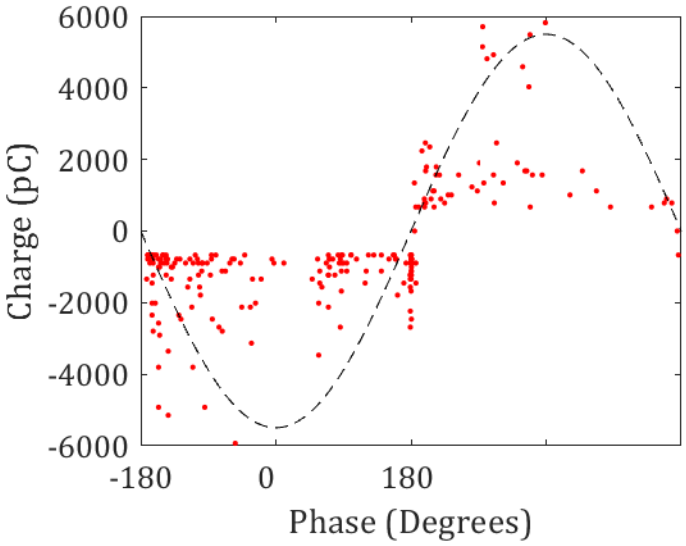

Figure 49 – PRPD plot for AC testing of parallel void PP samples.

5.2.1.3. *Serial Voids*

The samples containing serial void defects, produced PRPD patterns as shown in Figure 50 for the LDPE samples, and Figure 51 for the polypropylene samples. As with the previous PRPD plots presented in this chapter, these patterns are indicative of void-type defects. Also, as with the above patterns, the LDPE sample shows a greater distribution of PD events across the AC cycle, while the polypropylene sample shows a great distribution across the peak apparent charge values.

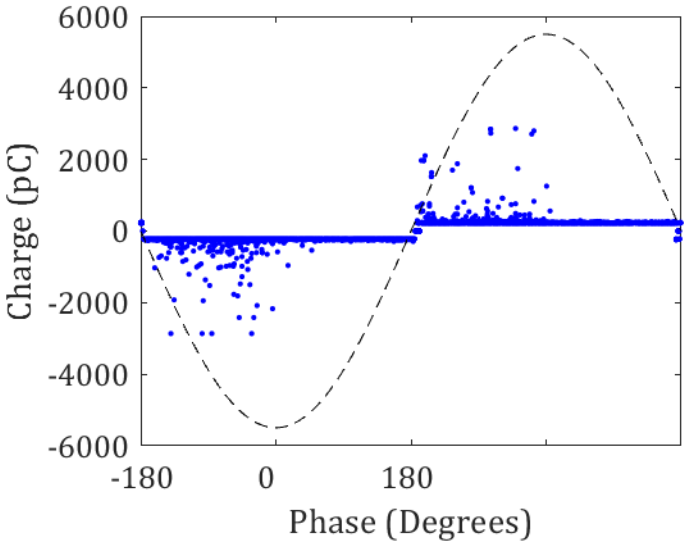

Figure 50 – PRPD plot for AC testing of serial void LDPE samples.

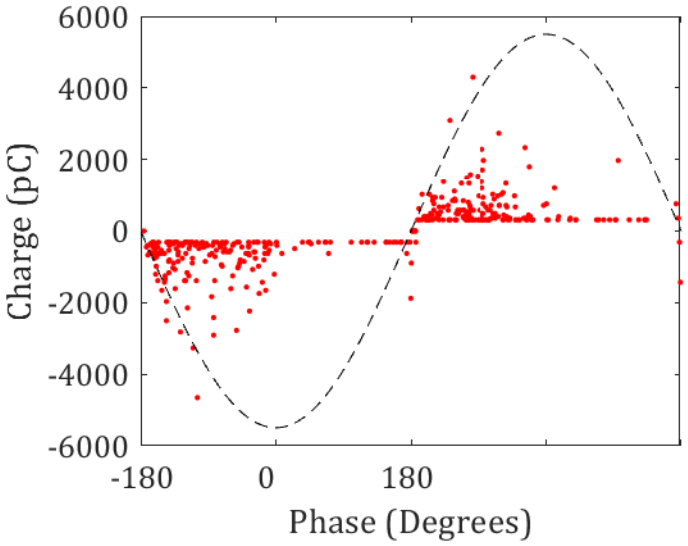

Figure 51 – PRPD plot for AC testing of serial void PP samples.

However, this difference is less pronounced, with the two patterns being more similar than was the case for the previously presented void configurations.

5.2.1.4. *Conclusions*

Overall, the PRPD patterns demonstrated the existence of void-type PD within each of the samples. It was found that there were greater similarities among different void configurations in the same material, than between the same void configuration in different materials.

5.2.2. ϕ-q-n

ϕ-q-n plots were generated for each of the void configurations in both materials, which take the PRPD patterns and add a dimension showing the number of pulses that occur at a given value of both phase and apparent charge.

5.2.2.1. *Low-Density Polyethylene Samples*

Figure 52 shows the ϕ-q-n plot for the single void LDPE sample. As with the PRPD plot, the pattern found ('rabbit-like') is strongly suggestive of PD within a void-type defect. The PD events were concentrated in the first and third quadrants, with a spread of events across the rest of the phase. This behaviour was suggested by the PRPD plots but is clearer using this representation.

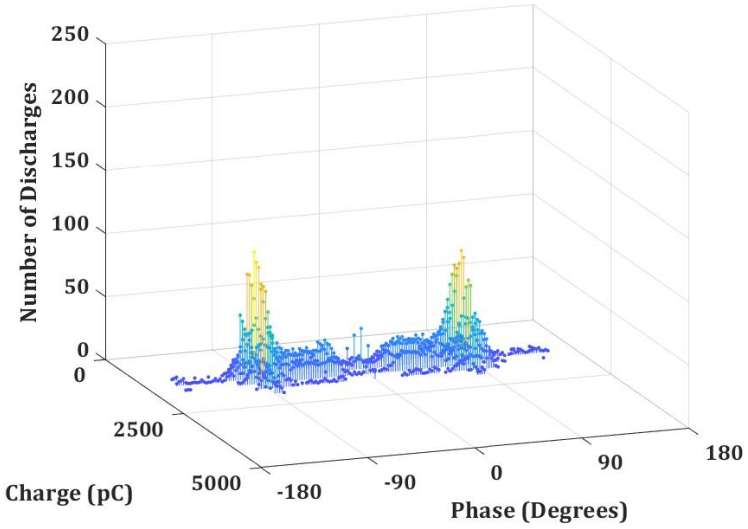

Figure 52 – ϕ-q-n plot for AC testing of single void LDPE samples.
Colours indicate the relative number of values at each point from yellow (highest) to dark blue (lowest).

The ϕ-q-n plot for the LDPE sample containing the two voids in parallel is shown in Figure 53. As with the single void LDPE sample, this plot also displayed the rabbit-like pattern of a void-type defect. In this case the 'ears' of the rabbit pattern are longer, and the 'body' of the pattern is also larger in all dimensions. This suggests that the parallel void sample is more active than the single void sample, while still maintaining a similar phase and charge distribution.

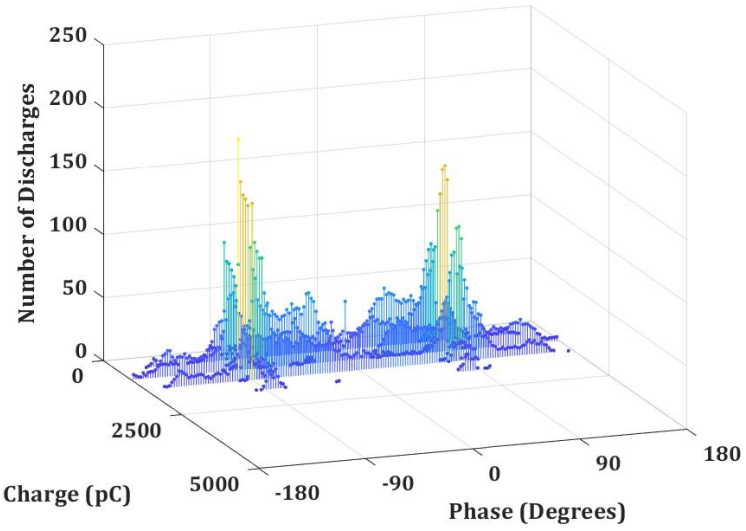

Figure 53 – ϕ-q-n plot for AC testing of parallel void LDPE samples.
Colours indicate the relative number of values at each point from yellow (highest) to dark blue (lowest).

Figure 54 shows the ϕ-q-n plot for the serial void LDPE sample, again with the indicative rabbit-like pattern. The serial void behaviour has 'ears' more similar to the single void samples, with a 'body' more similar to the parallel void samples. This suggests that the serial void samples were less active than the parallel void samples, while being more active than the single void samples. It is likely that PD activity is happening in each void (increasing the overall number of PD pulses detected) in both of the multiple void samples. However, it appears that the orientation with respect to the electric field has an impact on this, with the two parallel voids showing nearly a doubling of the activity of the single void, while the serial voids do not increase by as much. This suggests that there is a greater interaction between the PD activity in the parallel voids compared to the serial voids.

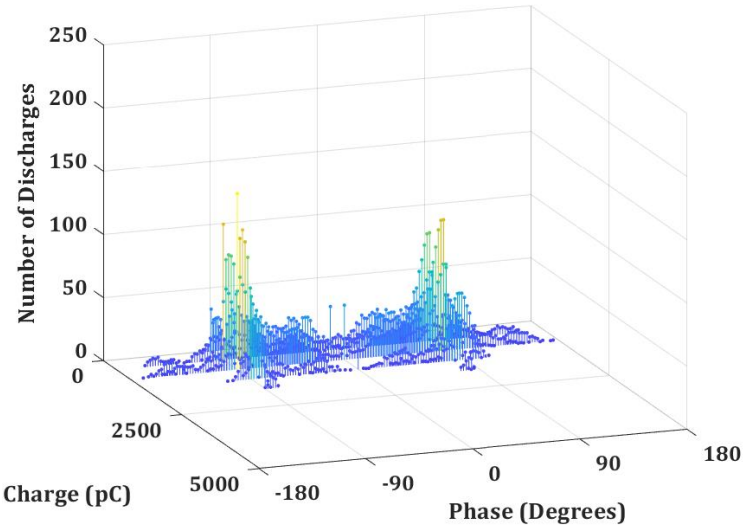

Figure 54 – ϕ-q-n plot for AC testing of serial void LDPE samples.
Colours indicate the relative number of values at each point from yellow (highest) to dark blue (lowest).

5.2.2.2. *Polypropylene Samples*

The ϕ-q-n plot for the single void polypropylene samples is shown in Figure 55, with the parallel void sample plot in Figure 56, and the serial void plot in Figure 57. All three plots show the void-type defect indicating rabbit like pattern.

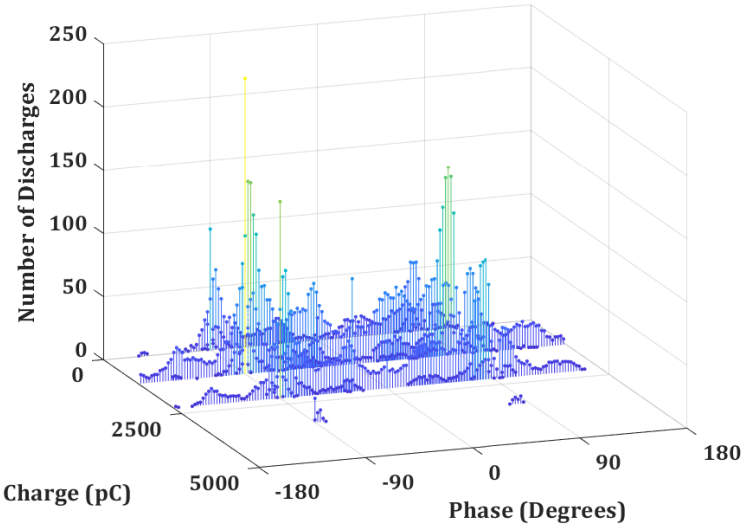

Figure 55 – ϕ-q-n plot for AC testing of single void PP samples.
Colours indicate the relative number of values at each point from yellow (highest) to dark blue (lowest).

The single void polypropylene samples produced a pattern with a larger 'body' than those of the LDPE samples, with a greater spread across values of apparent

charge, and less concentration (the 'ears' of the pattern) than previously. There was also an asymmetry present in the 'ears' with pulses more concentrated in the first quadrant than the third quadrant, unlike the relatively even distributions in the LDPE samples.

This asymmetry was also present in the parallel void polypropylene samples, while the 'body' of the pattern was more similar to the LDPE sample patterns, with less distribution across values of apparent charge.

Finally, the pattern for the serial void polypropylene samples, also demonstrated the asymmetry between the first and third quadrants, with a similar distribution in the rest of the pattern to that of the LDPE samples.

This implies that, unlike in the LDPE samples, the polarity of the voltage may have an impact on the PD in the voids in the polypropylene samples, as the two quadrants in question correspond to opposite peaks of the AC waveform.

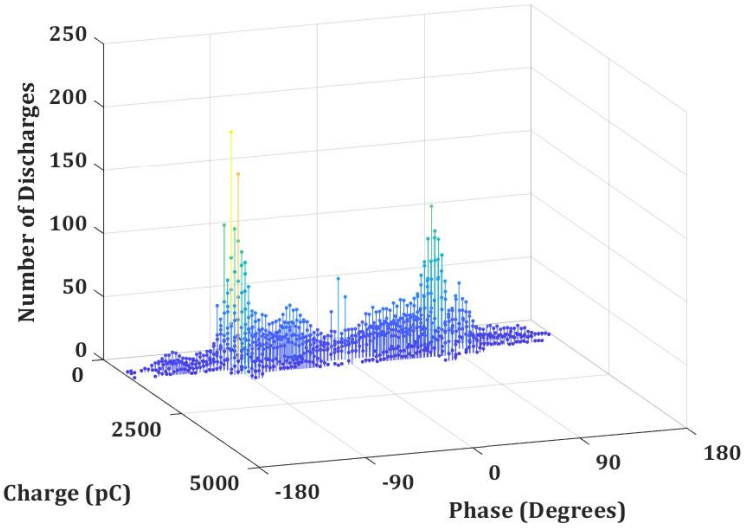

Figure 56 – ϕ-q-n plot for AC testing of parallel void PP samples.
Colours indicate the relative number of values at each point from yellow (highest) to dark blue (lowest).

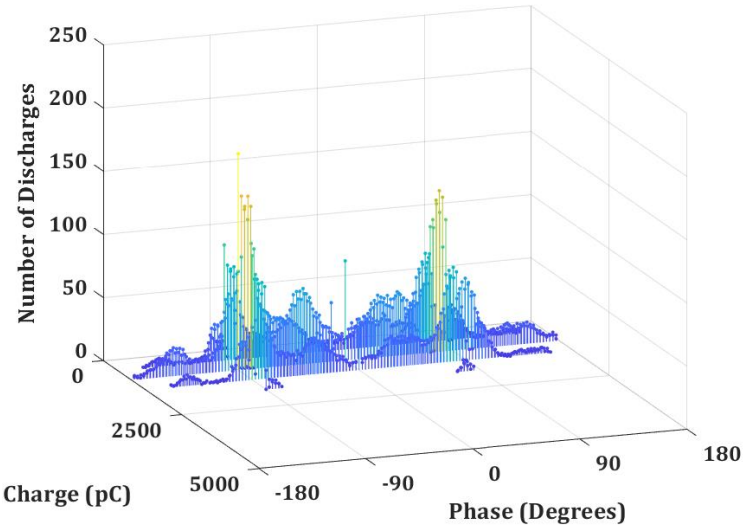

Figure 57 – ϕ-q-n plots for AC testing of serial void PP samples.
Colours indicate the relative number of values at each point from yellow (highest) to dark blue (lowest).

5.2.2.3. *Conclusions*

The ϕ-q-n patterns demonstrated some differences between different void configurations, but, as with the PRPD plots, there were greater differences between material types than void configurations. In the LDPE samples, the 'ears' of the pattern, were of a similar size, while in the polypropylene samples, the number of pulses in the first quadrant peak was greater than in the third quadrant. The first quadrant peak corresponds with the positive peak of the AC waveform, while the third corresponds with the negative AC waveform peak, suggesting that the polarity of the voltage has an impact on the PD development. This suggests therefore that the PD in the polypropylene is more sensitive to the voltage polarity than the polyethylene.

5.2.3. Pulse Sequence Analysis

Frequency distributions of charge characteristics (peak apparent charge, time between pulses, and the difference in peak apparent charge from the previous pulse) were also generated.

5.2.3.1. *Pulse Amplitude Frequency*

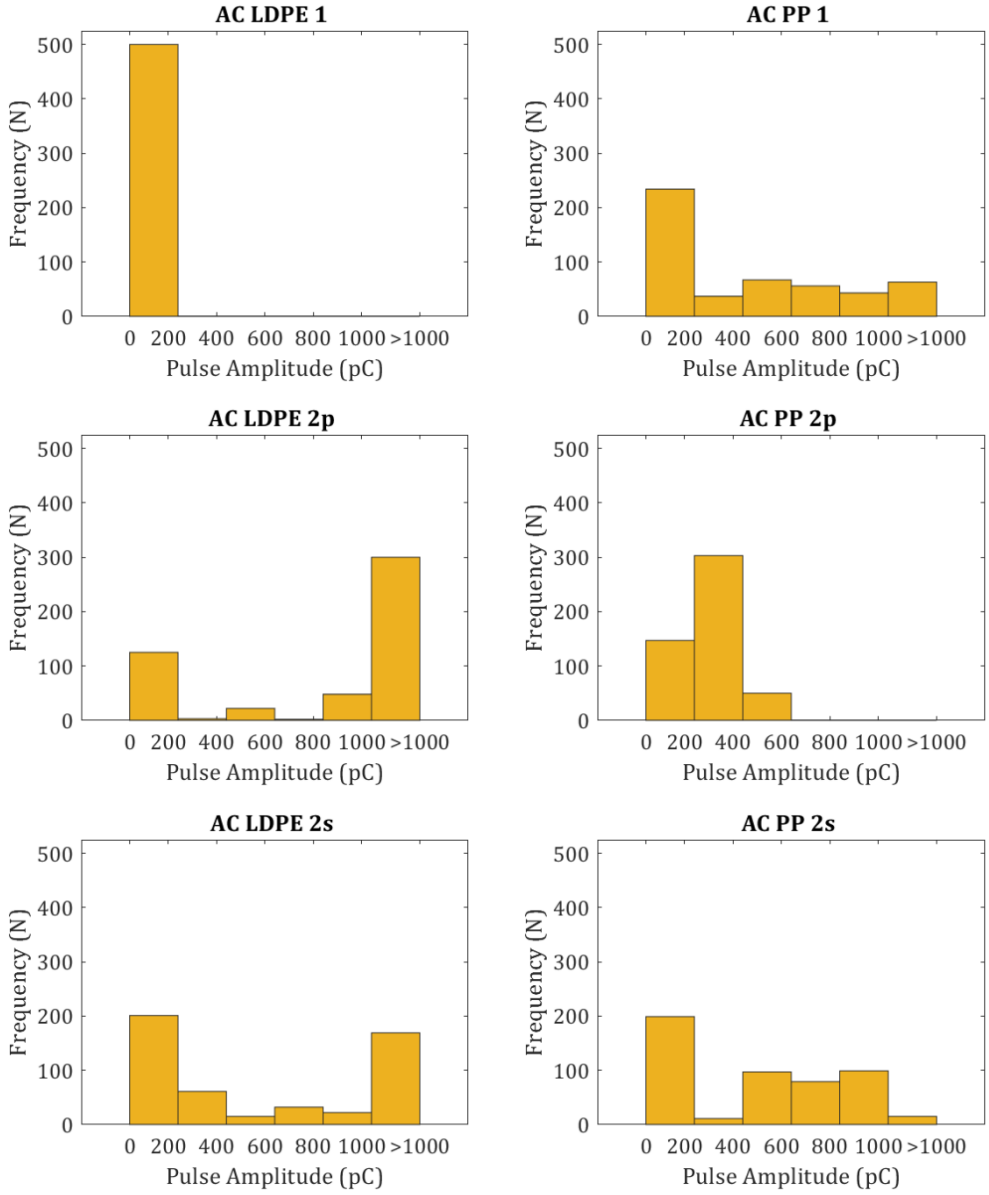

Figure 58 – Plots of frequency of peak pulse amplitude for each material and void configuration.

Frequency plots of peak apparent charge for each of the void configurations for both of the material types are shown in Figure 58. Comparing the different void configurations first, some differences in behaviour can be noted. Firstly, the majority of pulses in the single void samples of both LDPE and polypropylene, fall into the lowest bin of peak apparent charge (0-200 pC), particularly so in the LDPE sample. In the parallel and serial void samples, this is not the case. In the parallel samples, the majority of pulses fall into a higher bin (200-400 pC for the polypropylene, and >1000pC for the LDPE), while the serial void samples have a

more even split between the lowest bin (0-200 pC) and higher bins (>1000pC for the LDPE sample, and the 600-1000 pC bins for the PP). Comparing the two material types, does not suggest a consistency in behaviour between the LDPE and polypropylene samples, which conforms with the results found from the PRPD patterns and ϕ-q-n patterns.

5.2.3.2. *Successive Pulse Amplitude Difference*

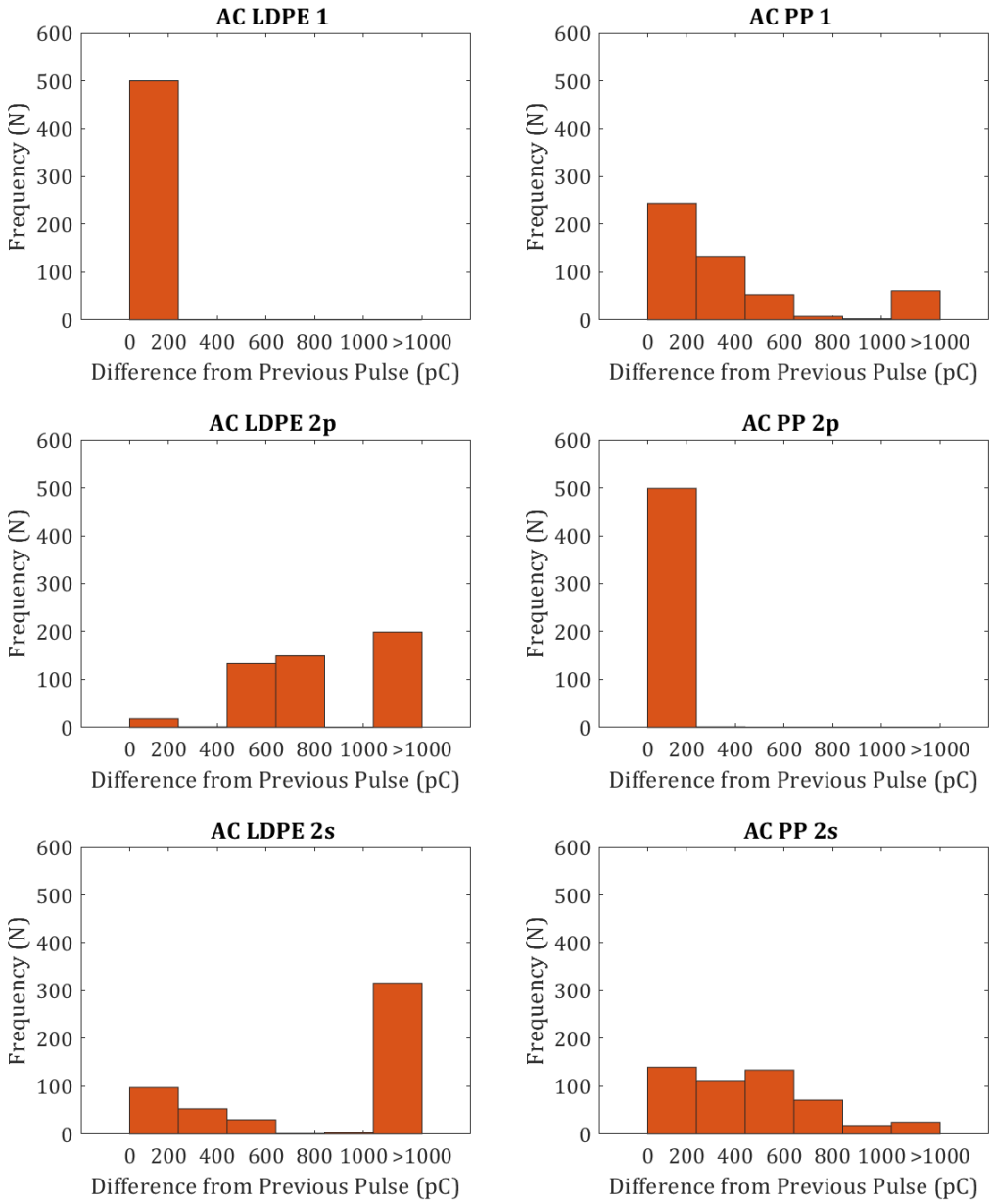

Figure 59 – Plots of frequency of difference in peak pulse amplitude between subsequent pulses for each material and void configuration.

Figure 59 shows the frequency of occurrence of the difference in peak apparent charge in a PD pulse when compared to the previous PD pulse. As might be expected, the PD sample types with the lowest range of peak apparent charge values (the single void LDPE and two parallel voids polypropylene samples), also have the lowest likely difference between pulses (between 0-200 pC). Considering the other samples there is a clear difference between the samples of the two materials. In the LDPE, PD events are more likely than not to be significantly different from the pulses preceding them, while in the polypropylene samples, this is not true, with the probability decreasing as the difference in apparent charge increases. This result is interesting and may be explained by looking at the average time between PD pulses, which are examined below.

5.2.3.1. *Time Between Pulses*

As discussed above, under AC conditions, PD reoccurs due to the alternating polarity, or every 10 ms. However multiple PD events can occur in one cycle, so the average time is likely to be less than this. The frequency plots of the time between pulses is shown in Figure 60. Once again, the LDPE single void samples, and polypropylene two parallel voids samples appear different from the other sample types. In the LDPE single void case, it appears that for most cycles recorded, there was only a single PD event, in each cycle. A significant concentration of single event cycles is also found in the polypropylene two parallel voids samples.

Comparing the other samples (Figure 60) similar distributions are seen throughout, with a spread across the bins covering 2.5-15 ms. The bin with the largest count is different for most of the different sample types, being 2.5-5 ms for the single void polypropylene samples, 7.5-10 ms for the two parallel void LDPE samples and two serial void polypropylene sample, and 5-7.5ms for the two serial voids LDPE samples.

The time between discharges does not appear to show consistent differences between void configurations or material types. While both do have a clear impact

on this metric, this relationship is not clear from the results found, and so conclusions on the causes of this impact are not clear.

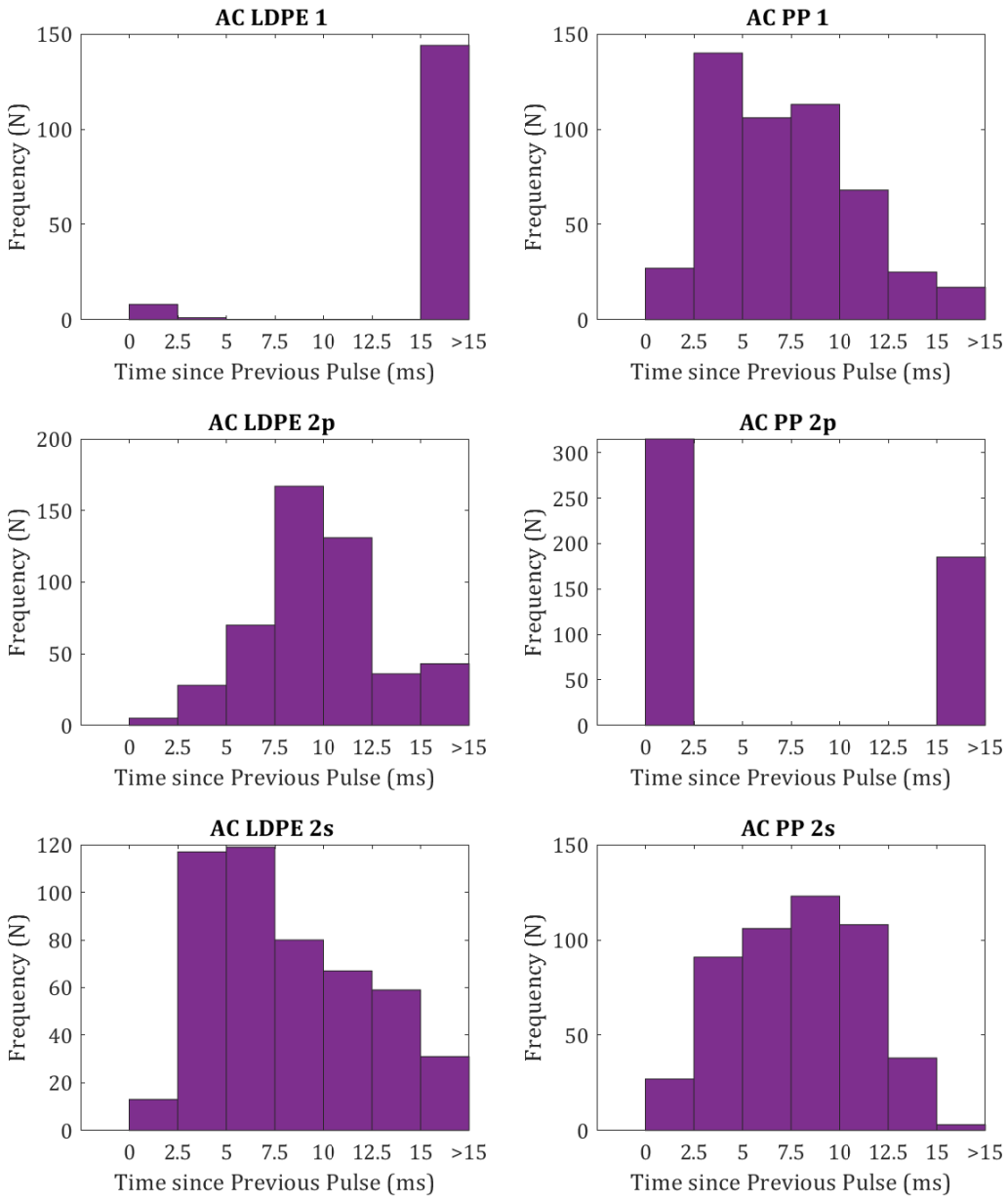

Figure 60 – Plots of frequency of time between subsequent pulses for each material and void configuration.

5.2.3.2. *Cumulative Charge*

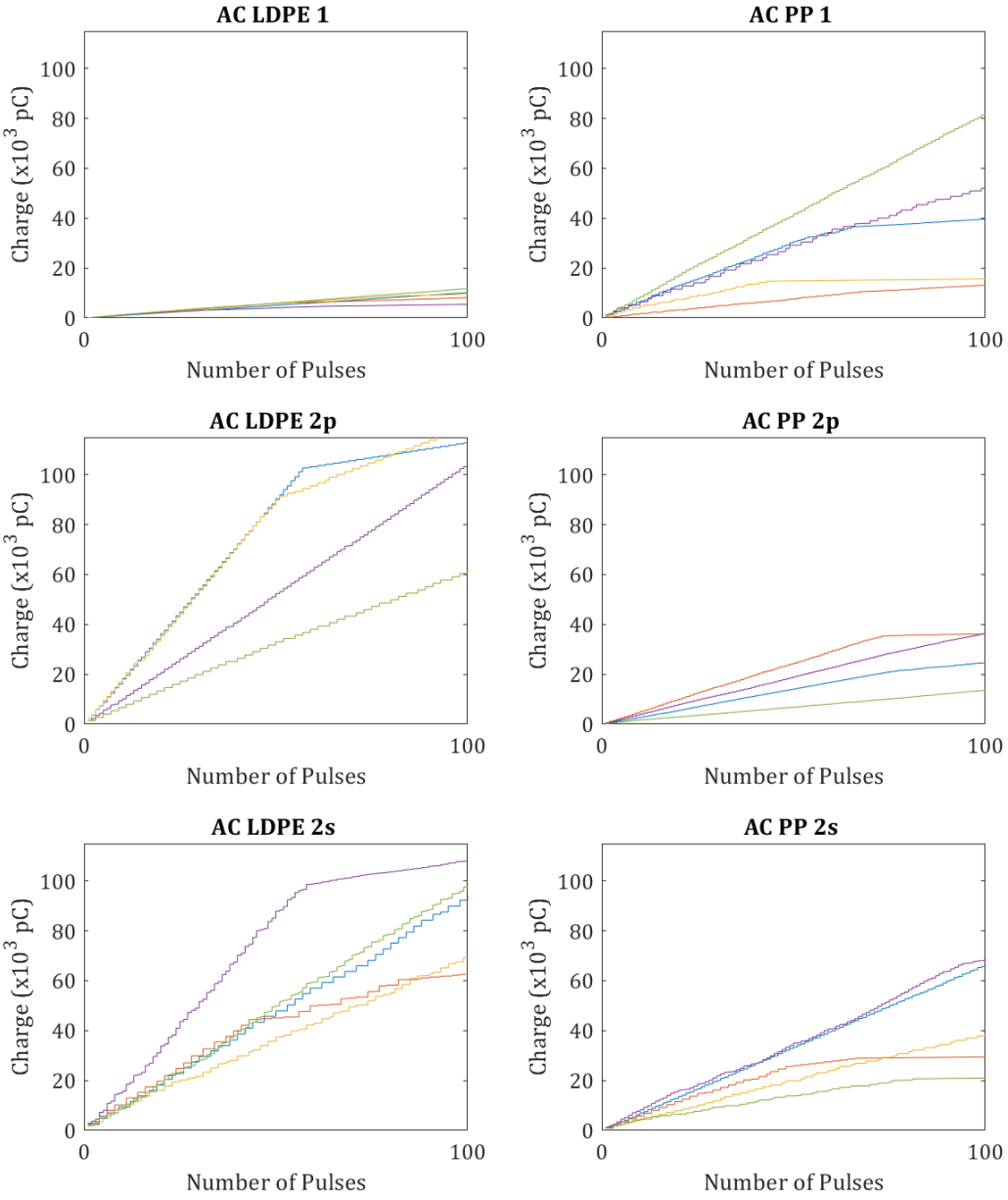

Figure 61 – Plots of cumulative charge for each material and void configuration, with plots for different samples in different colours.

The cumulative charge plots for each sample of each void configuration and material type are shown in Figure 61. Comparing these, it can be noted that greater differences are found between material types, than between void configurations. When multiple voids are present (either in serial or parallel configuration), the total charge over one hundred PD pulses, is significantly higher than when a single void is present in LDPE, while in PP the presence of multiple voids has significantly less impact.

5.2.3.3. *Conclusions*

Overall, pulse sequence analysis performed on the metrics of: peak apparent charge, peak apparent charge of pulses compared to their predecessor, time between pulses, and the cumulative charge over the pulses recorded, demonstrated some differences in behaviour between material types, and between void configurations. This behaviour was most distinct in the frequency of occurrence of peak apparent charges, with the difference in peak apparent charge compared to the previous pulse, and the time between pulses demonstrating significantly more variable behaviour.

5.3. Conclusions

The aim of this chapter was to present results captured from AC testing on samples of polyethylene and polypropylene, containing voids in the configurations of: a single void, two voids in a parallel configuration and two voids in a serial configuration, in order to determine what impact, if any, the different materials and void configurations have on the presentation and development of PD. Knowing these patterns can allow for better detection of PD, as well as determination of fault types and configurations.

The first metric analysed was the partial discharge inception voltage. Here it was found that the LDPE samples consistently had a higher PDIV than the polypropylene samples, this contrasted with the results from the more sensitive LDS-6. Additionally, it was found that presence of two voids in a serial configuration did not have a significant impact on the PDIV, whereas two voids in a parallel configuration did, reducing the PDIV significantly. This impact occurred in both materials tested. It is speculated that this is due to the orientation of the voids with respect to the electric field lines, in relation to the thickness of insulating material.

Next the phase resolved partial discharge and ϕ-q-n plots were analysed. From the former, it was found that each of the samples did have patterns that were consistent with void-type defects. It was also found that the material type had a greater impact on the recorded patterns than the void configuration, with a

consistently greater distribution of PD events across the phase of the AC waveform in the LDPE, and a greater distribution of PD events across the values of peak apparent charge in the polypropylene samples. Considering the ϕ-q-n plots, the same was also found, with greater differences between material types than void types. Specifically, the LDPE patterns showed greater symmetry, while the polypropylene patterns found higher PD in the first than the third quadrant, when considering the 'ears' of the pattern. This suggested a greater sensitivity to voltage polarity in the polypropylene than in the LDPE. Differences were also present in the 'body' of the pattern, with a more spread out body found in the polypropylene than in the LDPE, which was consistent with the findings from the PRPD plots.

Other metrics from pulse sequence analysis were also considered. Here it was easier to identify differences in behaviour between different void configurations, as well as further differences between material types. Considering the frequency of peak apparent charge values, it was found that single void PD events tended to fall in the lower end of recorded events, while in samples containing multiple voids (both serial and parallel) this was not the case. Additionally, the presence of parallel voids tended to cause the bulk of PD events to have higher apparent charge values, while the serial voids produced both lower and higher values of apparent charge compared to the single void samples. The difference in apparent charge values compared to the value of the previous pulse, and the time between charges, showed differences between each of the material types and void configurations, however these were not consistent between each category, making drawing conclusions from these results difficult.

Overall, the void configuration was found to have the greatest impact on PDIV, and then subsequently the values of apparent charge of the PD pulses, while the materials were found to have a greater impact on both the PRPD and ϕ-q-n patterns. With more field experience this information could inform PD defect assessment, as different than expected values of PDIV or PD patterns could indicate the presence of multiple voids.

5.4. Evaluation

This chapter was successful in presenting the results captured by the LeCroy Waverunner 104Xi of the different sample types. A good number of samples of each type allowed for confirmation of findings (unlike in Chapter 4). Although polyethylene and polypropylene are the most common insulating materials in cables today, other materials, such as high-performance thermoplastic elastomers, as well as polymers doped with nanoparticles, are also increasingly available. Potential extension to the work in this chapter would be to determine how these materials impact the activity of PD in defects within them.

6. DC Analysis of Void Configurations in Layered Polymers

This chapter explores the results from the DC testing of the thin film samples, with the different void configurations. As before, samples had a single void, or two voids in either a parallel and serial configuration (created as described in Chapter 3). Five samples of each type were tested under both positive and negative polarity DC stress. New samples were used for each polarity. The data presented in this chapter were recorded using the LeCroy Waverunner 104Xi.

6.1. PD Inception Voltages

The PD inception voltages were determined using the method detailed in Chapter 3. The mean measured input voltage at PD inception on the LV side of the transformer, the range of these values, the output voltage on the HV side of the transformer (the PDIV), and the voltage the samples of that type were tested at are shown in Table 8. As in previous chapters, the test voltage was 10% higher than the PDIV.

Table 8 – Partial discharge inception voltages for DC tests of thin film samples.

			PD Inception Voltage			Test (kV)
Voltage	**Sample Material**	**Void Configuration**	**LV Input (V)**	**Range**	**HV Output (kV)**	
−DC	LDPE	Single	49.9	%4	**18.6**	20.5
		Parallel	37.8	%2	**14.1**	15.5
		Serial	56.7	%3	**21.1**	23.2
+DC		Single	50.1	%3	**18.6**	20.5
		Parallel	40.4	%3	**15.0**	16.5
		Serial	52.5	%3	**19.5**	21.5

As indicated by IEC 60270, the PDIV values for the DC testing was significantly higher (2-3 times) than the AC testing of samples of the same configuration. The reason for this difference are explained by the differences in mechanisms for PD under AC and DC as explored in Chapter 2. As with the PDIVs for the AC testing, the results using the 104Xi are higher than using the LDS-6, this is also likely due to the increased sensitivity of the LDS-6.

Comparing the results under different polarities first, the negative polarity DC produced PDIV values that were lower than the positive polarity in the single and parallel void configurations, while producing higher values in the serial void configuration.

Comparing the different void configurations, it can be seen that, as with the AC testing, the parallel voids reduced the PDIV, while the presence of serial voids had led to a smaller increase in PDIV. As discussed in the previous chapter, it has been suggested that the orientation of defects with respect to the field lines of the electric field stressing the sample is what causes this difference in behaviour, so these results find that this effect is also present under DC conditions. This is despite the physical mechanisms for PD under DC being different from under AC as discussed in Chapter 2, thus this removes the possibility that this impact is related to the change in the electric field as the polarity shifts under AC conditions.

The test voltages applied therefore were (for both polarities) lowest for the parallel void samples, higher for the single void samples, and finally highest for the serial void samples.

6.2. Test Results

After determination of the test voltages, the samples were tested, as per the methodology described in Chapter 3, with the peak apparent charge, and time of occurrence, of the pulse recorded for each pulse over the test period. The results are presented in this section in the form of |Δq|-dt-n plots, as well as pulse sequence analysis histograms. These show peak apparent charge magnitude, the difference between apparent charge of pulses compared the previous pulse, and the time between pulses. Finally, cumulative charge plots are presented.

6.2.1. |Δq|-dt-n

The |Δq|-dt-n plots present the number of PD pulses which fall into bins corresponding to values of peak apparent charge, and the time elapsed between the previous pulse and the detection of the present pulse. The bin sizes were selected based on the range of values detected. The charge bins were given a width of 500 pC, from 0 pC up to 5000 pC, with a final bin for the values detected

outside this range. The time bins were given a width of 10s, from 0 to 60s, with a final bin for values outside of this range. This gave a total of 77 bins in to which each pulse could be sorted with each bin giving the time window and the magnitude range.

Figure 62 shows the |Δq|-dt-n plots for the single void samples, tested under both positive and negative polarity DC voltages. There was a significant difference in how the PD presented under these different polarities. Under negative polarity DC the PD pulses were large and occurred infrequently, while the positive polarity DC produced pulses that had smaller apparent charges, but that recurred much more frequently. This behaviour is interesting and could be related to the recurrence mechanism of PD under DC conditions, as discussed in Chapter 2. As indicated, the longer between PD pulses, the greater the overvoltage past the breakdown field strength across the void, and thus the greater value of apparent charge. As to why the time between discharges would be lower under DC conditions, one explanation could be that the test voltage was higher under positive DC polarity. However, as the PDIV under both polarities was very similar, the difference in test voltage was not significant, making this unlikely. Another explanation could be that residual voltage was higher for the pulses under positive polarity DC, which could be related to how the charge dissipates into the material. These results suggest, therefore, that the polarity of the DC voltage applied to the sample, has an impact on how the charge generated in the void dissipates, this can be further explored through the use of pulse sequence analysis comparing the relationship of pulses to the pulses preceding them, which is performed in section 6.2.2.

The |Δq|-dt-n plots for the parallel void sample tests under negative and positive DC polarity are shown in Figure 63.

Again, different behaviour is found in the samples stressed under positive polarity and those stressed under negative polarity.

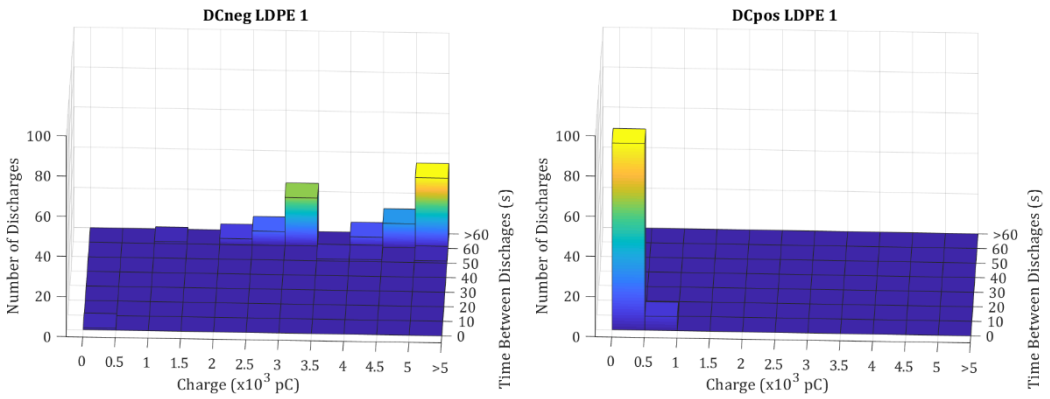

Figure 62 – |Δq|-dt-n plots for –DC (left) and +DC (right) tests of single void LDPE samples. Colours indicate the relative number of values falling in each bin from yellow (highest) to dark blue (lowest).

The pulses from the samples stressed under the negative polarity DC are more spread-out than those stressed under positive polarity DC, both by apparent charge values, and the time between the pulses. The negative polarity pulses are also clustered around a higher value of apparent charge, as well as a lower value of time between discharges. While this difference is not as pronounced as in the single void samples, it is clear that the polarity of the applied voltage has a similar impact i.e. decreasing the time between discharges, and thus increasing the peak apparent charge values. When multiple voids are present, the time between discharges is for pulses in either void, which will likely impact the relationship between time between discharges and apparent charge. As before, this suggests a relationship between the voltage polarity and the charge dissipation into the material.

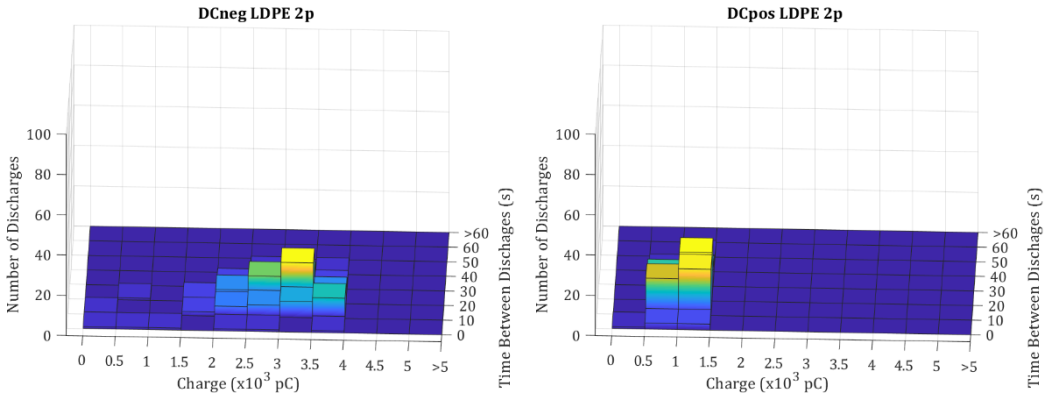

Figure 63 – |Δq|-dt-n plots for –DC (left) and +DC (right) tests of parallel void LDPE samples. Colours indicate the relative number of values falling in each bin from yellow (highest) to dark blue (lowest).

Lastly, the |Δq|-dt-n plots for the serial void samples are shown in Figure 64, for both positive and negative polarity DC voltages. As with the parallel void samples, the pulses were more spread-out in terms of both peak apparent charge, and time between charges under negative polarity DC stress, than positive polarity.

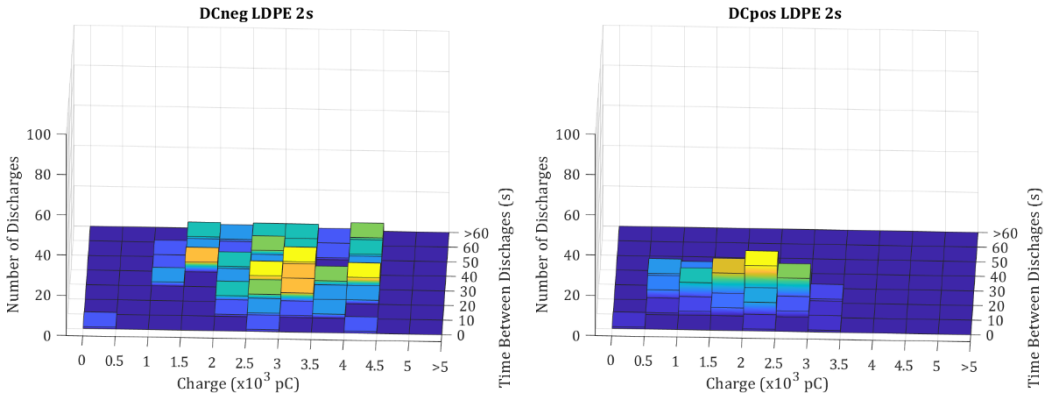

Figure 64 – |Δq|-dt-n plots for –DC (left) and +DC (right) tests of serial void LDPE samples. Colours indicate the relative number of values at each point from yellow (highest) to dark blue (lowest).

The negative polarity PD pulses were very well spread-out amongst the available bins of both time window and pulse magnitude. The positive polarity pulses were spread out to a lesser degree, with more clustering around high values of peak apparent charge, and lower values of time between discharges. There was less of this clustering present in both the single void or two parallel void configurations. This once again suggests that the polarity has an impact on the time between discharges, and, by reducing these, causing increased peak apparent charge values. This again implies that the voltage polarity has an impact on how the charge dissipates into the material, which, again, can be explored further by the use of pulse sequence analysis, as done in section 6.2.2.

6.2.1.1. *Conclusions*

Overall the |Δq|-dt-n plots highlight several differences between the behaviour of the partial discharge pulses under negative polarity DC when compared to positive polarity DC. In all void configurations, the time between pulses was shorter under positive DC, while the peak apparent charge values were lower. It is suggested that this is related to the charge dissipation into the material (which is the mechanism of PD recurrence under DC). Additionally, the presence of multiple voids also had an impact, with a greater spread of both peak apparent

charge, and time between charges, when either parallel or serial voids were present, with a greater impact from the serial voids.

6.2.2. Pulse Sequence Analysis

6.2.2.1. *Pulse Amplitude Frequency*

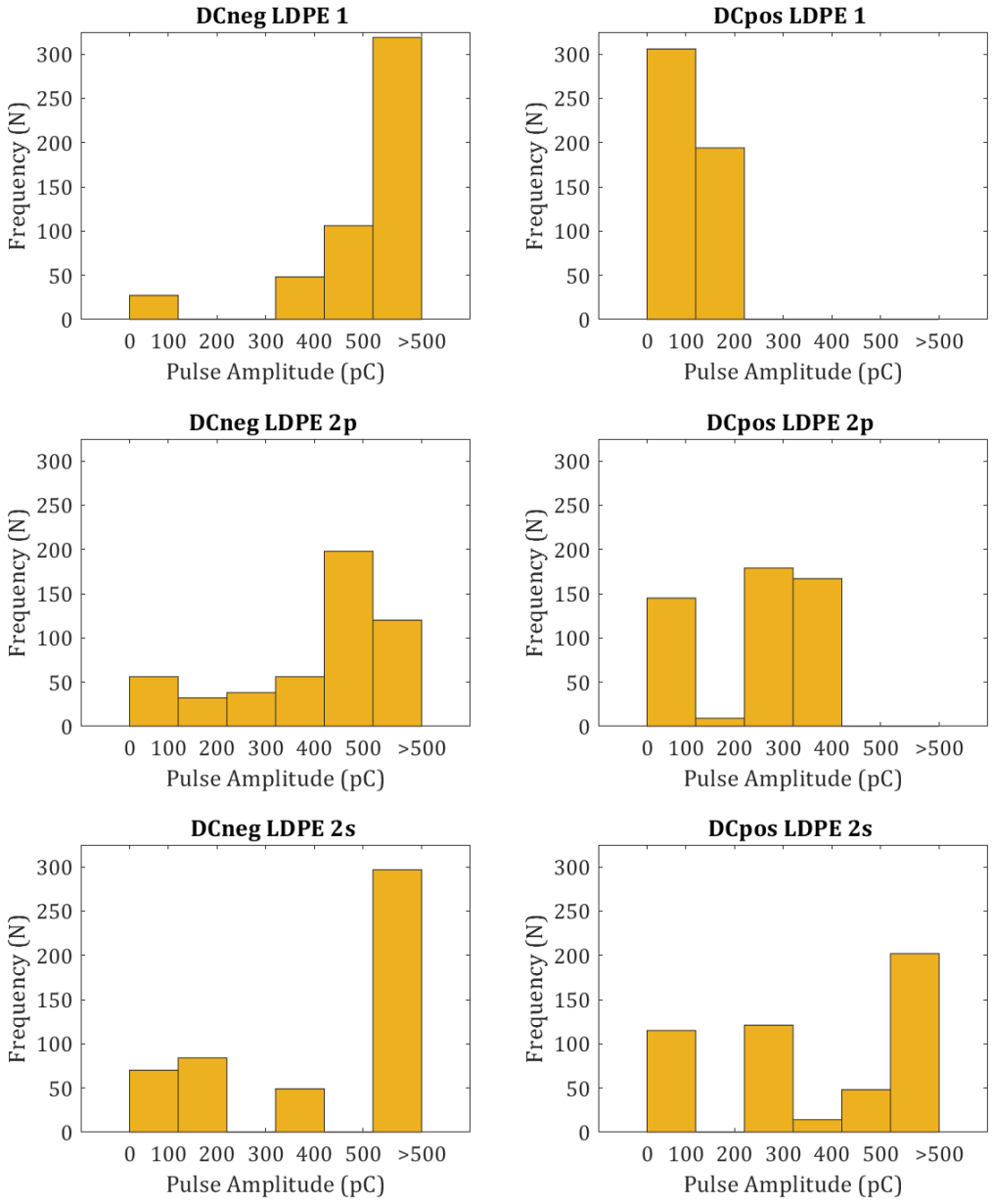

Figure 65 – Plots of frequency of occurrence of peak pulse amplitude for tests on the LDPE samples under (left) –DC and (right) +DC.

The frequencies of peak apparent charge magnitudes for each of the samples of the different void configuration, and under both positive and negative polarities, are shown in Figure 65. Comparing the results for the different samples, for the

negative polarity first, it can be seen that the average apparent charge is more similar for the single and serial voids, with generally higher peak apparent charges, compared to the parallel voids, which were more spread-out. Part of the reason for this could be that the PDIVs (and therefore test voltages) for the serial and single void configurations was similar, while the PDIV for the parallel void samples was significantly lower, as there is a positive correlation between applied voltage and pulse magnitude, a lower test voltage would produce on average pulses of smaller magnitude. This was also true for the tests under positive polarity DC; however, these samples all behave differently in terms of frequency of peak apparent charge values. In these samples, the single void had the most concentrated spread of apparent charge values, with a greater spread in the parallel samples, and the greatest in the serial void samples. Overall, under both DC polarities, the presence of multiple voids leads to a greater range of apparent charges, while the negative DC tends towards higher values on average.

Comparing these results with the AC results from the previous chapter, some differences are apparent. It is usually assumed that PD under DC conditions will have lower values of apparent charge than under AC conditions[71]. From these results, this is true for all of the sample configurations, with the exception of the single void LDPE sample, which had unusually low values of apparent charge when compared to the rest of the AC testing results.

As discussed in Chapter 2, the PD repetition rate under DC conditions is dependent on the test voltage, which is also true for the peak apparent charge of the pulses, so as the test voltages for the samples tested under DC were 2-3 times higher than for the samples tested under AC, this may explain why the differences in peak apparent charge are not as great as might be expected from the assumption (discussed in Chapter 2) that PD pulses that occur under DC have significantly lower magnitudes than those which occur under AC. As low values of peak apparent charge would occur at lower test voltages, where the repetition rate did not reach the one event per minute threshold.

6.2.2.2. *Subsequent Pulse Amplitude Difference*

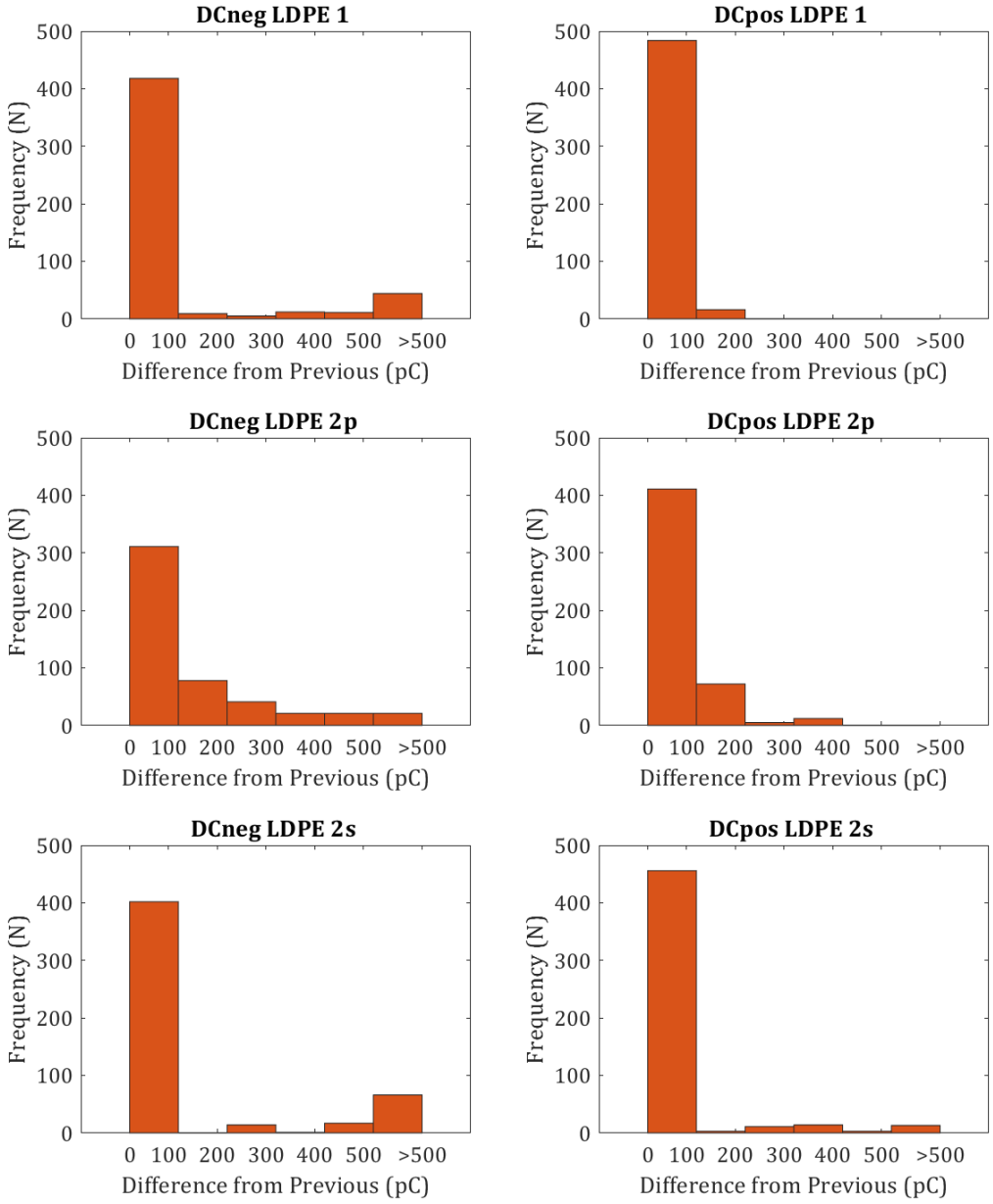

Figure 66 – Plots of frequency of difference between subsequent pulse amplitudes for tests on the LDPE samples, under (left) –DC, and (right) +DC.

Figure 66 shows the frequency plots of the difference in PD pulse apparent charges compared to the previous pulse. For each of the void configurations, under both negative and positive DC polarity, it is clear that the present PD pulse is most likely to have a very similar value of peak apparent charge to its predecessor. The samples tested under negative polarity DC are more likely than those tested under positive DC to have values outside of the smallest bin, with a

range found up to the highest bin in each of the void configurations. For the positive DC tests, this range is only found within the serial void configuration.

As with the values of peak apparent charge, the range of values is lowest in the single void configuration, greater in the parallel void configuration, and greatest in the serial void configuration. As before, overall, the presence of multiple voids led to a great spread of values than in the single void configurations.

Comparing these results to the AC testing of the LDPE samples of each configuration highlights some differences in PD pulse behaviour. The single void sample behaves similarly under AC conditions as under negative (and particularly) positive DC conditions, with the bulk of PD pulses having a difference of less than 200 pC from the previous pulse. The behaviour of the samples containing multiple voids was markedly different however, with very few pulses closely resembling the pulse that preceded them.

6.2.2.3. *Frequency of Time Between Pulses*

The frequency of time between pulses for each void configuration and voltage polarity is shown in Figure 67. From this, clear differences can be seen between the behaviour of PD pulses under different testing conditions. Looking at the single void samples, there is a clear distinction between the pulses tested under negative DC polarity, as compared to those tested under positive polarity DC. Under negative polarity testing, the pulses were fairly well spread-out, while under positive polarity the time between pulses was consistently short. This behaviour is also markedly different from the behaviour when multiple voids are present.

When multiple voids are present, the time between pulses follows a similar pattern to the positive polarity DC single void samples, with the largest number of pulses falling into the bin covering the smallest time between pulses, with a decreasing number of pulses falling into subsequent bins. The parallel void samples also showed a greater number of pulses falling into the shortest time between pulse range, than the serial samples under both DC polarities. This is interesting as the time between pulses analysis is the first analytical technique to

find greater differences between different void configurations than between different voltage polarities (although the voltage polarity still has an impact, particularly on the single void sample). While pulse amplitude and time between pulses are related (as per Chapter 2), comparing these metrics separately shows that similar distributions of time between pulses can still produce distinct distributions of peak pulse amplitude.

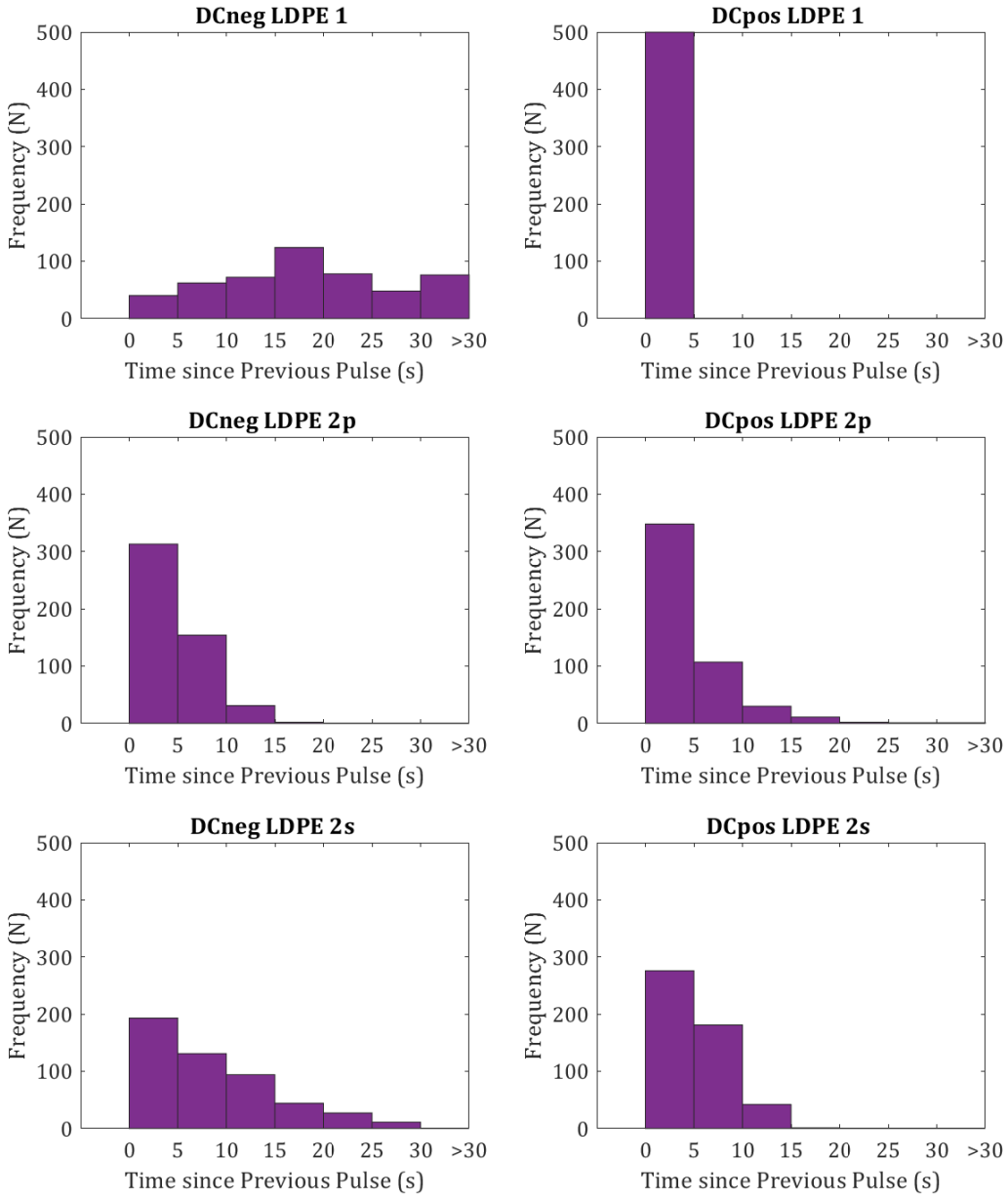

Figure 67 – Plots of frequency of time between subsequent pulse amplitudes for tests on the LDPE samples under, (left) –DC, and (right) +DC.

These results cannot be compared with the AC testing of the LDPE samples from Chapter 5, as the AC recurrence is much more frequent (on the scale of milliseconds rather than seconds).

6.2.2.4. *Cumulative Charge*

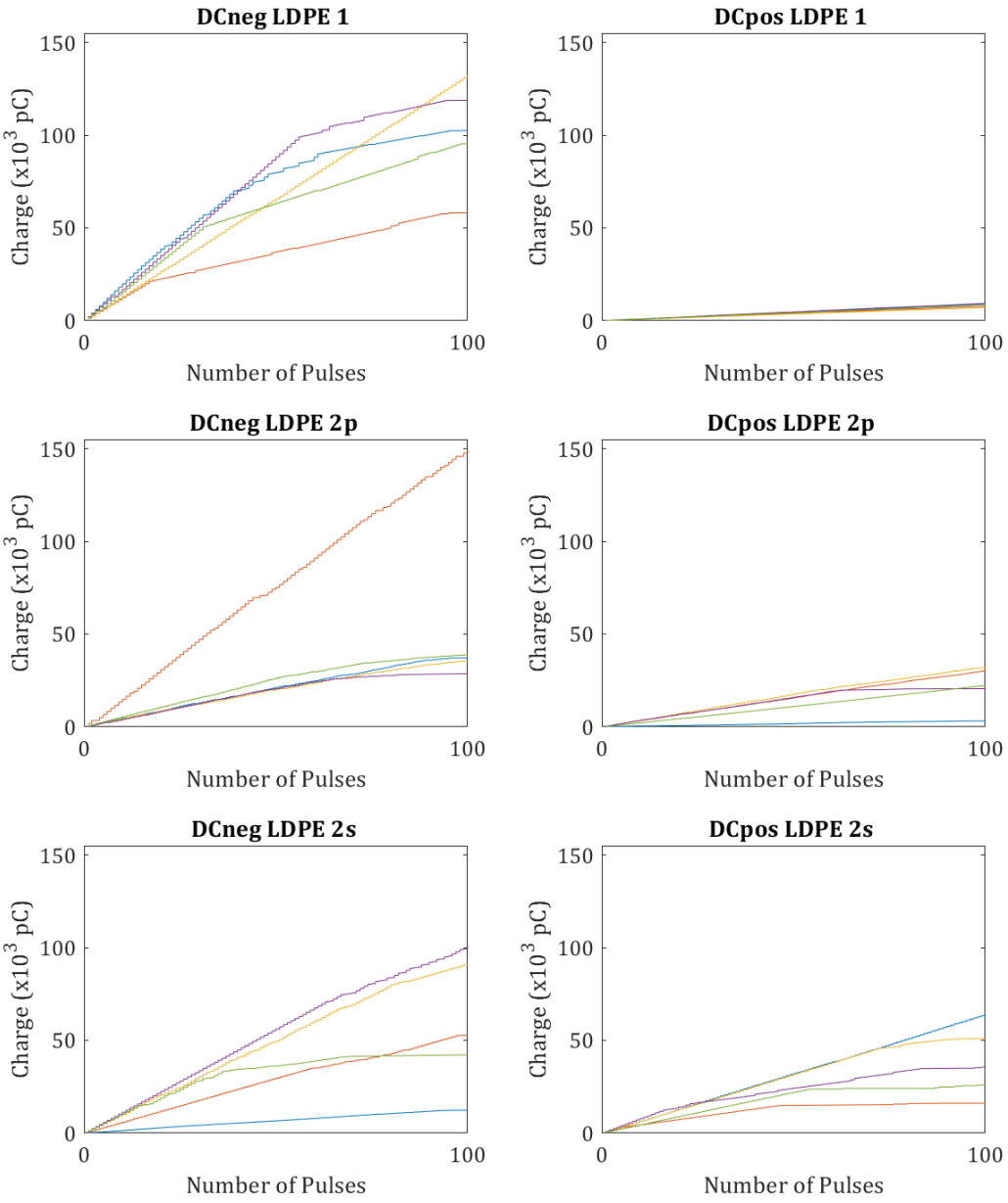

Figure 68 – Plots of cumulative charge for –DC (left) and +DC (right) DC testing of the LDPE samples.

Figure 68 shows the cumulative charge plots for the different samples of each void configuration, and DC voltage polarity. The most noticeable variation is between the total charge reached by the samples stressed under negative polarity

DC compared to positive polarity DC. The samples stressed under negative polarity DC saw a significantly higher total charge than those stressed under positive DC.

As discussed in previous sections, the negative DC pulses were generally of higher apparent charge, so this would account for the same number of pulses having a noticeably lower total charge under positive polarity DC. Under positive polarity DC, the presence of multiple voids increases the total charge over the test pulses, with the serial voids having a greater effect than the parallel voids. The negative polarity DC tests in contrast, show a similar range of charge cumulations for the single void and serials voids, while the parallel void samples tend to have a lower total charge (similar to the positive polarity parallel void samples tests) with the exception of one of the samples.

Overall, the presence of multiple voids under both polarities led to a greater range of total apparent charge values over the test period, with the negative polarity DC values being generally higher than those for the positive polarity DC.

6.2.2.5. *Conclusions*

Overall, several differences were noted from the pulse sequence analysis of the results of the DC testing when comparing both the voltage polarity and the void configuration. The peak pulse amplitude, difference in pulse amplitude from previous pulse, and cumulative charge measurements all presented differently under different voltage polarities, with smaller variations from void configuration, while the time between pulses was more impacted by void configuration than voltage polarity.

6.3. Conclusions

The aim of this chapter was to present results captured from DC testing of thin film samples of polyethylene with different void configurations, and under both negative and positive polarity DC. Void configurations tested were, single void, two voids in a parallel configuration, and two voids in a serial configuration. The results were presented to determine if the presence of multiple voids, or the

polarity of the DC voltage (or both) had an impact on the presentation and characteristics of partial discharge in the samples.

Firstly, the partial discharge inception voltages were determined. Initially, it was found that the PDIVs under both positive and negative DC were significantly higher than for the samples of the same void configuration tested under AC conditions, which conformed to expectations. It was discovered that, as had previously been found in AC testing, the presence of serial voids did not have a significant impact on the PDIV (increasing it slightly). Parallel voids, on the other hand, reduced the PDIV significantly. This suggests that the orientation of the void with respect to the electric field lines is significant in the determination of PDIV, this had been found previously under AC conditions, and so it is of interest that this is also true for DC conditions. The polarity of the applied test voltage did not have a consistent effect on the PDIV values, with negative polarity DC leading to a higher value for the serial void samples, and a lower value for both samples containing and single void and samples containing parallel voids.

The next analysis performed was the use of plots of the number of PD pulses that fall into assigned bins of magnitude of peak apparent charge on one axis, and time since the previous pulse on the other axis, or |Δq|-dt-n plots. Through these plots it was possible to determine several differences in PD activity between different void configurations and voltage polarities. Specifically, it was found that positive polarity DC led to shorter times between pulses, and thus lower peak apparent charges. It was theorised that this is related to charge dissipation into the insulation material. The presence of multiple voids also impacted PD activity, with a greater spread of both time between discharges, and peak apparent charge values, when multiple voids were present. This impact was strongest with serial voids as compared to parallel voids.

Pulse sequence analysis was also performed, with consideration of the frequency of occurrence of peak apparent charge values, the difference in value of peak apparent charge when compared to the preceding pulse, the time between discharges, and the cumulative charge of all the pulses recorded.

Peak apparent charge frequency plots showed that the presence of multiple voids increased the spread of values of apparent charge, with negative DC tending towards higher values in total. Serial voids in particular led to a majority of PD pulses falling in the highest bin.

Considering the frequency of difference in peak apparent charge from the previous pulse, found very similar behaviour under both polarities, and all void configurations, with most pulses closely resembling their predecessor. Negative DC conditions were more likely to produce pulses that were significantly different, while the presence of multiple voids only made this more likely under positive DC.

The frequency of time between pulses also highlighted different behaviour under the different conditions tested. In single void samples, the negative PD let to pulses that had a wide range of times between them, while the positive PD pulses were all in quick succession. However, when multiple voids were present, the PD behaviour tended to be similar, with most of the pulses occurring soon after the previous one, with the probability of a longer delay decreasing with the length of that delay. This finding is interesting, as the patterns of frequency of peak apparent charge (generally dependant on the time between discharges) were very different, even with similar patterns of frequency of time between discharges.

Lastly, plots of cumulative charge were considered. From these it was clear that the application of negative DC voltage consistently led to higher total charge values when compared to positive DC. One explanation for this could be asymmetries in the void defects. Although care was taken to ensure the voids were as close to cylindrical as possible, in practical terms the voids will not have been perfectly symmetrical. This lack of symmetry may have led to differences in field distribution at the upper and lower surfaces of the void, which, in turn, could lead to the voltage polarity having an impact on the development of the partial discharges.

Additionally, the presence of multiple voids led to a greater spread of total charge values whatever the polarity of the applied voltage.

In summary, both voltage polarity and the presence of multiple voids (and their configuration) have a measurable impact on PD activity in samples of polyethylene. This is of interest in terms of the use of PD monitoring, as suggests that if the polarity at which the cable is energised is known, then more accurate detection of PD would be possible. It was hypothesised that the potentially asymmetrical nature of the artificial voids contributed to this impact, so, since void defects which develop naturally will also be asymmetrical, this effect would be expected to be similar in a practical situation. In additional to voltage polarity considerations, differences in PD activity for different void configurations suggests that information about the nature of the defect may also be determinable.

6.4. Evaluation

Overall, this chapter was successful in achieving its aims, with the data collected being sufficient for analysis to be performed. 100 PD events was chosen as the number to record for each sample due to time and scope memory considerations (higher than this occasionally led to corruption in the files saved by the scope). This allowed for direct comparison between positive and negative DC, however due to the faster reoccurrence of positive DC, the recording time was occasionally less than the IEC 60270 recommendation of 30 minutes.

Unlike in the previous chapter, only samples of LDPE were tested, this was due to issues with inducing PD in the polypropylene samples under DC conditions. These issues were partially due to the reduced sensitivity of the LeCroy Waverunner 104Xi compared to the Lemke Diagnostics LDS-6, which prevented detection of PD in the PP before the breakdown strength of the material was reached. It was hoped that the LDS-6 could be repaired prior to the completion of this project but, despite best efforts, this was not achieved.

7. AC and DC Testing of Artificial Voids in XLPE Cable

This chapter is concerned with the results from AC and both positive and negative polarity DC testing of the XLPE cable sample, with the introduced artificial single void defect. These results are analysed using the techniques previously used on the thin film samples in Chapters 5 and 6, in order to confirm the validity of the artificial void creation method (as detailed in Chapter 3), as well as to identify features of PD behaviour in the cable sample. The results for this chapter were captured using the LeCroy Waverunner 104Xi.

7.1. Partial Discharge Inception Voltage

Determination of the partial discharge inception voltages was achieved using the method as described in Chapter 3. Table 9 shows the PDIV for the XLPE cable sample under AC, and both negative and positive DC polarity stresses, including the mean measured voltage on the input side of the HV transformer, the percentage range of these values, the inferred voltage on the output side (the PDIV), and the determined test voltage (10% greater than the PDIV).

Table 9 – Partial discharge inception voltages for DC tests of cable sample.

			PD Inception Voltage			Test (kV)
Voltage	**Sample Material**	**Void Configuration**	**LV Input (V)**	**Range**	**HV Output (kV)**	
AC	XLPE	Single	43.4	%4	**16.1**	17.7
−DC			54.2	%4	**20.2**	22.2
+DC			49.3	%4	**18.3**	20.1

For the cable the values of PDIV were higher for the DC voltages than for the AC voltages, although with less of a difference than the tests on the thin film polyethylene. One explanation for this could be that the voltage required for PD pulses of sufficient magnitude to be detected within the cable under AC conditions was higher than the actual breakdown voltage. This could be possible as there is a larger physical separation between the void where the PD is occurring and the earthing the HFCT is coupled with, than in the thin film test rig, meaning the pulse signal will attenuate more before detection.

The negative DC polarity PDIV was higher than the value for the positive polarity, suggesting the voltage polarity has an impact on the PD present in the XLPE cable. Unlike with the thin film samples, only one cable sample was tested, with at least 24 hours of grounding after cable de-energisation between tests. The order of testing was (as presented in the table) AC, negative polarity DC, positive polarity DC. This repeated testing may also have had an impact on the values of PDIV, although initial values of PDIVs were determined first for each voltage type to allow for the main testing, a PDIV was then recorded for each test.

7.2. Test Results

The samples were tested at the test voltages listed in Table 9 using the method described in Chapter 3. Apparent charge and time of occurrence were recorded for all tests, with phase as referenced to the output AC waveform recorded for the AC testing. For the AC tests only, phase-resolved partial discharge and ϕ-q-n plots are presented, while pulse sequence analysis histograms for: peak apparent charge, difference in peak apparent charge in successive pulses, and time between pulses. In addition, cumulative charge plots, and |Δq|-dt-n plots are presented for all tests.

7.2.1. PRPD

The PRPD plot for the AC tests on the XLPE cable is shown in Figure 69. The positive and negative peaks are found in the first and third quadrant of the AC reference phase, slightly leading both the positive and negative peaks, with more activity in the negative half-cycle than the positive one. This behaviour is typical of void type defects and confirms the presence of PD within the cable sample. There is also a range of small PD events across the phase (the distribution of which is difficult to determine using a PRPD plot). This behaviour is similar to what was found for the tests on the single void LDPE thin film samples, and contrasts with the less spread out values found in the polypropylene samples. This suggests that the behaviour of PD is similar in polyethylene, whether low-density or cross-linked, at least in comparison to PD in other materials, this is expected as the electrical properties of XLPE and LDPE, including charge accumulation, are similar[154].

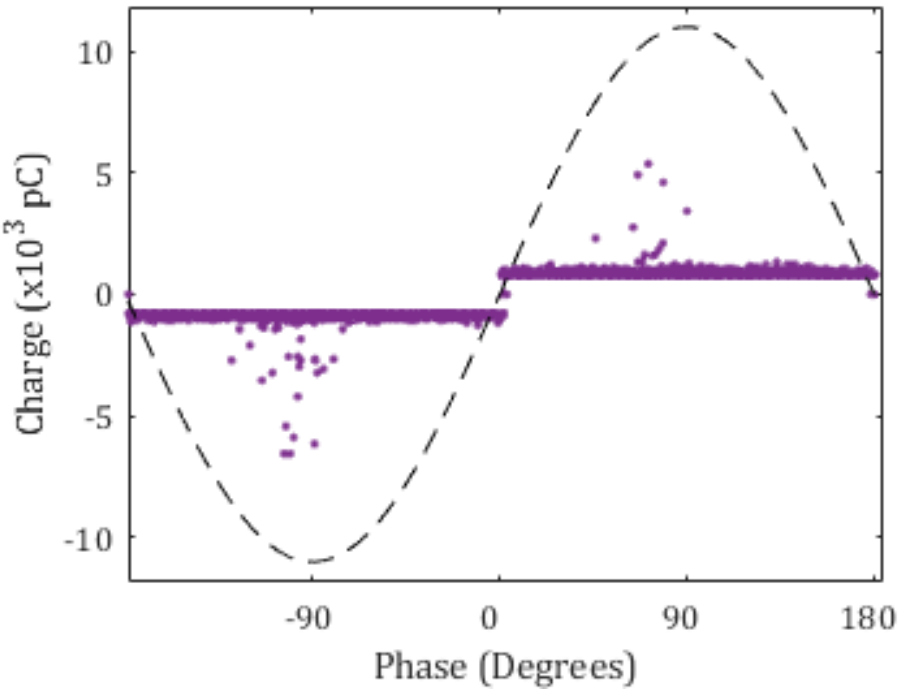

Figure 69 – PRPD plot for AC tests on the XLPE sample.

7.2.2. ϕ-q-n

Figure 70 shows the ϕ-q-n plot for the AC testing of the XLPE cable sample. From this the pattern indicative of void-type discharge, as discussed in previous chapters, can be seen clearly. This again is strongly suggestive of a void-type defect. As was found from the PRPD plot, PD events are spread across the phase, with particular concentrations at the first and third quadrants (leading the peaks of the AC waveform), forming the 'ears' of the pattern. The 'body' of the pattern shows that the largest peak apparent charge values also occur leading the AC waveform peaks. This behaviour is similar to that which was observed in the AC tests on void type defects in previous chapters.

In particular the distribution of PD pulses most closely resembles the single void LDPE samples. This again suggests similar behaviour in both XLPE and LDPE, in comparison to the behaviour in polypropylene. This is useful as it suggests that conclusions reached from the testing of LDPE in previous chapter are applicable to practical XLPE cables.

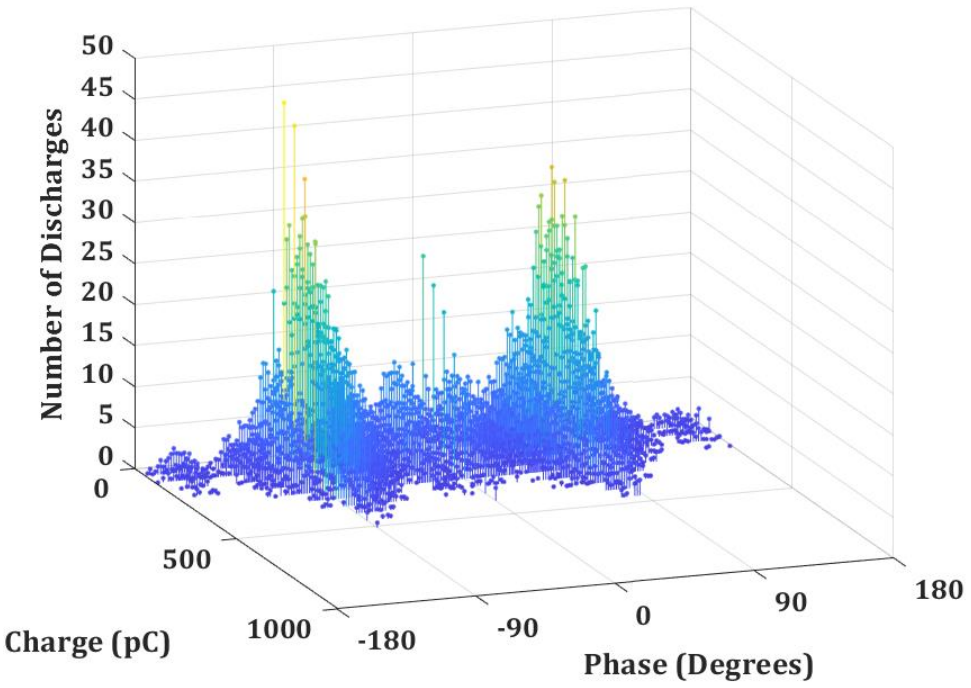

Figure 70 – ϕ-q-n plot for AC tests on the XLPE sample.
Colours indicate the relative number of values at each point from yellow (highest) to dark blue (lowest).

7.2.3. Pulse Sequence Analysis

7.2.3.1. *Pulse amplitude frequency*

The frequency plots of the peak apparent charge magnitude for the pulses recorded under all voltage types are shown in Figure 71. Considering the AC plot first, it is notable that the bulk of PD pulses occur over a small range towards the upper end of the available bins. This small range is similar to the behaviour in the single void LDPE samples which also showed the lowest range of recorded pulses of all the samples tested, however in that case the pulse amplitudes were at the lower end of those recorded.

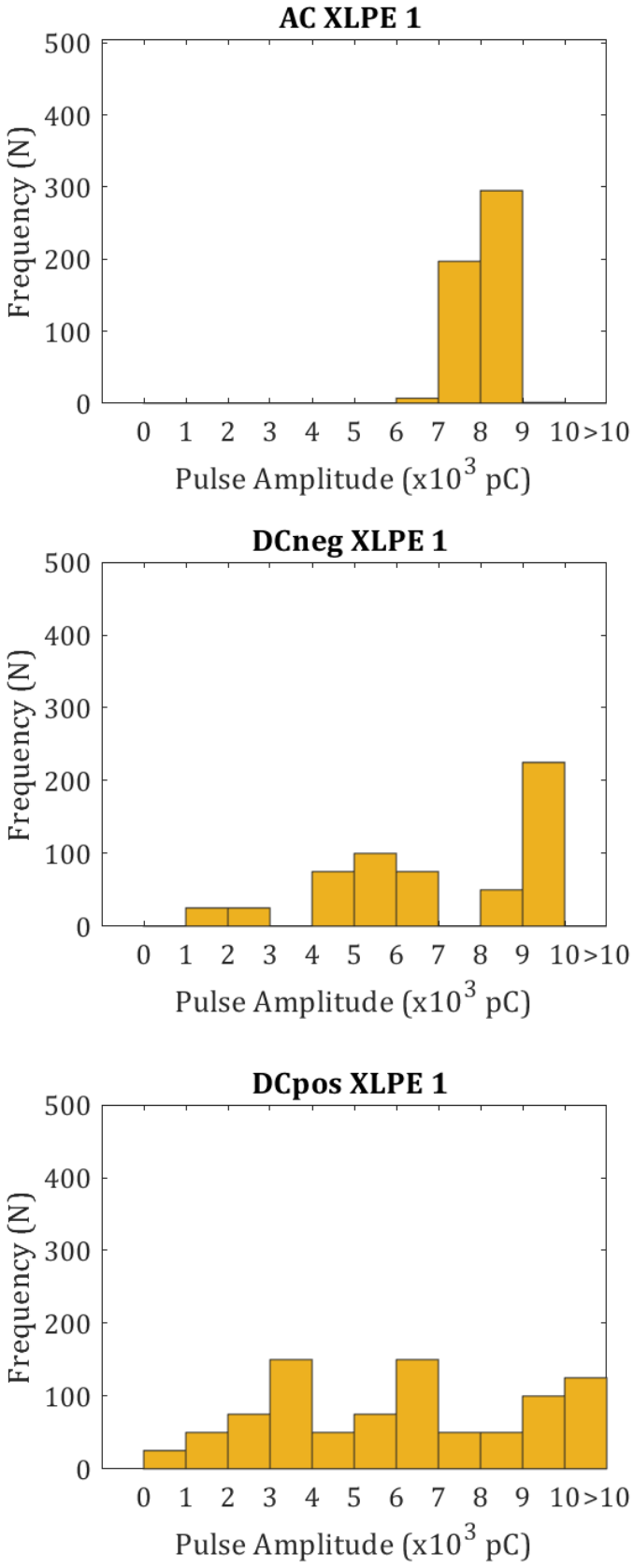

Figure 71 – Plots of frequency of occurrence of peak pulse amplitude for tests on the XLPE sample under (top) AC, (middle) –DC, and (bottom) +DC.

Considering the plots for the negative and positive polarity DC tests, it is noticeable that the behaviour of the PD, with regards to peak apparent charge amplitudes, is similar in both cases. In both polarities, there is a wide spread of values of peak apparent charge, with values slightly more concentrated in the negative polarity case. In the negative polarity case also, there is a trend towards values of peak apparent charge being more probably towards the higher end of the range. This behaviour was also found in the LDPE single void samples when tested under negative polarity DC voltage. However, the behaviour of the single void LDPE samples under positive polarity voltage does not strongly resemble the testing of the XLPE cable. Overall, there are some similarities between the behaviour of the XLPE cable when compared to the LDPE samples, with the AC and negative polarity DC having the least variation, and the positive polarity DC being the most distinct. This could be due to the difference in material; cross-linked instead of low-density, polyethylene. Although XLPE is created from LDPE, and there is a limited difference in the electrical properties of the two materials [154]. Therefore, it is more likely that the difference in physical set-up, the testing of a cable sample in comparison to the use of thin film samples in test rig, is the reason for the differences in PD presentation. Previous chapters have suggested an impact of electric field orientation on PD development, and the cable testing will have a different electric field pattern than the tests using the test rig due to the change from parallel electrodes to the cylindrical electrode of the cable conductor illustrated in .

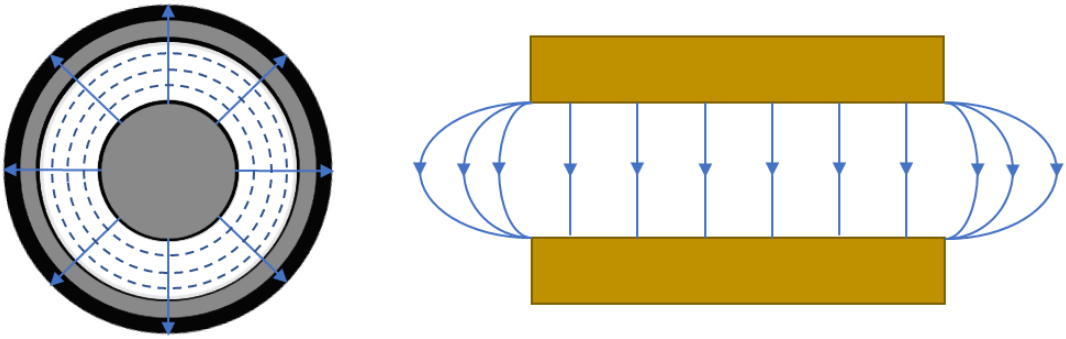

Figure 72 – Illustration of cross-section of electric field lines in (left) cable sample and (right) parallel electrodes of test rig.

7.2.3.2. *Successive Pulse Amplitude Difference*

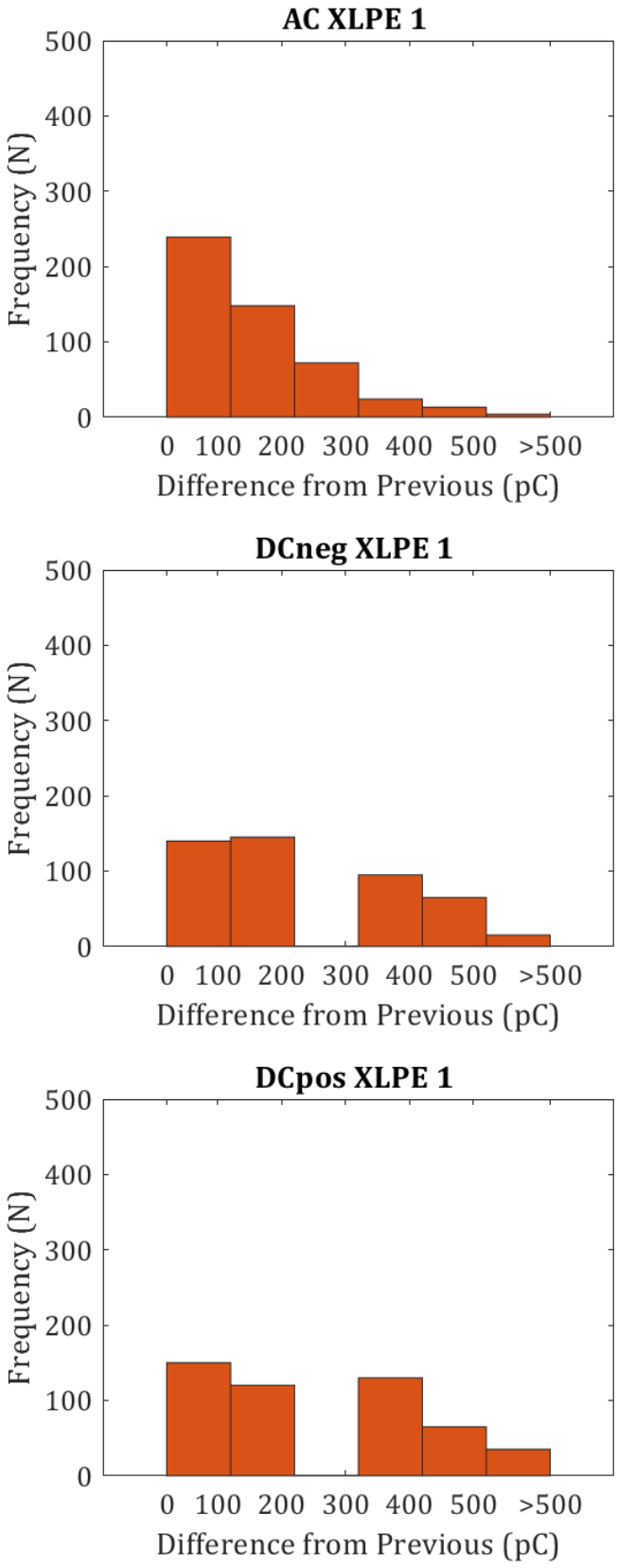

Figure 73 – Plots of frequency of different between subsequent pulse amplitudes for tests on the XLPE sample under (top) AC, (middle) –DC, and (bottom) +DC.

Figure 73 shows the frequency plots of the difference in peak apparent charge value of the PD pulses when compared to their immediate predecessor. The PD which occurred under AC voltage, were most likely to have a value of peak apparent charge that closely resembled the pulse immediately preceding them, with the probability of decreasing the greater the change in value. This was true to an even larger extent in the single void LDPE thin film samples, where all pulses closely resembled the pulse preceding them. This probability trend does not hold for the pulses found under either negative or positive polarity DC stresses. In both these cases, there was a far more even distribution of differences between pulses, with a roughly even likelihood of pulses falling into the first, second, and fourth bins, and a decreased likelihood of falling into bins greater than this. Curiously in both cases, no pulses fell into the third bin. This behaviour again differs from the single void LDPE samples, in which the significant majority of pulses closely resembled those preceding them. As with the peak apparent charge values themselves, this could be due to the difference in the applied electric fields between the different test methods.

7.2.3.3. *Time Between Pulses*

The frequency plots of the time between pulses are shown in Figure 74, due to the different methods of PD recurrence (discussed in Chapter 2) the timescale for the AC pulses was in milliseconds, while for the DC pulses this was in seconds. Considering the AC plot, pulses were more likely to occur less than 30 ms after the previous pulse, which corresponds to at least one pulse on each AC waveform cycle. The number of longer gaps, suggests cycles where no PD occurred were common, although less common than cycles containing PD. This behaviour is different from that which was found in the single void LDPE samples tested under AC stresses, where cycles without PD were not detected once the PDIV was reached. This may be due to different PD behaviour in XLPE when compared to LDPE or could be down to smaller PD pulses occurring that were not detected by the measurement system. The plots for the DC results highlight differences in behaviour between the pulses recorded under negative polarity, and positive polarity, DC voltages. The negative polarity DC pulses are more likely to occur

towards the upper end of the range of values of time between discharges, while the positive polarity pulses tended to occur with significantly less delay.

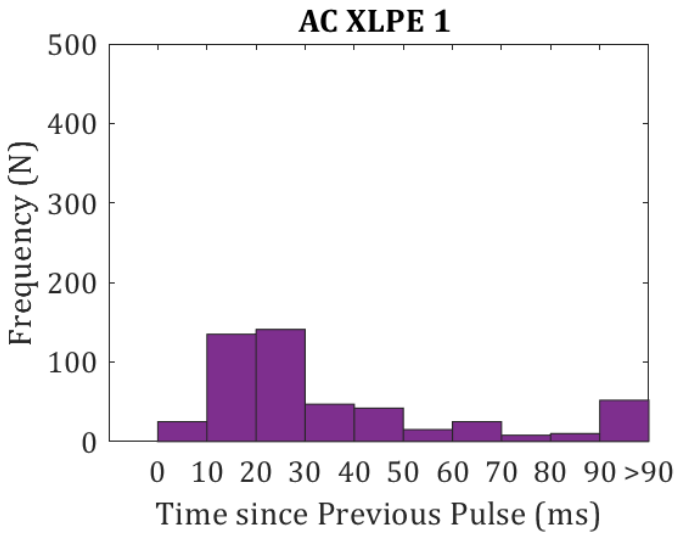

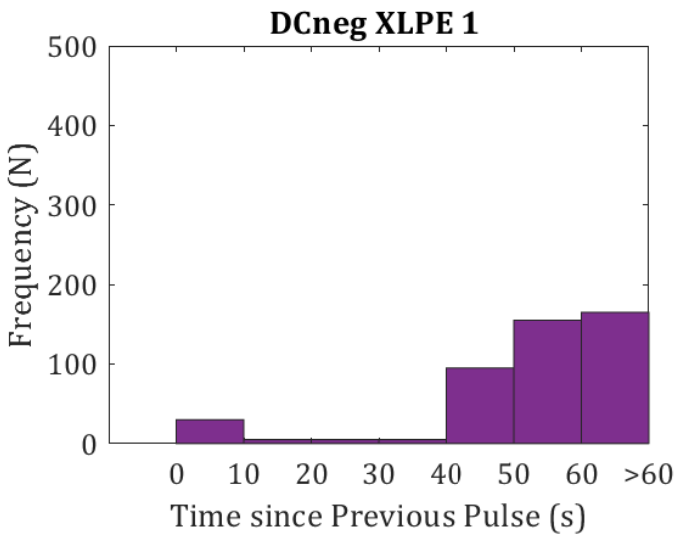

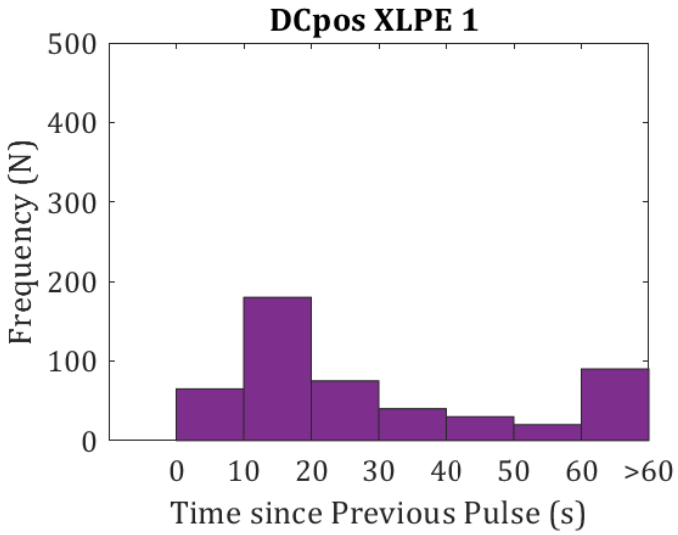

Figure 74 – Plots of frequency of time between subsequent pulse amplitudes for tests on the XLPE sample under (top) AC, (middle) –DC, and (bottom) +DC.

This behaviour was also found in the single void LDPE samples, which also had a longer average time between pulses under positive polarity DC than negative polarity DC. It was speculated in Chapter 6 that this was related to charge dissipation into the surrounding material (due to the mechanisms of PD recurrence under DC discussed in Chapter 2), so this may be true of XLPE as well as LDPE, since, as discussed above, these materials have similar electrical properties, including charge accumulation.

7.2.3.4. *Cumulative Charge*

The cumulative charge plots for the AC tests on the XLPE cable sample are shown in Figure 75. The five tests show a similar, steady, increase over the test period, with a similar total charge reached in each case. This small range of differences in cumulative charge plots was common in the previous testing of thin film samples where a single void was present, in particular the single void LDPE samples. This is another example of the XLPE cable sample behaving in a similar manner to the LDPE thin film samples containing a single void.

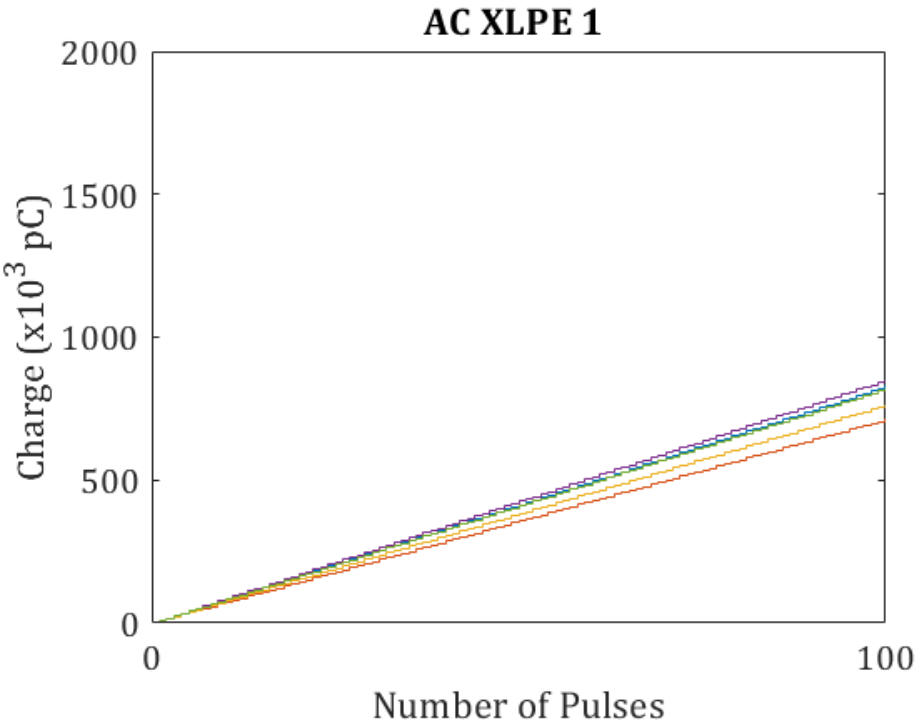

Figure 75 – Plots of cumulative charge for AC testing of XLPE sample.

Figure 76 shows the cumulative charge plot for the negative polarity DC testing of the XLPE cable. As with the AC plots, there is little variation between the different tests, with a greater consistency between plots than was found in the negative polarity DC testing of the LDPE samples. This could be due to the fact that several thin film samples were tested for each voltage type and void configuration, while only one cable sample was tested, leading to greater consistency. As with the AC testing, a similar value of total charge was reached in each case, although this value was higher than the AC testing, due to the higher average peak apparent charge values.

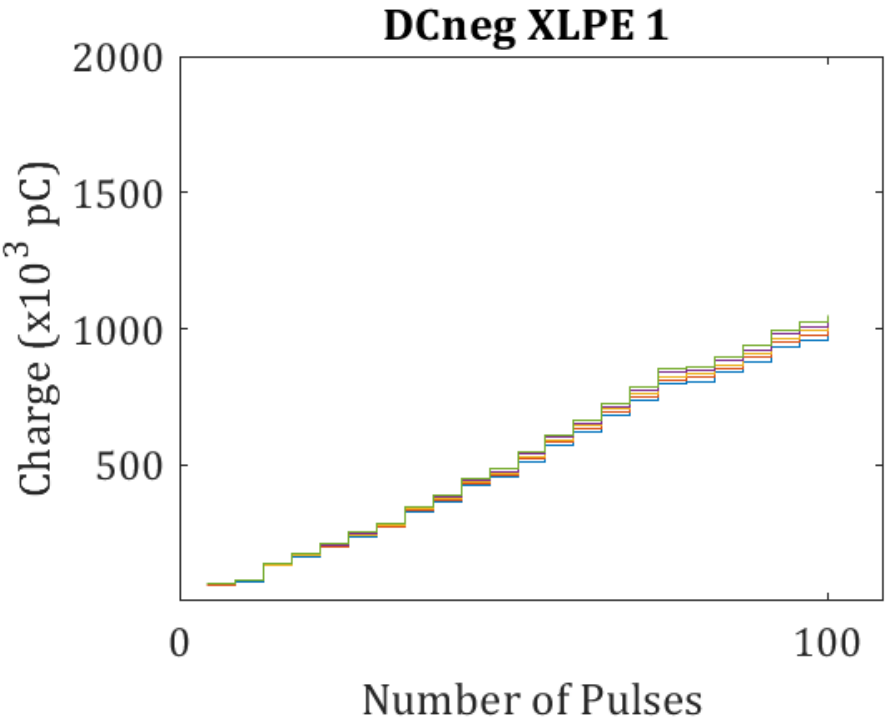

Figure 76 – Plots of cumulative charge for –DC testing of XLPE sample.

The final cumulative charge plot, Figure 77, shows the results from the positive polarity DC testing. As with the previous plots, the five tests of the cable sample produced similar results, both in terms of the pattern, and the final value of total apparent charge. As before, this lack of diversity is possibly due to the same sample being repeatedly tested. Unlike with the tests performed on the LDPE samples, the final total charge value is higher under the positive, rather than negative polarity DC. This is due to a greater number of PD pulses which occurred

under positive DC polarity falling into the higher ranges of peak apparent charge values.

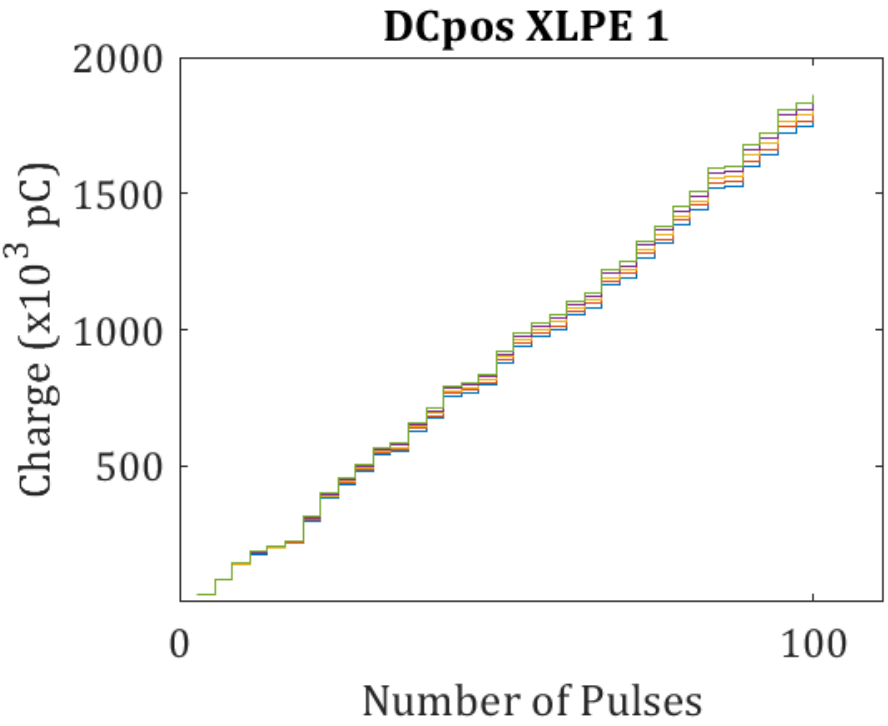

Figure 77 – Plots of cumulative charge for +DC testing of XLPE sample.

7.2.4. |Δq|-dt-n

The |Δq|-dt-n plot for the tests performed under AC conditions on the XLPE cable is shown in Figure 78. This displays a lack of correlation under AC conditions between the time between discharges, and the peak apparent charge. The peak apparent charge values occur in a small range, over the recorded range of time between discharges. This could be due to the fact that pulses overall have to be larger to be detected within the cable sample (as discussed above, there is a greater physical separation from the void and the earthing which the HFCT is connected to).

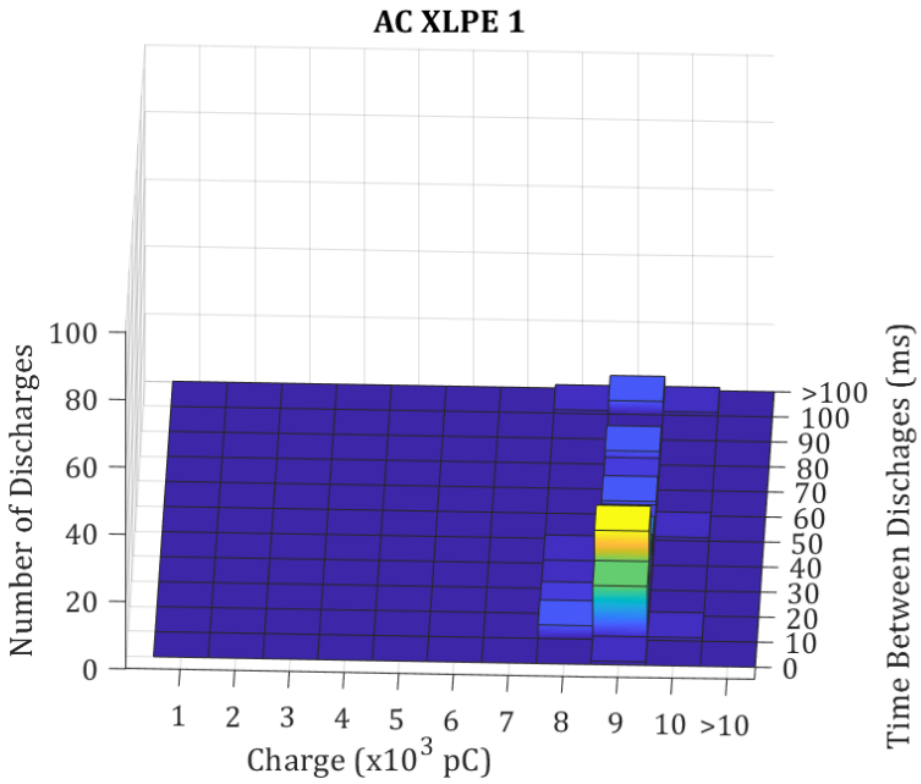

Figure 78 – |Δq|-dt-n plot for AC tests of XLPE sample.
Colours indicate the relative number of values falling in each bin from yellow (highest) to dark blue (lowest).

Figure 79 shows the |Δq|-dt-n plot for the negative polarity DC tests of the XLPE cable. The bulk of the PD pulses fell into the bin representing the largest peak apparent charge and the longest time between discharges. The pulses which did not fall into these categories still fell into the top ranges of either. This suggests that the pulses under negative DC were largely uniform. As with other metrics, this uniformity could be a result of the same sample being tested repeatedly, rather than different samples, as was the case with the thin film testing. However, despite this, the |Δq|-dt-n plot bears a resemblance to the same plot for the thin film LDPE samples when tested under negative polarity DC.

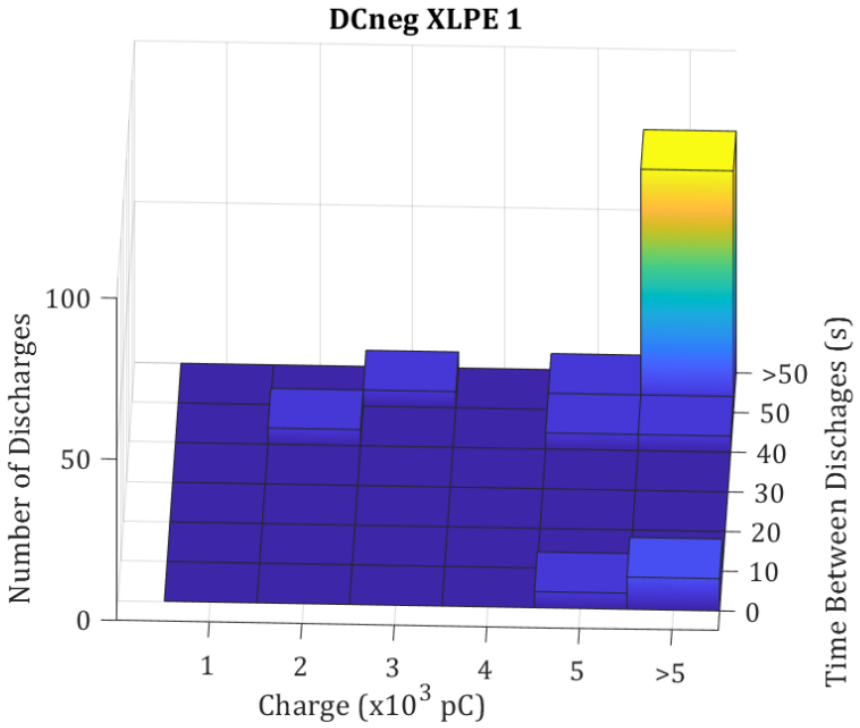

Figure 79 – |Δq|-dt-n plots for –DC tests of XLPE sample.
Colours indicate the relative number of values falling in each bin from yellow (highest) to dark blue (lowest).

The |Δq|-dt-n plot for the positive polarity DC testing of the XLPE cable sample is shown in Figure 80 as before, the scale of the time between discharges is seconds for plots of the pulses captured under DC conditions rather than milliseconds as for AC. This shows a distribution of pulses that is less uniform than the distribution for the negative polarity DC. While the bulk of pulses still occur in the high end of the peak apparent charge range, the associated values of time between discharges are lower. In addition, more pulses occur across both this range, and the time between discharges range when compared to the negative polarity DC. There is also less of a correlation between time between discharges and peak apparent charge than might be expected, both from the mechanisms of PD recurrence under DC conditions, and compared to the plots from previous testing on both the thin film samples, and the negative polarity testing of the cable sample.

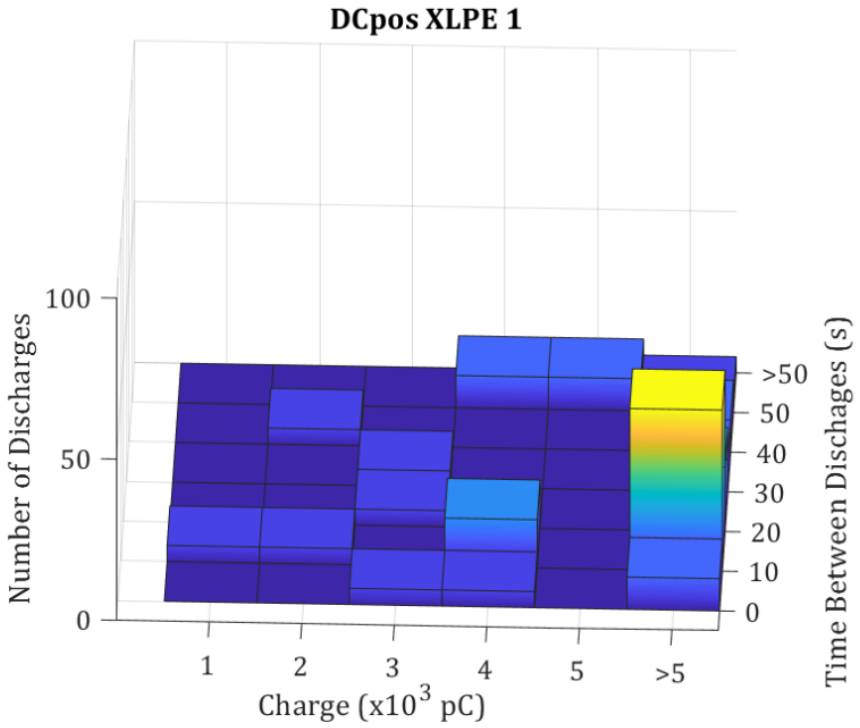

Figure 80 – |Δq|-dt-n plots for +DC tests of XLPE sample.
Colours indicate the relative number of values falling in each bin from yellow (highest) to dark blue (lowest).

7.3. Conclusions

The aim of this chapter was to present results from the testing of an XLPE cable sample, with an artificial void introduced by a coring method. The sample was tested under AC, negative polarity DC, and positive polarity DC voltages. Various analysis techniques, including partial discharge inception voltage, phase-resolved partial discharge plots (for AC testing only), ϕ-q-n plots, pulse sequence analysis, and |Δq|-dt-n plots were presented. From these, it was clear that an artificial PD-producing void had be successfully created in the cable sample.

Information on how the PD presented under the different voltage conditions was also obtained, with comparison with thin film sample testing from previous chapters possible.

Initially, consideration of the PDIVs showed that the values under AC conditions were lower than under DC conditions of either polarity. This difference was less than that which was found for the thin film samples, potentially due to the greater

attenuation of the detected signals due to the greater separation between the void and the detection equipment.

The PRPD and ϕ-q-n plots confirmed the presence of a PD-producing void within the XLPE cable sample. Typical patterns, peaks leading the AC waveform for the PRPD plot, and rabbit-like for the ϕ-q-n plot, were found. These patterns bore a similarity to the results for the single void testing of the thin film LDPE samples, suggesting that the behaviour of PD in XLPE was similar to that as in LDPE.

The pulse sequence analysis highlighted differences in how the PD presented in the XLPE cable sample under AC as compared to DC conditions. The values of peak apparent charge where much more spread out under DC conditions, while under AC these were much more concentrated. These results were also similar to the single void LDPE samples for both the AC and negative polarity DC, with the positive polarity DC remaining more distinct, with higher values of pulse magnitude than might be expected from the LDPE results. Values of difference in apparent charge values as compared to the previous PD pulse, also showed differences in AC and DC behaviour. Under AC the probability of the value of magnitude of the difference decreased as that magnitude itself increased, while under DC, there was a roughly equal likelihood across a range of values. Unlike previous metrics, these results did not closely match the results from the LDPE thin film samples. Consideration of the time between discharges, in turn, demonstrated difference between negative and positive polarity DC. PD pulses occurring under negative polarity DC were more likely to occur after a longer time delay than under positive polarity DC. This suggests, as indicated in previous chapters, a difference in how charges dissipate into the insulating material depending on the voltage polarity. The AC results were distinct from those found for the LDPE samples, with cycles where no PD was detected being far more common in the XLPE cable sample.

Cumulative charge plots were also produced for all three voltage types. These found a low variation between different tests in each case, which was similar behaviour to the LDPE thin film samples containing a single void. However, unlike in the LDPE, the negative polarity tests reached a lower total charge than the

positive polarity tests, due to lower average peak apparent charge. This may be due to the same sample being repeatedly tested, as positive polarity DC tests were performed after negative polarity tests.

The |Δq|-dt-n plots again showed differences in behaviour under different DC polarities. The expected correlation between time between discharges and peak apparent charge of discharges was strong under negative polarity DC, but weaker under positive polarity. This correlation was strong for the LDPE single void samples, so this represents another metric where the negative polarity DC behaviour in the XLPE strongly resembles the behaviour in the LDPE, while the positive polarity DC does not show this resemblance. This again could be impacted by multiple tests being performed on the same cable.

Overall however, the similarities between the XLPE and LDPE samples suggest strongly the results from the previous chapters would be applicable to practical cables, and thus potentially of industrial use. Specifically understanding of PD patterns is important for finding PD signals in noisy environments.

7.4. Evaluation

As indicated above, the overall aims of this chapter were met, with the validity of the coring method for producing artificial voids in cables confirmed to produce detectable PD within that void. Additionally, results from AC and DC were presented and analysed. This allows for partial discharge testing in practical cable samples, which, as also demonstrated by these results, could have an impact on the presentation of PD even in electrically similar materials.

One limitation, discussed within the chapter, is that the same cable sample was tested repeatedly. Although efforts were taken to reduce the impact of this (long grounding periods, determination of PDIV before main testing) it is not possible to rule out that this may have had an impact on the results presented. In future, it would be better to test multiple cable samples, unless the development of PD behaviour over time is specifically being investigated. Due to oil contamination in the thin film samples after they were removed from the test rig, it was not

possible to test film samples to determine the impact of applying different voltage types in turn on PD behaviour to correlate these with the cable tests.

Also, for better comparison to the work in previous chapters, it would be useful to test difference void configurations within cable samples, this was not possible due to time constraints, but is technically feasible, using the coring method.

As with previous chapters, it would be useful to have used the more sensitive Lemke Diagnostics LDS-6, in particular due to the likely smaller size of the PD signals once they reached the measurement equipment, as confirmed during calibration.

Lastly, again for better comparison, cable samples of different insulation types could be tested (in particular, a sample of polypropylene paper laminate). It was not possible, despite efforts, to procure a sample for testing in this case.

8. Analysis of PD Pulse Characteristics

This chapter is concerned with statistical analysis of the PD pulses under the different conditions investigated previously. Data for this chapter were captured by the LeCroy Waverunner 104Xi (data captured by the Lemke LDS-6 could not be analysed in this manner, as only the apparent charge of the pulse, and, for AC, the phase, are captured).

Specifically, metrics concerning the PD pulses themselves are considered to determine if the size and shape of pulses is affected by insulation material, voltage type, or defect configuration. The shape of PD pulses is important for the designing of denoising algorithms. This is to be achieved by presenting charge-duration scatter plots for each of the captured pulses, as well as analysis of the peak apparent charge, rise time, pulse width, and fall time of these pulses. Lastly an average pulse is constructed from the average of each of these values for each of the different variables, with these plotted together and compared.

8.1. Charge-Duration Clusters

8.1.1. AC Tests on Thin Film LDPE Samples

Figure 81 shows a scatter plot of the amplitude (peak apparent charge) and duration (pulse width) of the PD pulses captured from the AC testing of the thin film samples (using the methodology described in Chapter 3) of the three void types investigated (single void, two voids in a parallel configuration, and two voids in a serial configuration). From this plot, three clusters, corresponding to the three void configurations appear very distinct. The first cluster, corresponding to the pulses from single void defect samples, appears at the bottom of the plot with the lowest amplitude, and across 25-40 ns in duration. The next cluster, consisting of the pulses from the parallel void defect samples, occurs over the same duration (25-40 ns) but over a range of amplitudes from 1000-2500 pC. The final cluster, for the pulse from the serial void defect pulses, overlaps somewhat with the second cluster, having durations from greater than 25 ns to less than 35 ns, and amplitudes from 1000 pC up to 3500 pC.

It is clear from this plot, that the presence of multiple voids in LDPE increases the range and average amplitudes of PD pulses under AC stresses (this was also seen in Figure 58). In addition, the presence of parallel voids, under these conditions, has little effect on the distribution of pulse durations, while serial voids reduce the range of pulse durations.

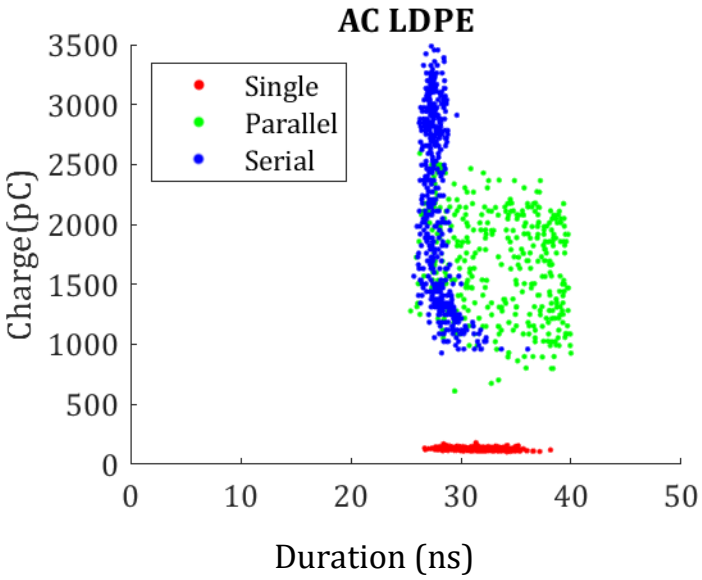

Figure 81 – Scatter plot of peak apparent charge against pulse width for AC testing of LDPE samples.

8.1.2. Negative DC Tests on Thin Film LDPE Samples

The scatter plot of pulse amplitude and duration for the negative polarity DC testing of the LDPE thin film samples is shown is Figure 82. From this plot it is again possible to determine three clusters, however these are much less distinct than in the previous plot for the AC results. The first cluster, for pulses from the samples containing a single defect, is found within the bounds of 35-45 ns, from 300 to 1100 pC. Overlapping with this, but extending beyond it is the second cluster, for pulse from the samples containing two voids in parallel, which largely occur from 30-55 ns in duration (although some outside this range to beyond 100 ns) with amplitudes ranging from 25 to 1100 pC. The final cluster overlaps in part with both previously identified clusters, occurring from 35-50 ns, with amplitudes of 25 to 800 pC.

As mentioned above, these clusters are less distinct in the case of the negative polarity DC testing, however the impact of defect type is still clear. The presence of multiple voids causes a greater range of pulse duration to be recorded, much more so in the case of voids in parallel than in serial configuration. Additionally, the average amplitudes are also reduced by the presence of multiple voids, in this case much more when serial voids are present than when parallel voids are tested.

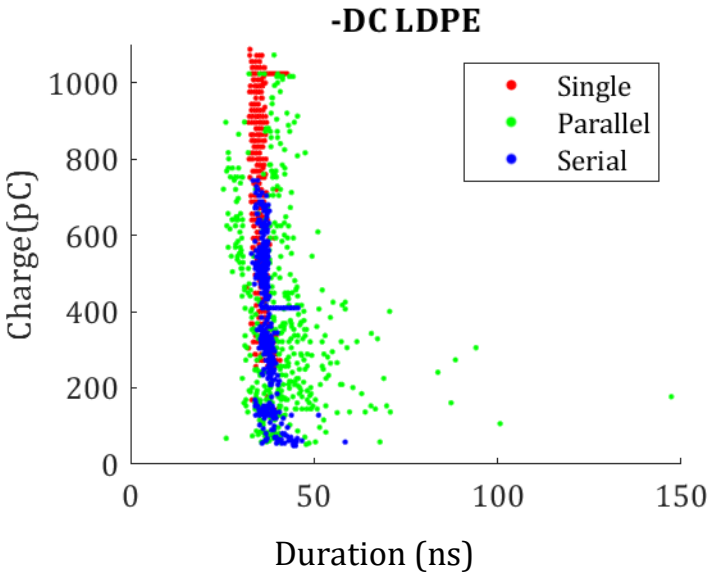

Figure 82 – Scatter plot of peak apparent charge against pulse width for -DC testing of LDPE samples.

8.1.3. Positive DC Tests on Thin Film LDPE Samples

The scatter plot of the amplitudes and durations of the pulses recorded under negative polarity DC is shown in Figure 83. Three clusters, corresponding to the defect types, are again clear. These clusters are more distinct than in the scatter plot for the pulses recorded under negative polarity DC. The first cluster, containing pulses recorded from the single void samples, occurs largely over the duration 55 to 80 ns, and, as with the AC testing, is found at the lower end of the amplitude range (25 to 200 pC). The second cluster, for the pulses from the parallel void samples, is centred around duration values between 30-50 ns, with most pulses having amplitudes between 25 and 400 pC (with a number occurring up to 800 pC). The final cluster, for pulses from the serial void samples, occur over a narrow range of durations from 35-40 ns, and a range of pulse amplitudes from

400-1000 pC, this is similar to the pulses from this defect type, found from the negative polarity DC testing.

In the case of negative polarity DC, as was found in the AC testing, the presence of multiple voids increases the range of pulse amplitudes found. In addition, multiple void defects appear to also reduce the range of amplitudes that are detected (particularly in the case of the pulses recorded from the serial void samples).

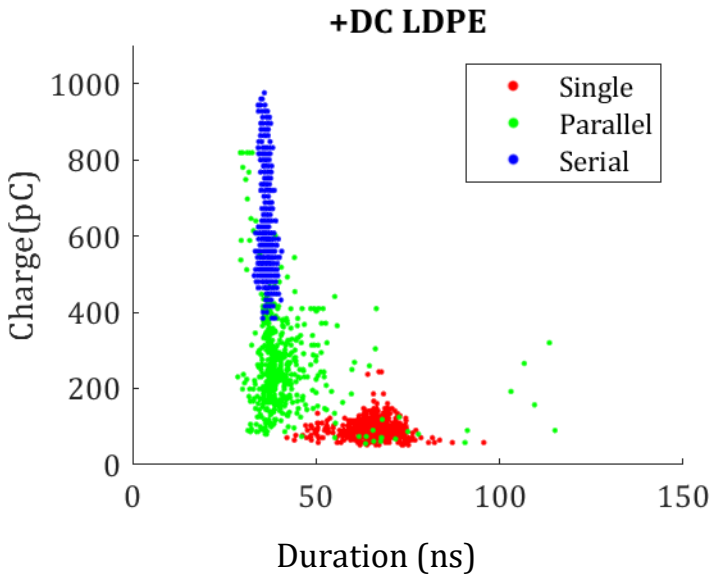

Figure 83 – Scatter plot of peak apparent charge against pulse width for +DC testing of LDPE samples.

8.1.4. AC Tests on Thin Film Polypropylene Samples

Figure 84 shows the scatter plot of the amplitudes and durations of the pulses recorded from the AC tests on the thin film polypropylene samples. Unlike in the previous samples, only two distinct clusters are found. The first, contains the pulses from samples with a single void or with two voids in a serial configuration. The pulses occur from around 30-35 ns and have amplitudes from 500 up to 2000 pC. The second cluster, containing the pulses from the testing of the samples containing two voids in a parallel configuration, occur over a smaller range of amplitude values with a lower average value, between 25-500 pC. These pulses also occurred over a wider range of durations, with most falling between 30-40 ns.

This behaviour is markedly different to what was found in the LDPE, where each void type had a distinct impact on the resultant pulse amplitudes and durations, leading to three clear clusters. In this case however, the presence of multiple voids only had an impact on the presentation of PD if the voids were in the parallel configuration, while the pulses found in the serial configurations testing were indistinguishable from those found from the testing of the samples containing a single void.

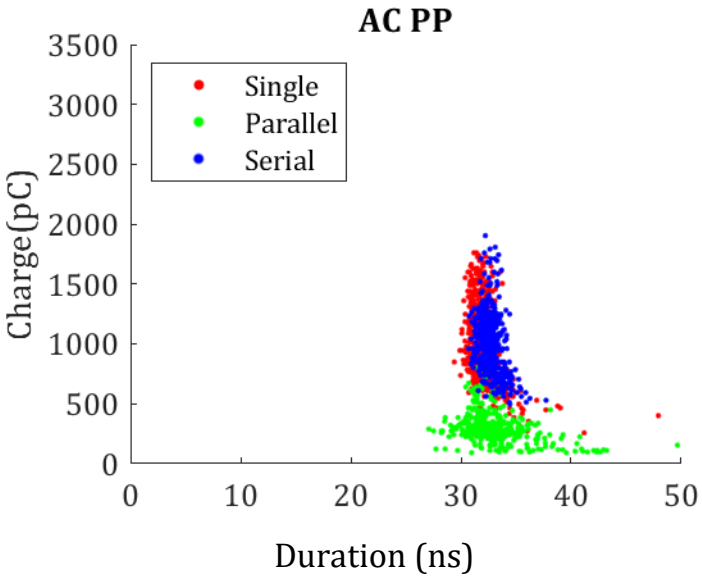

Figure 84 – Scatter plot of peak apparent charge against pulse width for AC testing of PP samples.

8.1.5. All Tests on XLPE Cable Sample

The scatter plot of the amplitudes and duration of the pulses recorded during the AC and DC testing of the XLPE cable sample is shown in Figure 85. In this case, two clusters are notable. The first, for the AC testing, which show a shorter duration than any of the previous clusters, of around 0-3 ns, and amplitudes between 7000-9000 pC. The second cluster, containing the results from the DC testing, also had shorter durations than were found on previous plots for the thin film samples, but still had a range of greater than the AC pulses, of between 5-15 nC, with a greater range of amplitudes, occurring between 4000-10000 pC. It is not possible to distinguish between the positive and negative polarity DC, suggesting that, in the XLPE, the polarity of the DC did not have a significant

impact on the pulse shape. This is different from the behaviour in the LDPE, where both polarities produced distinct behaviour.

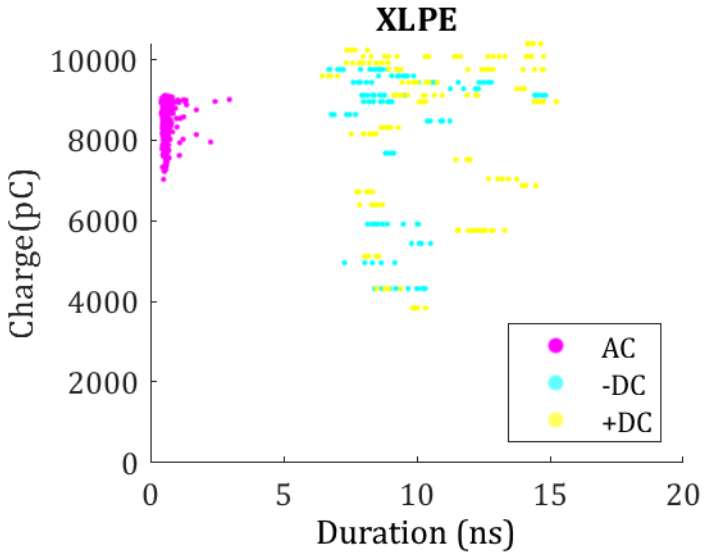

Figure 85 – Scatter plot of peak apparent charge against pulse width for AC and DC testing of XLPE sample.

8.1.6. Conclusions

Overall, the scatter plots are largely successful in distinguishing PD pulses from different void configurations. However the scatter plots were of limited use for determining applied voltage polarity in the case of the DC tests on the XLPE. The clusters found from the AC testing of the LDPE samples were very distinct, with it being possible to determine clusters for the single, parallel and serial voids. The same was true of the positive polarity DC pulses, where again, three clear clusters were found. However, the negative polarity DC pulses were less successful distinguished, with one cluster for all events. The PP pulses were more distinct than this, with a cluster for the single void and serial void pulses, and a second cluster for the parallel void pulses.

8.2. Pulse Characteristics Tables

As discussed in chapter 2, common metrics for describing PD pulses include the rise and fall times, pulse width, and peak apparent charge.

Tables for each of these values, as well as the peak apparent charge itself are presented, showing, for each voltage, material, and void configuration, the mean value, as well as the standard deviation, skewness and kurtosis. (N.B. in the tables

single voids are indicated by '1', two voids in parallel and indicated by '2//' and two voids in series are indicated by '2--').

8.2.1. Peak Apparent Charge

The statistical breakdown of the measurements of peak apparent charge are presented in Table 10. The greatest mean values occur for the testing of the XLPE cable sample, with the DC testing in particular having a very large standard deviation, suggesting a wide range of apparent charge values. The pulses from the AC testing of the LDPE samples, for each void configuration, were near normally distributed (mesokurtic – see section 2.4.1.3). However, the samples produced a wider variation when tested under DC, with platykurtic distributions found under negative polarity DC, and a mix of platykurtic and leptokurtic distributions under positive polarity DC.

Table 10 – Measures and statistics for peak apparent charge of PD pulses. For the means and standard deviations, the colour gradient shows the range from smallest (orange) to largest (purple) in pC. The skewness and kurtosis are represented graphically.

Voltage	Material	Void	Mean	SD	Skew	Kurtosis
AC	LDPE	1	125.63	11.19	0.81	3.71
		2//	1727.5	346.65	-0.58	3.17
		2--	2229.7	611.99	-0.11	2.6
	PP	1	987.48	314.05	0.42	2.58
		2//	310.26	110.28	1.5	5.01
		2--	1027.7	227.78	-0.24	3.96
	XLPE	1	8553.4	458.63	-1.07	3.29
-DC	LDPE	1	1340.4	460.35	-0.36	2.14
		2//	782.61	443.97	0.75	2.46
		2--	778.31	321.47	-0.27	1.74
	XLPE	1	7032.8	2597.1	-0.55	2.26
+DC	LDPE	1	94.05	25.83	1.49	8.22
		2//	264.76	108.59	1.15	4.13
		2--	614.18	104.59	-0.33	2.31
	XLPE	1	6093.1	2969.3	-0.07	1.79

8.2.2. Rise Time

Table 11 shows the breakdown of the statistical measures from the rise time of the PD pulses. Shorter average rise times were generally found in the negative polarity DC testing, the average from pulses from the AC testing fell in the middle and longer times were found in the average from pulses from the positive polarity DC testing. An exception to this was the AC testing of the XLPE which was found to have a were short average rise time. In addition, in most cases, the presence of parallel voids led to an increase in average rise time, while serial voids lead to a decrease. The DC testing for both polarities had significantly larger standard deviation values than the AC testing, suggesting that these values tended to be more spread out. Despite this, high kurtosis values suggest that outliers were less common in the DC testing when compared with the AC testing.

Table 11 – Measures and statistics for rise time of PD pulses.
For the means and standard deviations, the colour gradient shows the range from smallest (orange) to largest (purple). The skew and kurtosis are represented graphically.

Voltage	Material	Void	Mean	SD	Skew	Kurtosis
AC	LDPE	1	19.21 ns	2.78 ns	0.66	3.03
		2//	22.02 ns	6.79 ns	0.49	1.46
		2--	16.51 ns	1.22 ns	2.37	10.79
	PP	1	16.65 ns	1.44 ns	1.41	6.05
		2//	19.46 ns	3.48 ns	1.23	6.32
		2--	17.06 ns	1.50 ns	1.37	4.2
	XLPE	1	0.49 ns	0.35 ns	2.99	13.15
-DC	LDPE	1	15.09 ns	2.07 ns	0.68	10.68
		2//	24.11 ns	9.71 ns	1.82	9.2
		2--	15.46 ns	2.41 ns	1.68	17.13
	XLPE	1	11.05 ns	8.88 ns	2.04	6.05
+DC	LDPE	1	38.78 ns	9.14 ns	0.17	3.35
		2//	26.63 ns	13.01 ns	2.95	14.82
		2--	14.97 ns	1.50 ns	-0.84	4.89
	XLPE	1	12.96 ns	10.52 ns	1.71	4.84

8.2.3. Pulse Width

The pulse width statistics are shown in Table 12. From this it is clear that the pulses found under DC testing have a longer average width that those found from the AC testing. This is particularly true for the pulses found during the positive DC testing. As with the rise times, the XLPE pulses had a significantly lower average pulse width (particularly under AC conditions) than those found in the thin film testing.

Table 12 – Measures and statistics for width of PD pulses.
For the means and standard deviations, the colour gradient shows the range from smallest (orange) to largest (purple). The skew and kurtosis are represented graphically.

Voltage	Material	Void	Mean	SD	Skew	Kurtosis
AC	LDPE	1	31.30 ns	1.91 ns	0.24	2.85
		2//	33.53 ns	4.24 ns	-0.15	1.64
		2--	27.85 ns	1.03 ns	1.01	5.12
	PP	1	32.11 ns	1.39 ns	2.07	11.66
		2//	32.94 ns	2.29 ns	0.88	4.95
		2--	32.69 ns	0.85 ns	0.63	4.04
	XLPE	1	0.61 ns	0.23 ns	3.58	18.83
-DC	LDPE	1	35.58 ns	1.63 ns	0.56	3.45
		2//	40.85 ns	10.44 ns	2.76	16.76
		2--	37.43 ns	1.92 ns	1.22	9.46
	XLPE	1	9.42 ns	1.77 ns	1.23	4.41
+DC	LDPE	1	65.37 ns	6.38 ns	-0.42	5.29
		2//	41.70 ns	9.82 ns	3.2	22.34
		2--	36.63 ns	1.20 ns	-0.12	2.96
	XLPE	1	12.35 ns	6.87 ns	3.17	12.68

8.2.4. Fall Time

Table 13 shows the statistics for the fall times of the captured PD pulses. As with previous metrics, the averages for the XLPE testing stand out as being lower (significantly in the case of the AC testing) than the thin film testing. Also, as before, the positive polarity DC testing, tends towards lower averages. In this case, the AC testing and negative polarity DC testing produce similar results in terms of average fall times.

Table 13 – Measures and statistics for fall time of PD pulses.
For the means and standard deviations, the colour gradient shows the range from smallest (orange) to largest (purple). The skew and kurtosis are represented graphically.

Voltage	Material	Void	Mean	SD	Skew	Kurtosis
AC	LDPE	1	24.20 ns	3.70 ns	0.6	4.02
		2//	21.50 ns	4.00 ns	-0.07	1.69
		2--	19.30 ns	2.00 ns	0.11	1.97
	PP	1	22.30 ns	1.50 ns	-0.13	3.23
		2//	23.50 ns	2.40 ns	0.11	3.44
		2--	24.40 ns	1.60 ns	-0.27	2.52
	XLPE	1	0.50 ns	0.30 ns	2.97	13.76
-DC	LDPE	1	24.50 ns	2.70 ns	-0.85	4.39
		2//	24.40 ns	12.20 ns	4.96	33.23
		2--	27.50 ns	3.40 ns	-0.84	3.99
	XLPE	1	7.20 ns	1.60 ns	1.21	4.96
+DC	LDPE	1	40.30 ns	11.60 ns	0.45	1.88
		2//	21.40 ns	5.30 ns	1.64	11.12
		2--	26.70 ns	2.50 ns	-0.28	2.73
	XLPE	1	11.00 ns	8.10 ns	2.68	10.35

8.3. Comparison of Average PD Pulse Characteristics

8.3.1. Pulses Under AC Voltage

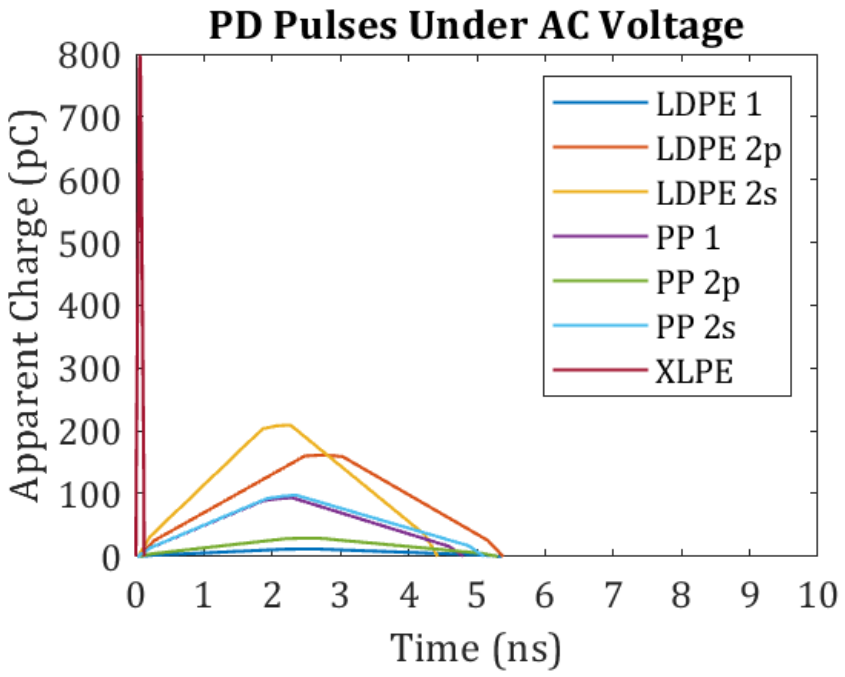

Figure 86 – Plot of PD pulses from average of measured values for AC testing.

The mean values of the characteristics described above were used to create average pulses, that were then plotted for comparison.

Figure 86 shows these average pulses for the testing performed under AC conditions. Several distinguishing features can be noted from the seven pulses constructed in this manner. Firstly, the XLPE pulse is notable for being both the largest in amplitude and shortest in width, rise, and fall times. Next, the multiple void (2 in series and 2 in parallel) LDPE samples produce pulses with a similar amplitude, with the 2 serial voids leading to shorter rise and fall times. In the polypropylene, the single void and two serial voids produce pulses with very similar characteristics in all respects. The single void LDPE and two parallel void polypropylene pulses have similar amplitudes as well as widths and rise and fall times. This has implications for the detection of PD pulses under these different conditions.

8.3.2. Pulses Under −DC Voltage

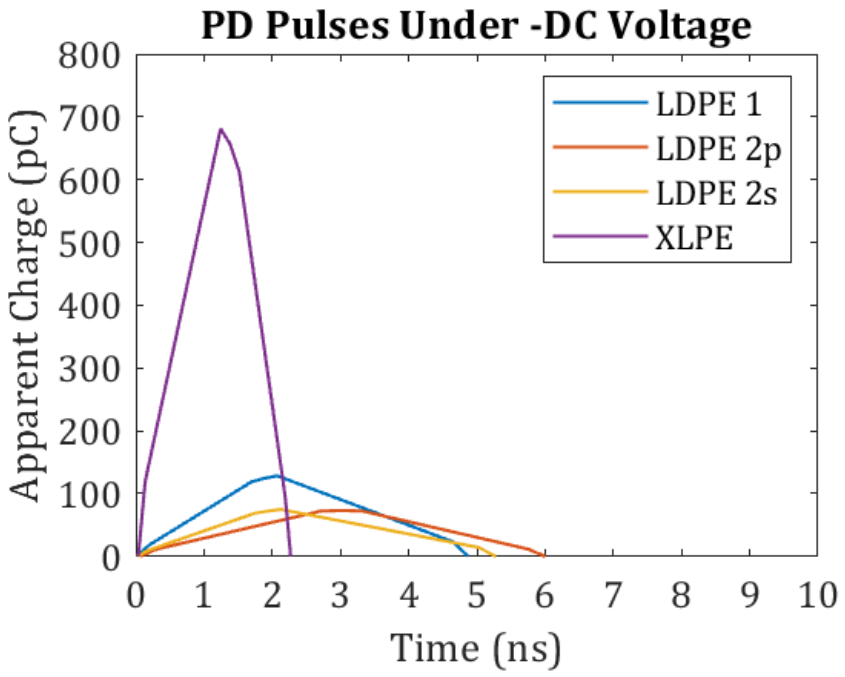

Figure 87 – Plot of PD pulses from average of measured values for –DC testing.

Figure 87 shows the average pulses for the tests under negative polarity DC. As with the AC tests, the most distinct average pulse is the one representing the XLPE pulses, which again has the largest amplitude and shortest duration. The average pulses for the multiple void samples had smaller amplitudes, but longer durations, with the parallel void pulse having a longer rise time, and the serial void pulse a longer fall time. This again has implications for the detection of PD under different conditions, especially when PD pulses must be extracted from background noise.

8.3.3. Pulses Under +DC Voltage

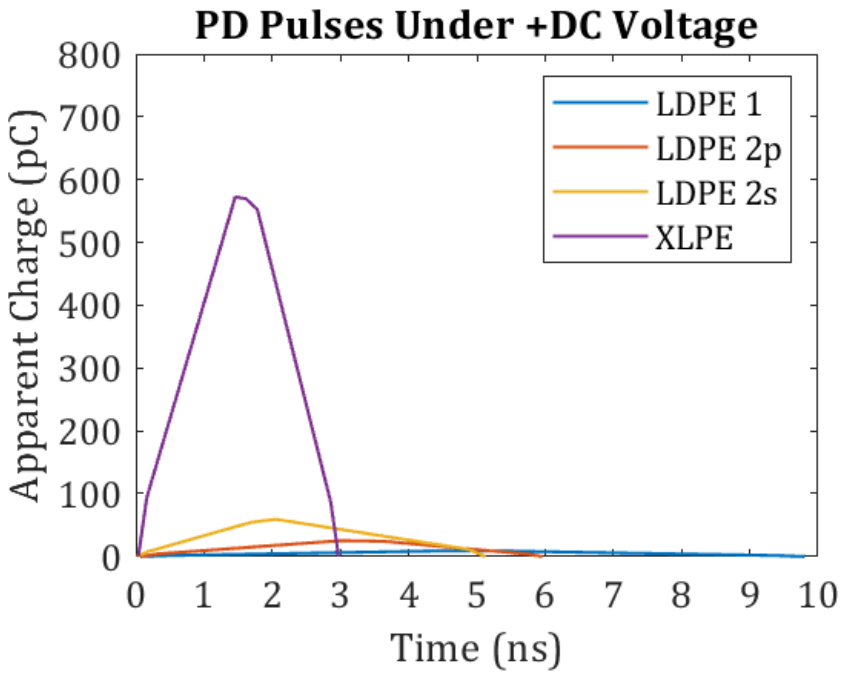

Figure 88 – Plot of PD pulses from average of measured values for +DC testing.

Figure 88 shows the average pulses for the positive polarity DC testing. As with the previous voltage types, the XLPE pulse is the most separate, with again a larger amplitude and shorter duration. The pulses for the different void configurations in the LDPE are also more divergent than under other voltage types. The two serial void pulse had a higher amplitude and shorter duration, while the single void has a lower amplitude and much longer duration, with the two parallel void pulse in the middle for both metrics.

8.3.4. Conclusions

Considering the LDPE pulses from Figure 86, Figure 87, and Figure 88, it is of note that when pulses are found to have lower amplitudes, this tends to lead to longer durations, while higher amplitudes tend to have lower duration. The pulses under positive polarity DC were of the lower amplitude longer duration type, while the negative polarity DC average pulses were the opposite, this suggests, as with previous analysis, that the characteristics of PD pulses under DC are impacted by the polarity of the applied voltage. The pulses themselves for the samples with two serial voids, regardless of the voltage type, had shorter rise

times and longer fall times, while the parallel void samples had even rise and fall times.

The XLPE pulses from the plots above also show this negative correlation between pulse width and amplitude. This may allow for PD pulses to be identified in noisy environments, where other signals will not have this property.

8.4. Conclusion

The aim of this chapter was to present statistical analyses on the PD pulses captured in different materials, under different voltage conditions, and with different void configurations.

Firstly, scatter plots of amplitude and duration were presented for each material and voltage type. From these, clear clusters were found for AC and positive polarity DC testing of the LDPE. While the negative polarity DC results were significantly less distinct. The AC testing of the polypropylene was more distinctive that the negative polarity DC testing of the LDPE, but it was not possible to distinguish between single void and serial void pulses. In the XLPE cable sample, the AC pulses were very distinct from the DC pulses, but the positive and negative polarity DC pulses were not distinguishable from each other. This suggests some use of the amplitude-duration plots in determining the nature of void defects, by analysing the amplitude and duration of collected pulses, and determining where on the scatter plot it would fall, although a larger database of pulses would be required for this.

Tables were presented for common measurement characteristics of PD pulses. Specifically, rise time, pulse width, fall time, and pulse amplitude were considered. Several finds were of note; the pulse amplitudes were more variable under DC testing than AC testing. The negative polarity DC testing produced pulses with the shortest rise times, AC pulses were in the middle, and positive polarity testing had the longest, with DC testing again proving more variable in this metric. The pulse widths were found to be generally longer in the DC testing compared to the AC. Fall times were similar in the AC and negative polarity DC testing, while being shorter in the positive polarity DC.

These differences were made clear through the plotting of average pulses constructed from the mean values of the considered measurements. The XLPE pulses were the most distinct in all cases. Average pulses in the LDPE when compared between the same void configuration across different voltage types were found to increase in amplitude as the pulse duration decreased, and vice-versa.

Overall, it is clear that the conditions under which a PD pulse occurs in a void type defect, considering the insulation material, voltage type, and void configuration, had an impact on the size and shape of that PD pulse. This suggests that the design of denoising algorithms should take into account the material type or voltage type (or both) that the PD pulses are expected to be detected in, to allow for greater accuracy in distinguishing PD pules from background noise.

8.5. Evaluation

This chapter was successful at providing further analysis of the captured PD pulses, with clear differences demonstrated between pulses that develop under different conditions.

Understanding the shape of PD pulses has important applications in denoising of PD signals, which is vital for detection when noise is a significant concern, such as detecting PD after they have been transmitted over longer distances.

To add to this work, multiple void testing of the XLPE cable would be useful to see if the short and high amplitude pulses were affected by void configuration. Testing on a PPLP cable as well as samples of thin film polypropylene would round out the analysis allowing for a more complete picture of the impact of insulating material, void configuration and voltage type on the size and shape of PD pulses.

9. Conclusions and Future Work

This chapter reviews the conclusions which have been presented throughout the thesis and gives some suggestions to how the work could be built upon in the future.

9.1. Conclusions

The conclusions from throughout the thesis are presented below.

9.1.1. Coring Method

Methods used to construct the test samples were explored in detail, with a 'coring' method for creating an artificial void within a cable sample introduced. This method was validated using the results presented in Chapter 7. This allowed for tests to be performed on a real cable sample, as well as the thin film samples.

9.1.2. Open Access Database

The data management procedures followed for the creation of the database of PD signals were also presented, with the database another key output of this research. Signals from the database have been used in the design of a novel wavelet algorithm for PD denoising, which was found to be more successful than conventional algorithms[24].

9.1.3. Comparison of PD in Polyethylene and Polypropylene

Results captured from the Lemke LDS-6 were used to compare the presentation of PD in low-density polyethylene and polypropylene. It was found that the characteristics of PD were very similar in both LDPE and polypropylene, with a greater variation between samples than was found between materials when considering standard PD plots. Pulse sequence analysis however did different PD behaviour in the different materials. While PD activity in both materials was found to 'settle down' in the second 2-hour test periods compared to the first, in the LDPE this came in the form of the number of PD pulses per cycle becoming steady (with continuing variability in the peak apparent charge values of these pulses), while in the polypropylene the number of PD events per cycle varied, while the peak apparent charge values were more consistent.

9.1.4. Use of Thin-film Samples for DC Testing

Results from the Lemke LDS-6 on DC testing of a single void LDPE sample showed evidence of a void type defect, confirming that the thin film layered method is suitable for testing under DC conditions.

9.1.5. Impact of Multiple Voids on PD under AC Conditions

Results captured from the AC testing of samples of polyethylene and polypropylene containing voids in different configurations were presented to determine what impact, if any, the different materials and void configurations have on the presentation and development of PD.

It was found that the LDPE samples consistently had a higher PDIV than the polypropylene samples. It was also found that the presence of two voids in a serial configuration did not have a significant impact on the PDIV, whereas two voids in a parallel configuration reduced the PDIV significantly. This impact occurred in both materials tested. It is speculated that this is due to the orientation of the void within the electric field lines, in relation to the thickness of insulating material.

From analysis of the PRPD, and ϕ-q-n plots it was found that the material type had a greater impact on the recorded patterns than the void configuration, with a consistently greater distribution of PD events across the phase of the AC waveform in the LDPE, and a greater distribution of PD events across the values of peak apparent charge in the PP samples. Considering the ϕ-q-n plots, the same was also found, with greater differences between material types than void types.

Pulse sequence analysis was also considered, where it was easier to identify differences in behaviour between different void configurations. The frequency of peak apparent charge values, indicated that single void PD events tended to fall in the lower end of recorded values, while in samples containing multiple voids (both serial and parallel) this was not the case. Additionally, the presence of parallel voids tended to cause the bulk of PD events to have higher apparent charge values, while the serial voids, produced both lower and higher values of apparent charge.

Overall, the void configuration was found to have the greatest impact on PDIV, and then subsequently the values of apparent charge of the PD pulses, while the materials types were found to have a greater impact on both the PRPD and ϕ-q-n patterns.

9.1.6. Impact of Multiple Voids on PD under DC Conditions

Results captured from DC testing of thin film samples of polyethylene with different void configurations, and under both negative and positive polarity DC, were presented with the aim of determining if the presence of multiple voids, or the polarity of the DC voltage (or both) had an impact on the presentation and characteristics of partial discharge in the samples.

It was found that the PDIVs under both positive and negative DC were significantly higher than for the samples of the same void configuration tested under AC conditions. It was discovered that the presence of serial voids did not have a significant impact on the PDIV (increasing it slightly). Parallel voids, on the other hand, reduced the PDIV significantly when compared to the PDIVs of the serial and single voids tested with the same voltage type. This suggests that the orientation of the void within electrical field lines is significant in the determination of PDIV under DC conditions.

Through |Δq|-dt-n plots it was possible to determine several differences in PD activity between different void configurations and voltage polarities. It was found that positive polarity DC led to shorter times between pulses, and thus lower peak apparent charges. It was theorised that this is related to charge dissipation into the insulation material or charge distribution on the void surface. The presence of multiple voids also impacted PD activity, with a greater spread of both time between discharges and peak apparent charge values when multiple voids were present. This impact was strongest with serial voids as compared to parallel voids.

Pulse sequence analysis found that the presence of multiple voids increased the spread of values of apparent charge, with negative DC tending towards higher values in total. Serial voids in particular led to a majority of PD pulses falling in

the highest bin. Negative DC conditions were more likely to produce pulses that were significantly different from their predecessor, while the presence of multiple voids only made this more likely under positive DC. Regarding single void samples, the negative polarity DC led to pulses that had a wide range of times between them, while the positive polarity DC pulses were all in quick succession. However, when multiple voids were present, the PD behaviour tended to be similar, with most of the pulses occurring soon after the previous one, with the likelihood of a longer delay decreasing with the length of that delay.

Overall, both voltage polarity and the presence of multiple voids (and their configuration) were found to have a measurable impact on PD activity under DC conditions.

9.1.7. Characteristics of PD in XLPE Cable Sample

Chapter 7 presented results from the AC and DC testing of the XLPE cable sample, with an artificial void introduced by a coring method. These results showed that an artificial PD-producing void had been successfully created in the cable sample.

PDIV values under AC conditions were lower than under DC conditions of either polarity. This difference was less than that which was found for the thin film samples.

PRPD and ϕ-q-n plots suggested that the PD behaviour in the XLPE cable sample was similar to that in the single void LDPE samples.

Values of peak apparent charge were much more spread out under DC conditions, similar to the LDPE samples. Values of difference in apparent charge from the preceding pulse showed that under AC the probably of a difference value decreased as that value itself increased, while under DC, there was a roughly equal likelihood across a range of values. The time between discharges showed that PD pulses occurring under negative polarity DC were more likely to occur after a longer time delay than would be the case under positive polarity DC.

9.1.8. Statistical Analysis of PD Pulse Characteristics

Statistical analysis of the PD pulses captured was presented. Scatter plots of amplitude and duration found clear clusters for all three void configurations in the AC and positive polarity DC testing of the LDPE. While the negative polarity DC results were significantly less distinct. The AC testing of the polypropylene was more distinctive that the negative polarity DC testing of the LDPE, but it was not possible to distinguish between single void and serial void pulses. In the XLPE cable sample, the AC pulses were very distinct from the DC pulses, but the positive and negative polarity DC pulses were not distinguishable from each other.

Common measurement characteristics of PD pulses- rise time, pulse width, fall time, and pulse amplitude were considered. It was found that the pulse amplitudes were more variable under DC testing than AC testing. The negative polarity DC testing produced pulses with the shortest rise times, AC pulses were in the middle, and positive polarity testing had the longest, with DC testing again proving more variable in this metric. The pulse widths were found to be generally longer in the DC testing compared to the AC. Fall times were similar in the AC and negative polarity DC testing, while being shorter in the positive polarity DC.

Average pulses constructed from the mean values of the considered measurements were also considered, with the XLPE pulses the most distinct in all cases. Average pulses in the LDPE, when compared between the same void configuration across different voltage types, were found to increase in amplitude as the pulse duration decreased, and vice-versa.

Overall, it was clear that the conditions under which a PD pulse occurred had an impact on the size and shape of that PD pulse. This has implications for the detection of PD, particularly in noisy environments, as it suggests that when distinguishing PD pulses from background noise, the conditions under which the PD is potentially being generated (e.g. voltage type, insulation type, and void configuration itself) should be considered. Specifically, if denoising algorithms were to take this information about the likely size and shape of the PD pulses into account it could allow for the better detection of PD, particularly when the source of the PD is far from the detector.

9.2. Future Work

Further work using the techniques presented in this thesis would be possible to further extend knowledge in the areas researched. Specifically, as analysis on DC testing of polypropylene was not undertaken, this would provide an interesting comparison for the DC LDPE results.

In addition, multiple void testing of the XLPE cable would be useful to see if the short and high amplitude pulses were affected by void configuration, additionally, testing of multiple cable samples would be useful to rule out the impact of repeatedly testing the same cable.

Testing on a PPLP cable as well as the above would round out the analysis allowing for a more complete picture of the impact of insulating material, void configuration and voltage type on the size and shape of PD pulses. Other cable insulation materials such as high-performance elastomers and nanoparticle doped XLPE would also provide interesting analysis in the future.

This would further extend the usefulness of this research in helping with the detection of PD pulses in noisy environments, or when the source of the PD is far from the detection equipment, as it would provide more reference information on the likely characteristics of PD pulses under more conditions, potentially allowing for better detection methods, or easier separation of PD signals from noise.

References

[1] R. Bartnikas, "Partial Discharges: Their Mechanism, Detection and Measurement," *IEEE Trans. Dielectr. Electr. Insul.*, vol. 9, no. 5, pp. 763–808, 1997.

[2] L. Niemeyer, "The Physics of Partial Discharges," *Int. Conf. Partial Disch.*, pp. 1–4, 1993.

[3] A. Kelen, "Ageing of insulating materials and equipment insulation in service and in tests," *IEEE Int. Symp. Electr. Insul.*, pp. 9–13, 1976.

[4] B. Fruth and L. Niemeyer, "The Importance of Statistical Characteristics of Partial Discharge Data," *IEEE Trans. Electr. Insul.*, vol. 27, no. 1, pp. 60–69, 1992.

[5] B. Sheng, C. Zhou, D. M. Hepburn, X. Dong, G. Peers, W. Zhou, and Z. Tang, "Partial discharge pulse propagation in power cable and partial discharge monitoring system," *IEEE Trans. Dielectr. Electr. Insul.*, vol. 21, no. 3, pp. 948–956, 2014.

[6] P. H. F. Morshuis and J. Beyer, "Quality assessment of HVDC components by PD analysis," *Conf. Electr. Insul. Dielectr. Phenom. (CEIDP), Annu. Rep.*, pp. 542–545, 1997.

[7] R. Bartnikas, "Use of a Multichannel Analyzer for Corona Pulse-Height Distribution Measurements on Cables and Other Electrical Apparatus," *IEEE Trans. Instrum. Meas.*, vol. 22, no. 4, pp. 403–407, 1973.

[8] E. Gulski and F. H. Kreuger, "Computer-aided recognition of Discharge Sources," *IEEE Trans. Electr. Insul.*, vol. 27, no. 1, pp. 82–92, 1992.

[9] G. Capponi and I. Elettrica, "Measurement of Partial Discharge in Solid Dielectrics with a Microprocessor-based System," *IEEE Trans. Electr. Insul.*, vol. 27, no. 1, pp. 106–113, 1992.

[10] E. C. T. Macedo, J. M. M. Villanueva, E. C. Guedes, R. C. S. Freire, J. M. R. De Souza Neto, and I. A. Glover, "The influence of void configuration in

statistical parameters of partial discharge signals," *Conf. Rec. - IEEE Instrum. Meas. Technol. Conf.*, pp. 952–956, 2013.

[11] C. Kane and A. Golubev, "Advantages of continuous monitoring of partial discharges in rotating equipment and switchgear," *IEEE Conf. Rec. Annu. Pulp Pap. Ind. Tech. Conf.*, pp. 117–122, 2003.

[12] M. P. Bahrman, "HVDC Transmission Overview," in *Transmission and Distribution Conference and Exposition*, 2008, pp. 1–7.

[13] P. Schavemaker and L. Van Der Sluis, *Electrical Power System Essentials*. John Wiley & Sons, Ltd, 2008.

[14] P. Bresesti, W. L. Kling, R. L. Hendriks, and R. Vailati, "HVDC Connection of Offshore Wind Farms to the Transmission System," *IEEE Trans. Energy Convers.*, vol. 22, no. 1, pp. 37–43, 2007.

[15] R. Prochazka, O. Sefl, and M. Knenicky, "Partial Discharges Activity within an Internal Void at AC Voltage Disturbed by High Frequency Components," *ICHVE 2018 - 2018 IEEE Int. Conf. High Volt. Eng. Appl.*, pp. 1–4, 2019.

[16] B. Ma, X. Wu, X. Li, X. Zhou, Q. Zhang, J. Li, and X. Han, "Study of the Influence of Void Defect Size on Partial Discharge Characteristics in Solid Insulation," *ICHVE 2018 - 2018 IEEE Int. Conf. High Volt. Eng. Appl.*, pp. 3–6, 2019.

[17] M. Knenicky, R. Prochazka, and J. Hlavacek, "Partial Discharge Patterns during Accelerated Aging of Medium Voltage Cable System," *ICHVE 2018 - 2018 IEEE Int. Conf. High Volt. Eng. Appl.*, pp. 1–4, 2019.

[18] Y. Zhan, G. Chen, and M. Hao, "Space charge modelling in HVDC extruded cable insulation," *IEEE Trans. Dielectr. Electr. Insul.*, vol. 26, no. 1, pp. 43–50, 2019.

[19] Y. Zhu, F. Yang, X. Xie, W. Cao, G. Sheng, and X. Jiang, "Studies on electric field distribution and partial discharges of XLPE cable at DC voltage," *Proc. IEEE Int. Conf. Prop. Appl. Dielectr. Mater.*, vol. 2018-May, no. 2, pp. 562–565, 2018.

[20] Z. Ahmed, J. V. Kluss, and D. A. Wallace, "Partial discharge measurements and techniques for pattern recognition and life prediction of medium voltage XLPE cables," *ICHVE 2018 - 2018 IEEE Int. Conf. High Volt. Eng. Appl.*, pp. 1–4, 2019.

[21] R. Hata, "Solid DC submarine cable insulated with polypropylene laminated paper (PPLP)," *SEI Tech. Rev.*, no. 62, pp. 3–9, 2006.

[22] S. Wenrong, L. Junhao, Y. Peng, and L. Yanming, "Digital detection, grouping and classification of partial discharge signals at DC voltage," *IEEE Trans. Dielectr. Electr. Insul.*, vol. 15, no. 6, pp. 1663–1674, 2008.

[23] E. A. Morris, "Partial Discharge Measurements of Voids in Layered Polymers and Cable Sample." University of Strathclyde, 2020.

[24] J. Liu, W. H. Siew, J. J. Soraghan, and E. A. Morris, "A Novel Wavelet Selection Scheme for Partial Discharge Signal Detection under Low SNR Condition," *Annu. Rep. - Conf. Electr. Insul. Dielectr. Phenomena, CEIDP*, vol. 2018-Octob, pp. 498–501, 2018.

[25] E. A. Morris, W. H. Siew, and M. J. Given, "DC Partial Discharge in Polymeric Cable Insulation," in *Conference on Electrical Insulation and Dielectric Phenomena*, 2018, pp. 494–497.

[26] E. A. Morris and W. H. Siew, "Partial Discharge Activity in Polymeric Cable Insulation under High Voltage AC and DC," in *International Universities Power Engineering Conference (UPEC)*, 2017, pp. 1–4.

[27] E. A. Morris and W. H. Siew, "A Comparison of AC And DC Partial Discharge Activity in Polymeric Cable Insulation," in *21st IEEE International Pulsed Power Conference*, 2017, pp. 1–4.

[28] W. Long and S. Nilsson, "HVDC transmission: Yesterday and today," *IEEE Power Energy Mag.*, vol. 5, no. 2, pp. 22–31, 2007.

[29] Siemens, "High Voltage Direct Current Transmission –Proven technology for power Exchange," 2011.

[30] G. Mazzanti and M. Marzinotto, "Fundamentals of HVDC Cable Transmission," in *Extruded Cables for High-Voltage Direct-Current Transmission:Advances in Research and Development*, 1st ed., Wiley-IEEE Press, 2013, p. 384.

[31] M. P. Bahrman, "Overview of HVDC transmission," *2006 IEEE PES Power Syst. Conf. Expo. PSCE 2006 - Proc.*, pp. 18–23, 2006.

[32] M. Jeroense, "HVDC, the next generation of transmission: Highlights with focus on extruded cable systems," in *International Symposium on Electrical Insulating Materials*, 2008, pp. 10–15.

[33] A. Alassi, S. Bañales, O. Ellabban, G. P. Adam, and C. MacIver, "HVDC Transmission: Technology Review, Market Trends and Future Outlook," *Renew. Sustain. Energy Rev.*, vol. 112, no. June, pp. 530–554, 2019.

[34] G. Mazzanti, "Extruded Cable Systems for HVDC Transmission," in *HubNet Colloquium on Power Cables and Cable Integrity*, 2016.

[35] B. J. Pawar and V. J. Gond, "Modular multilevel converters: A review on topologies, modulation, modeling and control schemes," *Proc. Int. Conf. Electron. Commun. Aerosp. Technol. ICECA 2017*, vol. 2017-Janua, pp. 431–440, 2017.

[36] P. Tu, S. Yang, and P. Wang, "Reliability- and Cost-Based Redundancy Design for modular multilevel converter," *IEEE Trans. Ind. Electron.*, vol. 66, no. 3, pp. 2333–2342, 2019.

[37] J. Wylie, P. D. Judge, and T. C. Green, "Modular Multi-level Converter for Medium Voltage Applications with Mixed Sub-module Voltages within Each Arm," *Proc. - 2018 IEEE PES Innov. Smart Grid Technol. Conf. Eur. ISGT-Europe 2018*, pp. 1–6, 2018.

[38] P. Ladoux, N. Serbia, and E. I. Carroll, "On the Potential of IGCTs in HVDC," *IEEE J. Emerg. Sel. Top. Power Electron.*, vol. 3, no. 3, pp. 780–793, 2015.

[39] P. Li, G. P. Adam, S. J. Finney, and D. Holliday, "Operation Analysis of

Thyristor-Based Front-to-Front Active-Forced-Commutated Bridge DC Transformer in LCC and VSC Hybrid HVDC Networks," *IEEE J. Emerg. Sel. Top. Power Electron.*, vol. 5, no. 4, pp. 1657–1669, 2017.

[40] C. Verdugo, J. I. Candela, and P. Rodriguez, "Grid support functionalities based on modular multilevel converters with synchronous power control," *2016 IEEE Int. Conf. Renew. Energy Res. Appl. ICRERA 2016*, vol. 5, pp. 572–577, 2017.

[41] A. A. Elserougi, A. S. Abdel-Khalik, A. M. Massoud, and S. Ahmed, "A new protection scheme for HVDC converters against DC-side faults with current suppression capability," *IEEE Trans. Power Deliv.*, vol. 29, no. 4, pp. 1569–1577, 2014.

[42] E. J. Corr, W. H. Siew, and W. Zhao, "Long Term Testing and Analysis of Dielectric Samples Under DC Excitation," in *IEEE Electrical Insulation Conference*, 2016, pp. 2–5.

[43] G. Mazzanti and M. Marzinotto, "Main Principles of HVDC Extruded Cable Design," in *Extruded Cables for High-Voltage Direct-Current Transmission:Advances in Research and Development*, Wiley-IEEE Press, 2013.

[44] G. Mazzanti and M. Marzinotto, *Extruded Cables for High-Voltage Direct-Current Transmission: Advances in Research and Development*, First Edit. Hoboken, USA: Wiley-IEEE Press, 2013.

[45] G. Chen and Z. Xu, "Polypropylene laminated paper (PPLP) insulation for HVDC power cables," *Proc. IEEE Int. Conf. Prop. Appl. Dielectr. Mater.*, vol. 2018-May, pp. 28–32, 2018.

[46] International Electrotechnical Commission - Technical Commitee 42 -High-voltage and high-current test techniques, *IEC 60270:2000 - High-voltage test techniques — Partial discharge measurements*, no. 3. 2000, pp. 1–99.

[47] G. C. Lichtenberg, "De Nova Methodo Naturam Ac Motum Fluidi Electrici Investigandi (Concerning the New Method Of Investigating the Nature and

Movement of Electric Fluid)," *Novi Comment. Soc. Regiae Sci. Gottingensis (Göttingen Acad. Sci. - New Comment.*, vol. 2, no. 1, 1777.

[48] D. A. Nattrass, "Partial Discharge XVII: The Early History of Partial Discharge Research," *IEEE Electr. Insul. Mag.*, vol. 9, no. 4, pp. 27–31, 1993.

[49] A. N. Arman and A. T. Starr, "The measurement of discharges in dielectrics," *J. Inst. Electr. Eng.*, vol. 79, no. 475, pp. 67–81, 1936.

[50] T. Moriuchi and M. Tan, "Partial discharge properties in spherical void in epoxy resins," *Conf. Rec. 1978 IEEE Int. Symp. Electr. Insul. ISEI 1978*, pp. 37–40, 1979.

[51] N. H. Malik, A. A. Al-Arainy, A. M. Kailani, and M. J. Khan, "Discharge Inception Voltages Due To Voids In Power Cables," *IEEE Trans. Electr. Insul.*, vol. EI-22, no. 6, pp. 787–793, 1987.

[52] T. Mizutani, T. Kondo, and K. Nakao, "Change in partial discharge properties of a void in LDPE," in *Conference on Electrical Insulation and Dielectric Phenomena*, 1999, pp. 257–260.

[53] T. Mizutani and T. Kondo, "PD Patterns and PD Current Shapes of a Void in LDPE," in *Properties and Applications of Dielectric Materials, 2000. Proceedings of the 6th International Conference on*, 2000, vol. 1, pp. 157–160.

[54] P. H. F. Morshuis, A. Cavallini, G. C. Montanari, F. Puletti, and A. Contin, "The behavior of physical and stochastic parameters from partial discharges in spherical voids," in *International Conference on Properties and Applications of Dielectric Materials*, 2000, pp. 304–309.

[55] E. Ildstad and T. Haave, "Conduction and partial discharge activity in HVDC cable insulation of lapped polypropylene films," in *International Conference on Solid Dielectrics*, 2001, pp. 137–140.

[56] C. S. Kim, T. Hirase, and T. Mizutani, "PD frequency characteristics for a void bounded with LDPE," *Electr. Insul. Dielectr. Phenomena, 2002 Annu. Rep.*

Conf., pp. 712–715, 2002.

[57] P. H. F. Morshuis, "Degradation of solid dielectrics due to internal partial discharge: Some thoughts on progress made and where to go now," *IEEE Trans. Dielectr. Electr. Insul.*, vol. 12, no. 5, pp. 905–913, 2005.

[58] H. A. Illias, G. Chen, and P. L. Lewin, "Partial discharge measurements for spherical cavities within solid dielectric materials under different stress and cavity conditions," *Annu. Rep. - Conf. Electr. Insul. Dielectr. Phenomena, CEIDP*, vol. 2, pp. 388–391, 2009.

[59] D. Adhikari, D. M. Hepburn, and B. G. Stewart, "Analysis of partial discharge characteristics in artificially created voids," *Univ. Power Eng. Conf. (UPEC), 2010 45th Int.*, pp. 1–4, 2010.

[60] M. Hikita, M. Kozako, H. Takada, M. Higashiyama, T. Hirose, S. Nakamura, and T. Umemura, "Partial discharge phenomena in artificial cavity in epoxy cast resin insulation system," *Conf. Rec. IEEE Int. Symp. Electr. Insul.*, vol. 1, no. c, 2010.

[61] H. A. Illias, G. Chen, and P. L. Lewin, "Partial discharge behavior within a spherical cavity in a solid dielectric material as a function of frequency and amplitude of the applied voltage," *IEEE Trans. Dielectr. Electr. Insul.*, vol. 18, no. 2, pp. 432–443, 2011.

[62] L. Niemeyer, "The Physics of Partial Discharges," in *1993 International Conference on Partial Discharge*, 1993.

[63] J. H. Mason, "Discharges," *IEEE Trans. Electr. Insul.*, vol. EI-13, no. 4, pp. 211–238, 1978.

[64] F. Paschen, "Ueber die zum Funkenübergang in Luft, Wasserstoff und Kohlensäure bei verschiedenen Drucken erforderliche Potentialdifferenz (On the potential difference required for spark initiation in air, hydrogen, and carbon dioxide at different pressures)," *Ann. der Phys. (Annals Physics)*, vol. 273, no. 5, pp. 69–75, 1889.

[65] D. C. Faircloth, "Technological Aspects: High Voltage," *CAS-CERN Accel. Sch. Ion Sources*, pp. 1–39, 2012.

[66] M. A. Lieberman and A. J. Lichtenberg, "Principles of plasma discharges and materials processing." Wiley-Interscience, Hoboken, N.J., 2005.

[67] U. Fromm and F. H. Kreuger, "Statistical behaviour of internal partial discharges at DC voltage," *Jpn. J. Appl. Phys.*, vol. 33, no. 12R, pp. 670–675, 1994.

[68] P. H. F. Morshuis and F. H. Kreuger, "Transition from streamer to townsend mechanisms in dielectric voids," *J. Phys. D. Appl. Phys.*, vol. 23, no. 12, pp. 1562–1568, 1990.

[69] E. Kuffel, W. S. Zaengl, and J. Kuffel, *High Voltage Engineering Fundamentals*. Elsevier, 2000.

[70] M. C. Kang, K. H. Kim, and Y. T. Yoon, "Pre-arcing time prediction in a making test for a 420 kV 63 kA high-speed earthing switch," *Energies*, vol. 10, no. 10, pp. 1–15, 2017.

[71] P. H. F. Morshuis and J. J. Smit, "Partial discharges at dc voltage: Their mechanism, detection and analysis," *IEEE Trans. Dielectr. Electr. Insul.*, vol. 12, no. 2, pp. 328–340, Apr. 2005.

[72] U. Fromm, "Interpretation of partial discharges at dc voltages," *IEEE Trans. Dielectr. Electr. Insul.*, vol. 2, no. 5, pp. 761–770, 1995.

[73] U. Fromm, "Partial discharge and Breakdown Testing at High DC Voltage," Delft University of Technology, 1995.

[74] U. Fromm and P. H. F. Morshuis, "Partial Discharge Classification at DC Voltage," in *IEEE 5th Annual Conference of Conduction and Breakdown in Solid Dielectrics*, 1995, pp. 403–407.

[75] D. R. James, I. Saures, A. R. Ellis, M. O. Pace, and D. J. Deschenes, "Effect of gas pressure on partial discharge in voids in epoxy," in *Conference on Electrical Insulation and Dielectric Phenomena*, 2003, pp. 628–632.

[76] S.-I. Jeon, D. S. Shin, Y. Do-Hong, H. Key-Man, and H. Min-Koo, "A Study on The Partial Discharge Characteristics According to The Distribution Pattern of Voids Within an Insulation," in *IEEE 5th International Conference on Conduction and Breakdown m Solid Dielectrics*, 1995, pp. 398–402.

[77] D. S. Shin, M. K. Han, J. H. Lee, B. K. Lee, and Y. H. Ohk, "Effects of the distribution pattern of multiple voids within LDPE on partial discharge characteristics," *Conf. Rec. IEEE Int. Symp. Electr. Insul.*, vol. 1, pp. 142–145, 1996.

[78] M. G. Danikas, "Partial Discharge Behaviour of Two (or More) Adjacent Cavities in Polyethylene Samples," *J. Electr. Eng.*, vol. 52, no. 01, pp. 36–39, 2001.

[79] D. Adhikari, D. M. Hepburn, and B. G. Stewart, "Analysis of deterioration of PET insulation with multiple voids due to electrical stressing," *2011 Electr. Insul. Conf. EIC 2011*, no. June, pp. 146–150, 2011.

[80] D. P. Agoris and N. D. Hatziargyriou, "Approach to partial discharge development in closely coupled cavities embedded in solid dielectrics by the lumped capacitance model," *IEE Proceedings, Part A Sci. Meas. Technol.*, vol. 140, no. 2, pp. 131–134, 1993.

[81] D. Adhikari, D. M. Hepburn, and B. G. Stewart, "PD degradation analysis of PET with enclosed voids and voids connected to closed and vented channels," *Proc. Univ. Power Eng. Conf.*, 2012.

[82] H. A. Illias, G. Chen, and P. L. Lewin, "Measurement of partial discharge activities within two artificial spherical voids in an epoxy resin," *Annu. Rep. - Conf. Electr. Insul. Dielectr. Phenomena, CEIDP*, pp. 489–492, 2011.

[83] P. K. Olsen, F. Mauseth, and E. Ildstad, "The effect of DC superimposed AC voltage on partial discharges in dielectric bounded cavities," *ICHVE 2014 - 2014 Int. Conf. High Volt. Eng. Appl.*, pp. 2–5, 2014.

[84] M. Lerchbacher, C. Sumereder, G. Lemesch, F. Ramsauer, and M. Muhr, "Impact of small voids in solid insulating materials," *Proc. IEEE Int. Conf.*

Prop. Appl. Dielectr. Mater., pp. 1–4, 2012.

[85] E. J. Corr, W. H. Siew, and W. Zhao, "PD activity in void type dielectric samples for varied DC polarity," *Annu. Rep. - Conf. Electr. Insul. Dielectr. Phenomena, CEIDP*, vol. 2016-Decem, pp. 510–513, 2016.

[86] M. R. Rahimi, R. Javadinezhad, and M. Vakilian, "DC partial discharge characteristics for corona, surface and void discharges," in *Proceedings of the IEEE International Conference on Properties and Applications of Dielectric Materials*, 2015, vol. 2015-Octob, pp. 260–263.

[87] T. Dezenzo, T. Betz, and A. Schwarzbacher, "The different stages of PRPD pattern for positive point to plane corona driven by a DC voltage containing ripple," *IEEE Trans. Dielectr. Electr. Insul.*, vol. 25, no. 1, pp. 30–37, 2018.

[88] M. Mahdipour, A. Akbari, and P. Werle, "Charge concept in partial discharge in power cables," *IEEE Trans. Dielectr. Electr. Insul.*, vol. 24, no. 2, pp. 817–825, 2017.

[89] M. Wu, H. Cao, J. Cao, H. L. Nguyen, J. B. Gomes, and S. P. Krishnaswamy, "An overview of state-of-the-art partial discharge analysis techniques for condition monitoring," *IEEE Electr. Insul. Mag.*, vol. 31, no. 6, pp. 22–35, 2015.

[90] M. D. Judd, S. D. J. McArthur, A. J. Reid, V. M. Catterson, L. Yang, B. Jacobson, K. O. Svensson, and M. Gunnarsson, "Investigation of radiometric partial discharge detection for use in switched HVDC testing," *2006 IEEE Power Eng. Soc. Gen. Meet. PES*, 2006.

[91] P. C. Baker, M. D. Judd, and S. D. J. McArthur, "A frequency-based RF partial discharge detector for low-power wireless sensing," *IEEE Trans. Dielectr. Electr. Insul.*, vol. 17, no. 1, pp. 133–140, 2010.

[92] G. Mazzanti, J. Castellon, G. Chen, J. C. Fothergill, M. Fu, N. Hozumi, J. H. Lee, J. Li, M. Marzinotto, F. Mauseth, P. H. F. Morshuis, C. Reed, I. Troia, A. Tzimas, and K. Wu, "The insulation of HVDC extruded cable system joints. Part 1: Review of materials, design and testing procedures," *IEEE Trans. Dielectr.*

Electr. Insul., vol. 26, no. 3, pp. 964–972, 2019.

[93] T. Klueter, J. Wulff, and F. Jenau, "Measurement and Statistical Analysis of Partial Discharges at DC Voltage," in *Universities Power Engineering Conference*, 2013, vol. 0, pp. 0–4.

[94] M. A. Fard, A. J. Reid, D. M. Hepburn, and H. Gallagher, "Influence of voltage harmonic phenomena on partial discharge behavior at HVDC," *Proc. 2016 IEEE Int. Conf. Dielectr. ICD 2016*, vol. 1, pp. 548–551, 2016.

[95] M. A. Fard, M. E. Farrag, S. G. McMeekin, and A. J. Reid, "Partial discharge behavior under operational and anomalous conditions in HVDC systems," *IEEE Trans. Dielectr. Electr. Insul.*, vol. 24, no. 3, pp. 1494–1502, 2017.

[96] T. Dezenzo, T. Betz, and A. Schwarzbacher, "Transfer and evaluation of the AC PRPD representation for internal PD at DC voltage," *Proc. 2016 IEEE Int. Conf. Dielectr. ICD 2016*, vol. 1, pp. 528–531, 2016.

[97] J. Li, H. Wang, X. He, L. Chen, C. Zhang, Y. Zhang, X. Li, and Y. Yu, "Comprehensive evaluation of insulation performance of DC XLPE cables," *China Int. Conf. Electr. Distrib. CICED*, no. 201804270000229, pp. 238–243, 2018.

[98] R. Aldrian, G. C. Montanari, A. Cavallini, and Suwarno, "Signal separation and identification of partial discharge in XLPE insulation under DC voltage," *ICEMPE 2017 - 1st Int. Conf. Electr. Mater. Power Equip.*, pp. 53–56, 2017.

[99] M. Hoof and R. Patsch, "Analyzing partial discharge pulse sequences-a new approach to investigate degradation phenomena," in *IEEE International Symposium on Electrical Insulation*, 1994, pp. 327–331.

[100] P. H. F. Morshuis, A. Cavallini, D. Fabiani, G. C. Montanari, and C. Azcarraga, "Stress conditions in HVDC equipment and routes to in service failure," *IEEE Trans. Dielectr. Electr. Insul.*, vol. 22, no. 1, pp. 81–91, 2015.

[101] A. Imburgia, P. Romano, F. Viola, A. Madonia, R. Candela, and I. Troia, "Space

charges and partial discharges simultaneous measurements under DC stress," *Annu. Rep. - Conf. Electr. Insul. Dielectr. Phenomena, CEIDP*, vol. 2016-Decem, pp. 514–517, 2016.

[102] A. Tzimas, G. Lucas, K. J. Dyke, F. Perrot, L. Boyer, P. Mirebeau, S. Dodd, J. Castellon, and P. Notingher, "Space charge Evolution in XLPE HVDC cable with Thermal-Step- Method and Pulse-Electro-Acoustic," in *International Conference on Insulated Power Cables*, 2015, pp. 6–11.

[103] J. Beyer, "Space charge and partial discharge phenomena in HVDC devices," Technische Universiteit Delf, 2002.

[104] A. J. Reid, D. M. Hepburn, and B. G. Stewart, "The Influence of External Magnetic Fields on the Partial Discharge Characteristics of Voids," in *Electrical Insulation Conference*, 2013, no. June, pp. 147–150.

[105] I.-J. Seo, U. A. Khan, J.-S. Hwang, J. G. Lee, and J.-Y. Koo, "Identification of Insulation Defects Based on Chaotic Analysis of Partial Discharge in HVDC Superconducting Cable," *IEEE Trans. Appl. Supercond.*, vol. 25, no. 3, Jun. 2015.

[106] T. Okamoto and T. Tanaka, "Partial discharge characteristics in phase domain for various cylindrical voids," *Conf. Electr. Insul. Dielectr. Phenom. - Annu. Rep. 1985*, pp. 498–503, 2016.

[107] W. Gao, N. Su, and Q. Yin, "Size effect of partial discharge in solid void defects," *Proc. IEEE Int. Conf. Prop. Appl. Dielectr. Mater.*, pp. 501–504, 2009.

[108] E. J. Corr and W. H. Siew, "Analyses of partial discharges in dielectric samples under DC excitation," in *Proceedings of the Universities Power Engineering Conference*, 2015, pp. 1–6.

[109] R. Gillie, A. Nesbitt, R. Ramirez-Iniguez, B. G. Stewart, and G. Kerr, "Analysis of HV cable faults based on correlated HFCT and IEC60270 measurements," *2014 IEEE Conf. Electr. Insul. Dielectr. Phenomena, CEIDP 2014*, pp. 168–171, 2014.

[110] H. A. Illias, G. Chen, and P. L. Lewin, "Modeling of partial discharge activity in spherical cavities within a dielectric material," *IEEE Electr. Insul. Mag.*, vol. 27, no. 1, pp. 38–45, 2011.

[111] F. Gutfleisch and L. Niemeyer, "Measurement and Simulation of PD in Epoxy Voids," *IEEE Trans. Dielectr. Electr. Insul.*, vol. 2, no. 5, pp. 729–743, 1995.

[112] H. A. Illias, Teo Soon Yuan, A. H. A. Bakar, H. Mokhlis, G. Chen, and P. L. Lewin, "Partial discharge patterns in high voltage insulation," *PECon 2012 - 2012 IEEE Int. Conf. Power Energy*, no. December, pp. 750–755, 2012.

[113] L. Wang, A. Cavallini, G. C. Montanari, and L. Testa, "Evolution of PD patterns in polyethylene insulation cavities under AC voltage," *IEEE Trans. Dielectr. Electr. Insul.*, vol. 19, no. 2, pp. 533–542, 2012.

[114] I. D. Bruce and B. G. Stewart, "Extension of Pulse-Sequence-Analysis for evaluating insulation PD characteristics," *Univ. Power Eng. Conf. (UPEC), 2009 Proc. 44th Int.*, pp. 1–5, 2009.

[115] R. Patsch and F. Berton, "Pulse sequence analysis - A diagnostic tool based on the physics behind partial discharges," *J. Phys. D. Appl. Phys.*, vol. 35, no. 1, pp. 25–32, 2002.

[116] J. Kim, D. Kim, K. Nam, W. Choi, B. Lee, and J.-Y. Koo, "Characteristics of partial discharge by AC and DC," *Proc. 2012 IEEE Int. Conf. Cond. Monit. Diagnosis, C. 2012*, no. September, pp. 489–492, 2012.

[117] F. P. Mohamed, W. H. Siew, S. M. Strachan, A. S. Ayub, and K. Mclellan, "Method to Discard Partial Discharge (PD) Pulses from Neighboring High Voltage Equipment," *High Volt. Eng.*, vol. 2015, pp. 1125–1131, 2015.

[118] J. A. Ardila-Rey, J. M. Martínez-Tarifa, G. Robles, and M. Rojas-Moreno, "Partial discharge and noise separation by means of spectral-power clustering techniques," *IEEE Trans. Dielectr. Electr. Insul.*, vol. 20, no. 4, pp. 1436–1443, 2013.

[119] G. C. Montanari, F. Negri, and F. Ciani, "Noise rejection and partial discharge

identification in HVDC insulation systems," *2017 IEEE Electr. Insul. Conf. EIC 2017*, no. June, pp. 425–428, 2017.

[120] M. S. Mashikian, F. Palmieri, R. Bansal, and R. B. Northrop, "Partial Discharges in Shielded Cables in the Presence of High Noise," *IEEE Trans. Electr. Insul.*, vol. 27, no. 1, pp. 37–43, 1992.

[121] P. H. F. Morshuis, G. C. Montanari, and L. Fornasari, "Partial discharge diagnostics — Critical steps towards on-line monitoring," *2014 IEEE PES T&D Conf. Expo.*, pp. 1–5, 2014.

[122] P. Craatz, R. Plath, R. Heinrich, and W. Kalkner, "Sensitive on-site PD measurement and location using directional coupler sensors in 110 kV prefabricated joints," *IEE Conf. Publ.*, vol. 5, no. 467, pp. 317–321, 1999.

[123] D. Pommerenke, T. Strehl, R. Heinrich, W. Kalkner, F. Schmidt, and W. Weißenberg, "Discrimination between internal PD and other pulses using directional coupling sensors on HV cable systems," *IEEE Trans. Dielectr. Electr. Insul.*, vol. 6, no. 6, pp. 814–824, 1999.

[124] L. Zhong, Y. Xu, G. Chen, A. E. Davies, Z. Richardson, and S. G. Swingler, "Use of capacitive couplers for partial discharge measurements in power cables and joints," *IEEE Int. Conf. Conduct. Break. Solid Dielectr.*, pp. 412–415, 2001.

[125] D. A. Ward and J. L. T. Exon, "Using Rogowski coils for transient current measurements," *Eng. Sci. Educ. J.*, vol. June, 1993.

[126] A. Van den Bossche and J. Ghijselen, "EMC combined di/dt current probe," *IEEE Int. Symp. Electromagn. Compat.*, vol. 2, pp. 569–573, 2000.

[127] J. Cooper, "On the high-frequency response of a Rogowski coil," *J. Nucl. Energy. Part C, Plasma Physics, Accel. Thermonucl. Res.*, vol. 5, no. 5, pp. 285–289, 1963.

[128] V. Nassisi and A. Luches, "Rogowski coils: Theory and experimental results," *Rev. Sci. Instrum.*, vol. 50, no. 7, pp. 900–902, 1979.

[129] F. P. Mohamed, W. H. Siew, J. J. Soraghan, S. M. Strachan, and J. McWilliam, "Partial discharge location in power cables using a double ended method based on time triggering with GPS," *IEEE Trans. Dielectr. Electr. Insul.*, vol. 20, no. 6, pp. 2212–2221, 2013.

[130] C. Y. Lee, S. H. Nam, S. G. Lee, D. Kim, and M. K. Choi, "High frequency Partial Discharge measurement by capacitive sensor for underground power cable system," *PowerCon 2000 - 2000 Int. Conf. Power Syst. Technol. Proc.*, vol. 3, pp. 1517–1520, 2000.

[131] E. F. Steennis, R. Ross, N. Van Schaik, W. Boone, and D. M. Van Aartrijk, "Partial discharge diagnostics of long and branched medium-voltage cables," *IEEE Int. Conf. Conduct. Break. Solid Dielectr.*, pp. 27–30, 2001.

[132] L. W. Van Veen, "Comparison of measurement methods for partial discharge measurement in power cables," no. April, pp. 1–116, 2014.

[133] F. P. Mohamed, S. M. Strachan, J. McWilliam, W. H. Siew, and J. J. Soraghan, "Remote monitoring of partial discharge data from insulated power cables," *IET Sci. Meas. Technol.*, vol. 8, no. 5, pp. 319–326, 2014.

[134] E. Pultrum and M. van Riet, "HF Partial Discharge Detection of HV Extruded Cable Accessories," *Jicable*, pp. 662–665, 1995.

[135] F. H. Kreuger, M. G. Wezelenburg, A. G. Wiemer, and W. A. Sonneveld, "Partial Discharge Part XVIII: Errors in the Location of Partial Discharges in High Voltage Solid Dielectric Cables," *IEEE Electr. Insul. Mag.*, vol. 9, no. 6, pp. 15–22, 1993.

[136] J. C. Devins, "Physics of Partial Discharges in Solid Dielectrics.," *Conf. Electr. Insul. Dielectr. Phenom. (CEIDP), Annu. Rep.*, pp. 15–31, 1984.

[137] H. A. Illias, G. Chen, and P. L. Lewin, "Comparison between three-capacitance, analytical-based and finite element analysis partial discharge models in condition monitoring," *IEEE Trans. Dielectr. Electr. Insul.*, vol. 24, no. 1, pp. 99–109, 2017.

[138] S. Whitehead, *Dielectric Breakdown of Solids*. London, UK: Oxford University Press, 1951.

[139] Z. Achillides, G. Georghiou, and E. Kyriakides, "Partial discharges and associated transients: The induced charge concept versus capacitive modeling," *IEEE Trans. Dielectr. Electr. Insul.*, vol. 15, no. 6, pp. 1507–1516, 2008.

[140] I. W. McAllister, G. C. Crichton, and A. Pedersen, "Partial Discharges in Ellipsoidal and Spheroidal Voids," *IEEE Trans. Electr. Insul.*, vol. 26, no. 3, pp. 537–539, 1991.

[141] A. Pedersen, G. C. Crichton, and I. W. McAllister, "The Functional Relation between Partial Discharges and Induced Charge," *IEEE Trans. Dielectr. Electr. Insul.*, vol. 2, no. 4, pp. 535–543, 1995.

[142] E. Lemke, "A critical review of partial-discharge models," *IEEE Electr. Insul. Mag.*, vol. 28, no. 6, pp. 11–16, 2012.

[143] G. Chen, H. A. Illias, and P. L. Lewin, "Partial discharge within a spherical cavity in a dielectric material as a function of cavity size and material temperature," *IET Sci. Meas. Technol.*, vol. 6, no. 2, pp. 52–62, 2012.

[144] Y. Su, Y. Xue, B. Xu, and D. Liu, "The feasibility analysis of partial discharge location of XLPE cables based on traveling waves fault location technology," *APAP 2011 - Proc. 2011 Int. Conf. Adv. Power Syst. Autom. Prot.*, vol. 3, pp. 2417–2423, 2011.

[145] H. A. Illias, G. Chen, and P. L. Lewin, "The influence of spherical cavity surface charge distribution on the sequence of partial discharge events," *J. Phys. D. Appl. Phys.*, vol. 44, no. 24, 2011.

[146] X. Hu, W. H. Siew, M. D. Judd, and X. Peng, "Transfer function characterization for HFCTs used in partial discharge detection," *IEEE Trans. Dielectr. Electr. Insul.*, vol. 24, no. 2, pp. 1088–1096, 2017.

[147] Goodfellow Cambridge Ltd., "Polyethylene - Low Density - Film - LDPE -

ET311151 Datasheet." 2020.

[148] S. M. Kurtz, *UHMWPE Biomaterials Handbook*, Second. Academic Press, 2009.

[149] Goodfellow Cambridge Ltd., "Polyproplyene - Film - PP - PP301350 Datasheet." 2020.

[150] R. O. Ebewele, *Polymer Science and Technology*, First. CRC Press, 2000.

[151] D. Adhikari, D. M. Hepburn, and B. G. Stewart, "Comparison of partial discharge characteristics and degradation in several polymeric insulators," *IET Sci. Meas. Technol.*, vol. 6, no. 6, p. 474, 2012.

[152] M. A. Fard, A. J. Reid, and D. M. Hepburn, "Analysis of HVDC superimposed harmonic voltage effects on partial discharge behavior in solid dielectric media," *IEEE Trans. Dielectr. Electr. Insul.*, vol. 24, no. 1, pp. 7–16, 2017.

[153] F. Gutfleisch and L. Niemeyer, "Measurment and Simulation of PD in Epoxy Voids," *IEEE Trans. Dielectr. Electr. Insul.*, vol. 2, no. 5, pp. 729–743, 1995.

[154] G. C. Montanari, C. Laurent, G. Teyssedre, A. Campus, and U. H. Nilsson, "From LDPE to XLPE: Investigating the change of electrical properties. Part I: Space charge, Conduction and lifetime," *IEEE Trans. Dielectr. Electr. Insul.*, vol. 12, no. 3, pp. 438–446, 2005.